UNCLASSIFIED

AD 282 255

Reproduced
by the

ARMED SERVICES TECHNICAL INFORMATION AGENCY
ARLINGTON HALL STATION
ARLINGTON 12, VIRGINIA

UNCLASSIFIED

NOTICE: When government or other drawings, speci-
fications or other data are used for any purpose
other than in connection with a definitely related
government procurement operation, the U. S.
Government thereby incurs no responsibility, nor any
obligation whatsoever; and the fact that the Govern-
ment may have formulated, furnished, or in any way
supplied the said drawings, specifications, or other
data is not to be regarded by implication or other-
wise as in any manner licensing the holder or any
other person or corporation, or conveying any rights
or permission to manufacture, use or sell any
patented invention that may in any way be related
thereto.

CALCULATION OF NON-LIFTING POTENTIAL FLOW
ABOUT ARBITRARY THREE-DIMENSIONAL BODIES

by

JOHN L. HESS and A.M.O. SMITH

Report No. E.S. 40622   15 March 1962

DOUGLAS AIRCRAFT DIVISION · LONG BEACH, CALIFORNIA

DOUGLAS

CALCULATION OF NON-LIFTING POTENTIAL FLOW ABOUT ARBITRARY THREE-DIMENSIONAL BODIES

by

JOHN L. HESS and A.M.O. SMITH

Report No. E.S. 40622   15 March 1962

Contract No. Nonr 2722(00)

Douglas Aircraft Co., Inc. ∎ Aircraft Division ∎ Long Beach, California

Half-model of a merchant ship hull. This photograph illustrates the manner in which a continuous three-dimensional shape is approximated by plane quadrilateral surface elements. The dots represent the points where velocities and pressures are calculated. (See Section 11.42).

1.0 ABSTRACT

This report describes a method for calculating, with the aid of an electronic computer, the incompressible potential flow about arbitrary, non-lifting, three-dimensional bodies. The method utilizes a source density distribution on the surface of the body and solves for the distribution necessary to make the normal velocity zero on the boundary. Plane quadrilateral surface elements are used to approximate the body surface, and the integral equation for the surface source density is replaced by a set of linear algebraic equations for the values of the source density on each of the quadrilateral elements. After this set of equations has been solved, which is accomplished by a Seidel iterative procedure, the flow velocities at points both on and off the body surface are calculated. This approach is completely general. Bodies are not required to be slender, analytically defined, or simply connected. In fact the flow about an ensemble of bodies may be calculated, so that interference problems may be investigated. It is only necessary that the body can be satisfactorily approximated by the maximum number of surface elements permitted by the storage capacity of the computing machine. For the IBM 7090 this number varies from 675 for completely general bodies to 4400 for bodies with three planes of symmetry.

In the text of the report, the basic formulas of the method are derived, and the computational procedure is described in detail. The accuracy of the calculated surface velocities is exhibited by comparing them with analytic solutions for a sphere, ellipsoids of revolution, and tri-axial ellipsoids. Finally, the scope of the method is illustrated by presenting calculated velocity or pressure distributions for a variety of bodies including wing-fuselage combinations, ducts, a body in a wind tunnel, two bodies side by side, and ship hulls.

2.0 TABLE OF CONTENTS

4

3.0 INDEX OF FIGURES

4.0 DEFINITION OF SYMBOLS

A area of a plane quadrilateral surface element

A_{ij} component of velocity normal to the body surface induced at the null point of the i-th element (i-th basic element in cases of symmetry) by a unit source-density on the j-th element (j-th basic and reflected elements in cases of symmetry)

$\begin{matrix} a_{11} & a_{12} & a_{13} \\ a_{21} & a_{22} & a_{23} \\ a_{31} & a_{32} & a_{33} \end{matrix}$ elements of the transformation matrix used to transform the coordinates of points and the components of vectors between the reference coordinate system and the element coordinate system

b base of an isosceles triangle (figure 23)

b_{12} quantity defined by eq.(33)

C_{p_i} pressure coefficient at the null point of the i-th element, $C_{p_i} = 1 - V_i^2$

$\begin{matrix} D_{12} & D_{23} \\ D_{34} & D_{41} \end{matrix}$ quantities defined by eq.(93)

d magnitude of the common projection distance of the four input points used to form an element into the plane of the element

d_k k = 1, 2, 3, 4. Signed projection distance of the four input points used to form an element into the plane of the element

$\begin{matrix} d_{12} & d_{23} \\ d_{34} & d_{41} \end{matrix}$ length of the four sides of a quadrilateral element (eq. (45), d_{12} also given by eq.(27)

e_k k = 1, 2, 3, 4. Quantities defined by eq.(48), e_1 and e_2 also given by equation (40)

F function defining the body surface

f perpendicular distance of a field point from the extension of a side of a quadrilateral (figure 8)

h altitude of an isosceles triangle (figure 23)

h_k k = 1, 2, 3, 4. Quantities defined by eq.(49), h_1 and h_2 also given by equation (41)

$I_{xx} \quad I_{xy} \quad I_{yy}$ second moments or moments of inertia of the area of a quadrilateral element about the origin of its element coordinate system

M_n number of input points on the n-th input ''column'' or n-line

8

Symbol	Definition
ΔM_n	$M_{n+1} - M_n$
$M_x \quad M_y$	first moments of the area of a quadrilateral element about the origin of its element coordinate system
m	integer denoting the position of an input point on an input "column" or r-line or an element formed from this point
$m_{12} \quad m_{23}$ $m_{34} \quad m_{41}$	slopes of the sides of a quadrilateral in its own plane (eq.(46), m_{12} also given by (32))
N	the number of quadrilateral elements formed from input points (basic elements in cases of symmetry). Also used in eqs.(66) and (67) to denote the length of the normal vector to an element
N_i	normal velocity induced at the null point of the i-th element by all quadrilateral elements together (eq.(124))
N_T	number of "columns" or n-lines of input points in a section
$N_x \quad N_y \quad N_z$	components of the vector normal to an element in the reference coordinate system
$\vec{N}$	vector normal to an element
n	integer denoting the "column" or n-line to which an input point belongs or an element formed from this point. Also used in Section 6.0 to denote distance normal to the body surface
$n_x \quad n_y \quad n_z$	components of the unit normal vector to an element in the reference coordinate system
$n_{ix} \quad n_{iy} \quad n_{iz}$	components of the unit normal vector to the i-th element (i-th basic element in cases of symmetry) in the reference coordinate system
$\vec{n}$	unit normal vector to an element
$\vec{n}_i$	unit normal vector to the i-th element (i-th basic element in cases of symmetry)
P	general field point where the potential and velocity components are evaluated
p	field point on the body surface where the potential and velocity components are evaluated. Also a quantity defined by eq.(62)
q	source point or integration point on the body surface. Also a quantity defined by eq.(62)
q_{12}	a quantity defined by eq.(34)

R'	the region exterior to the body surface
r	distance from a field point where the potential and velocity components are evaluated to a source point or integration point
r_k	k = 1, 2, 3, 4. Distances from a field point where the potential and velocity components are evaluated to the four corner points of a quadrilateral element (eq.(47), r_1 and r_2 also given by eq.(27) and figure 8)
r_o	distance from a field point, where the potential and velocity components are evaluated, to the origin of the coordinate system of an element
S	surface of the body about which the flow is computed
s	arc length along a side of a quadrilateral. Also used in figure 44 to denote arc length along the centerline of a duct
s_1 s_2	projection of r_1 and r_2 along the extension of a side of a quadrilateral (figure 8)
T_1	length of vector $\vec{T}_1$ (equation (74))
T_{1x} T_{1y} T_{1z}	components of vector $\vec{T}_1$ in the reference coordinate system
T_{2x} T_{2y} T_{2z}	components of vector $\vec{T}_2$ in the reference coordinate system
$\vec{T}_1$ $\vec{T}_2$	diagonal vectors of a quadrilateral element (equation (64))
t	maximum diagonal of an element. The larger of t_1 and t_2.
t_1 t_2	lengths of the diagonals of a quadrilateral element (eq.(84))
t_{1x} t_{1y} t_{1z}	components of the vector $\vec{t}_1$ in the reference coordinate system
t_{2x} t_{2y} t_{2z}	components of the vector $\vec{t}_2$ in the reference coordinate system
$\vec{t}_1$ $\vec{t}_2$	unit vectors in the plane of an element. These vectors are, respectively, along the x or ξ and y or η axes of the element coordinate system
u	the quantity $x - \xi$
V	magnitude of total flow velocity
V_i	magnitude of total flow velocity at the null point of the i-th element

$V_x \quad V_y \quad V_z$	velocity components in an element coordinate system; in particular, the velocity components induced by that element at a field point
$V'_x \quad V'_y \quad V'_z$	velocity components in the reference coordinate system
V_o	velocity magnitude in a constant diameter region of a duct where the velocity varies only slightly with position
V_∞	magnitude of the velocity of a uniform onset flow. Usually taken as unity
$V_{ix} \quad V_{iy} \quad V_{iz}$	components in the reference coordinate system of the total flow velocity at the null point of the i-th element
V_{n_i}	total normal velocity at the null point of the i-th element
$V_{x_{12}} \quad V_{y_{12}} \quad V_{z_{12}}$	components in the element coordinate system of the velocity at a field point due to the fundamental potential function of the side of a quadrilateral between corner point 1 and corner point 2
$V_{\infty x} V_{\infty y} V_{\infty z}$	components of a uniform onset flow in the reference coordinate system
$V_{\infty n_i}$	normal component of a uniform onset flow at the null point of the i-th element
$\vec{V}_i$	total flow velocity vector at the null point of the i-th element
$\vec{V}_\infty$	onset flow vector
$\vec{V}_{ij}$	vector velocity induced at the null point of the i-th element (i-th basic element in cases of symmetry) by a unit source density on the j-th element (j-th basic and reflected elements in cases of symmetry)
w	$1/r_o$; when subscripted with x, y, and z, this denotes the partial derivatives of w in the directions of the axes of the element coordinate system
$X_{ij} \quad Y_{ij} \quad Z_{ij}$	components of $\vec{V}_{ij}$ in the reference coordinate system
$x \quad y \quad z$	Cartesian coordinates of a point in space. In sections of the report where the coordinates of points are required in both the reference and element coordinate system, these variables are used for the coordinates in the element coordinate system, while primed coordinates are used for coordinates in the reference coordinate system. In sections where only one coordinate system is considered, either the reference or element coordinate system, these variables are used.

x' y' z'	Cartesian coordinates of a point in space. These variables are used for the coordinates of points in the reference coordinate system in sections of the report where the coordinates of points are required in both the reference and element coordinate system
x_p y_p	p-th approximation to the coordinates of the null point in the element coordinate system
x_o y_o z_o	coordinates of the origin of the element coordinate system in the reference coordinate system. Also used for the coordinates of the centroid of a quadrilateral in the reference coordinate system, since this point is used as the origin of the element coordinate system as soon as it is computed.
$\bar{x}$ $\bar{y}$ $\bar{z}$	coordinates of the average point in the reference coordinate system (eq.68))
x_k' y_k' z_k'	k = 1, 2, 3, 4. Coordinates of the four corner points of a quadrilateral element in the reference coordinate system
x_{np} y_{np}	coordinates of the null point of an element in the coordinate system of that element
x_{np}' y_{np}' z_{np}'	coordinates of the null point of an element in the reference coordinate system
x_k^i y_k^i z_k^i	k = 1, 2, 3, 4. Coordinates in the reference coordinate system of the four input points used to form a quadrilateral surface element
y_M	maximum distance of points on a ship hull from the midplane or ''keel plane'' of the ship. Equals half the beam of the ship.
z_M	maximum depth below the free surface of points on a ship hull. Equals the draft of the ship.
β_1 β_2	angles defined in figure 8.
$\gamma_{ix}\gamma_{iy}\gamma_{iz}$	direction cosines with respect to the axes of the reference coordinate system of the total flow velocity vector at the null point of the i-th element
Δ	Laplacian operator (except ΔM_n defined above)
η_{12}	η coordinate of a general point on the side of a quadrilateral between corner point 1 and corner point 2
Θ	angular variable used in several figures and defined pictorially on each one

$\xi \; \eta \; \zeta$	Cartesian coordinates of a point in an element coordinate system, especially a source point or integration point on a quadrilateral element
$\xi_k \; \eta_k$	$k = 1, 2, 3, 4$. Coordinates of the four corner points of a quadrilateral in its element coordinate system, in particular when that coordinate system has the centroid of the quadrilateral as the origin
$\xi_0 \; \eta_0$	coordinates of the centroid of a quadrilateral in its element coordinate system based on the average point as origin
$\xi_k^* \; \eta_k^*$	$k = 1, 2, 3, 4$. Coordinates of the four corner points of a quadrilateral in its element coordinate system based on the average point as origin
ρ_i	ratio of the values of $\delta \sigma_i$ obtained in two successive iterations during the solution of the linear equations for the values of the surface source density (eqs. (131) and (132)
σ	surface source density
$\sigma_i \; \sigma_j$	values of the surface source density on the i-th and j-th elements, respectively, (i-th and j-th basic elements in cases of symmetry)
$\delta \sigma_i$	change in the value of σ_i produced by one iteration in the solution of the linear equations for the surface source density (equation (128))
Φ	total potential of the flow
φ	disturbance potential due to the body. Also used as an angular variable in certain figures and defined pictorially on each one.
φ_∞	potential of a uniform onset flow
ψ	angular variable used in several figures and defined pictorially on each one

Subscripts

i	denotes quantities associated with the i-th element (i-th basic element in cases of symmetry), in particular velocity components evaluated at the null point of that element
j	denotes quantities associated with the j-th element (j-th basic and reflected elements in cases of symmetry)

k	integer subscript taking on the values 1, 2, 3, 4. It denotes quantities associated with the four corner points of a quadrilateral element, in particular their coordinates
ν	identifying subscript used to designate an off-body point and quantities associated with it, in particular velocity components evaluated there
x y z	when used with a vector quantity, these subscripts denote the components of that vector along the coordinate axes. When used with a scalar quantity, these subscripts denote the partial derivatives of that quantity with respect to that coordinate, except that when used with the moments of the area of a quadrilateral, M_x, I_{xx}, etc., these subscripts denote the coordinate axes about which the moments are taken.

Superscripts

p	denotes the value of a quantity after p applications of an iterative procedure, in particular the values of the surface source density σ, after p iterations of the Seidel procedure for the solution of the linear equations
r	denotes velocity components induced by a reflected element in cases of one plane of symmetry
1r 2r 3r	denote velocity components induced by first, second, and third reflected elements, respectively, in cases of two planes of symmetry. The superscripts $4r$, $5r$, $6r$, and $7r$ are used in cases of three planes of symmetry to denote velocity components induced by the fourth, fifth, sixth, and seventh reflected elements, respectively.
s	integer superscript having the values 1, 2, and 3, and denoting the onset flow. Normally, calculations are performed for three onset flows simultaneously, and this superscript is used to denote the components of a particular onset flow and all quantities, velocities, source densities, etc., associated with that onset flow. In the text, this superscript is used both as a general value, e.g., $A_{ij}^{(s)}$, and as a specific value, e.g., $A_{ij}^{(2)}$.
∞	denotes values of the source density after infinitely many iterations of the Seidel procedure for the solution of the linear equations

14

5.0 INTRODUCTION

This report describes a method of calculating, by means of an electronic computer, the non-lifting potential flow about arbitrary three-dimensional bodies. This work is an extension of that described in references 1 and 2, whose formulas permit the calculation of potential flow about arbitrary two-dimensional and axi-symmetric bodies. This method utilizes a distribution of source density on the surface of the body and solves for the distribution necessary to meet the specific boundary conditions. Once the source density distribution is known, the flow velocities both on and off the body surface may be calculated. The basic equation defining the source density distribution is a two-dimensional Fredholm integral equation of the second kind over the body surface.

The method of this report has two advantages over network methods. First, the equation that must be solved is a two-dimensional one over the body surface rather than a three-dimensional one over the entire exterior flow field. (In two-dimensional and axi-symmetric cases the reduction in dimensionality is from two to one.) Secondly, any body may be conveniently calculated without the difficulty network methods may encounter when the body surface intersects the coordinate net in an arbitrary manner. The advantage of this method over methods that utilize a distribution of singularities inside the body surface, e.g., in a plane, is that this method can calculate flows about arbitrary bodies. There is no restriction that the body be slender, analytic, or simply connected or that the disturbance velocities due to the body be small compared with the velocity of the onset flow. There is one further advantage. Although at present the method will handle only the case when the body is immersed in a uniform stream, a relatively minor modification will allow the case when the body is in an arbitrary, non-uniform, potential onset flow to be calculated. Cases for which the onset flow cannot be described by a potential function can also be calculated, but the significance of the results is not clear.

Section 6.0 formulates the mathematical problem and states the basic idea behind this method of solution. Section 7.0 is a general outline of the particular way in which the solution is carried out. Some alternative

15

possibilities are also discussed in this section. The formulas for the velocities induced by a plane quadrilateral source element that form the basis of this method are derived in Section 8.0. Section 9.0 gives a detailed description of the method of computation together with all the relevant equations. The accuracy of the method is exhibited in Section 10.0, where the calculations are compared with analytic solutions, while Section 11.0 shows examples of the flows calculated for a variety of bodies that were selected to show the versatility of the method. The derivations and results of Section 8.0 and the complete listing of equations given in Section 9.0 will probably not be of interest to most readers. Accordingly, these sections my be omitted without loss of continuity. Section 8.0 and the lengthier parts of Section 9.0, specifically 9.2, 9.3, 9.5, and 9.6, need not be read even by someone who intends to use the method. The remainder of Section 9.0, namely 9.1, 9.4, 9.7, 9.8, and 9.9, explains the input and output of the program and lists computation times and size limits for the cases.

The set of machine programs that perform the computations of this method has been designated the V150 series of programs for three-dimensional potential flow.

6.0 MATHEMATICAL STATEMENT OF THE PROBLEM

The problem considered here is that of the steady flow of a perfect fluid about a three-dimensional body. Let the surface of the body be denoted S, and let S have an equation of the form

$$F(x\ ,\ y\ ,\ z\ ) = 0 \tag{1}$$

where x , y , z are Cartesian coordinates as shown in figure 1. The onset
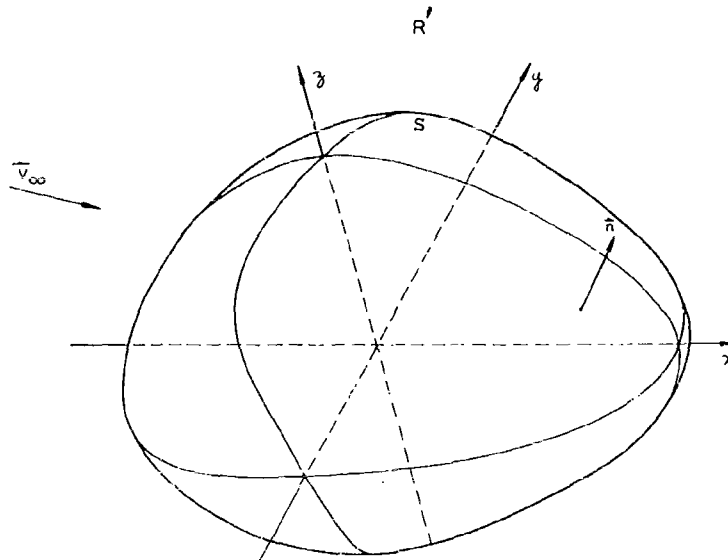
Figure 1. - The body surface.

flow is taken as a uniform stream of unit magnitude. Thus this flow may be represented by the constant vector $\vec{V}_\infty$ with components $V_{\infty x}$, $V_{\infty y}$, $V_{\infty z}$, respectively, along the coordinate axes x , y , z , where

$$V_\infty = \sqrt{V_{\infty x}^2 + V_{\infty y}^2 + V_{\infty z}^2} = 1 \tag{2}$$

The restriction to a uniform onset flow is not essential, but is made for definiteness and simplicity. Non-uniform onset flows may be considered with a minor increase in complexity.

The fluid velocity at a point may be expressed as the negative gradient of a potential function $\bar{\Phi}$. The function $\bar{\Phi}$ satisfies Laplace's equation in the region R' exterior to S, has a zero normal derivative on S, and approaches the proper uniform stream potential at infinity. Symbolically,

$$\Delta \bar{\Phi} = 0 \qquad \text{in} \quad R' \tag{3}$$

$$\left.\frac{\partial \bar{\Phi}}{\partial n}\right|_S = \bar{n} \cdot \left.\text{grad } \bar{\Phi}\right|_{F = 0} = 0 \tag{4}$$

$$\bar{\Phi} \to - (V_{\infty x}x + V_{\infty y}y + V_{\infty z}z) \quad \text{for} \quad x^2 + y^2 + z^2 \to \infty \tag{5}$$

Here Δ denotes the Laplacian operator and $\bar{n}$ is the unit outward normal vector at a point of the surface S, i.e.,

$$\bar{n} = \pm \left[\frac{\text{grad } F}{|\text{grad } F|}\right]_{F = 0} \tag{6}$$

where the sign in (6) is chosen to make $\bar{n}$ an outward normal vector. It is convenient to write $\bar{\Phi}$ as

$$\bar{\Phi} = \varphi_\infty + \varphi \tag{7}$$

where

$$\varphi_\infty = - (V_{\infty x}x + V_{\infty y}y + V_{\infty z}z) \tag{8}$$

is the uniform stream potential, and φ is the disturbance potential due to the body. Then φ satisfies

$$\Delta \varphi = 0 \qquad \text{in} \quad R' \tag{9}$$

$$\left.\frac{\partial \varphi}{\partial n}\right|_S = \bar{n} \cdot \left.\text{grad } \varphi\right|_{F = 0} = + \bar{n} \cdot \left.\bar{V}_\infty\right|_{F = 0} \tag{10}$$

$$\varphi \to 0 \qquad \text{for} \qquad x^2 + y^2 + z^2 \to \infty \tag{11}$$

It is shown in reference 3 that the body surface may be imagined to be covered with a surface source density distribution σ and that the potential φ may then be written

$$\varphi(x \ , \ y \ , \ z \ ) = \oiint_S \frac{\sigma(q)}{r(P, \ q)} \, dS \tag{12}$$

where $r(P, q)$ is the distance from the integration point q on the surface to the field point P with coordinates x , y , z where the potential is being evaluated (see figure 2).
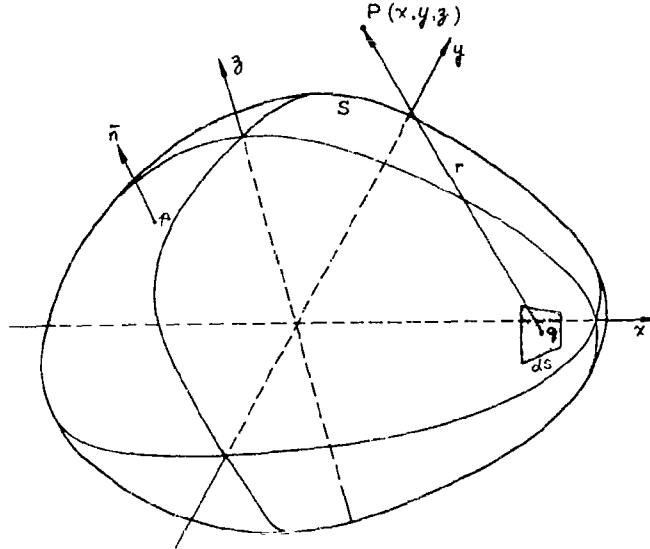
Figure 2. - Notation used in describing the potential due to a surface source density distribution.

The form of φ shown in equation (12) automatically satisfies equations (9) and (11) for any function σ. The function σ must be determined so that φ satisfies the normal derivative condition, equation (10). Applying equation (10) requires the evaluation of the normal derivative of the integral in equation (12) at a point p on the surface S. It is shown in reference 3 that as the surface S is approached, the derivative of this integral becomes singular and its principal part must be extracted. Physically, this corresponds to the contribution of the local source density to the local normal velocity. The contribution of the remainder of the surface to the local normal velocity is given by the derivative of an integral of the form given in equation (12) evaluated on the boundary, i.e., $P = p$, and this integral is now taken to mean the finite part. From reference 3 the principal value is $-2\pi\sigma(p)$, so on the body surface the normal derivative of φ is

19

$$\left.\frac{\partial \varphi}{\partial n}\right|_S = -2\pi\,\sigma(p) + \oiint_S \frac{\partial}{\partial n}\left(\frac{1}{r(p,\,q)}\right)\sigma(q)dS \qquad (13)$$

Inserting this into equation (10) gives the integral equation for σ as

$$2\pi\,\sigma(p) - \oiint_S \frac{\partial}{\partial n}\left(\frac{1}{r(p,\,q)}\right)\sigma(q)dS = -\,\hat{n}(p)\cdot\vec{V}_\infty \qquad (14)$$

where the unit normal vector has been written $\hat{n}(p)$ to explicitly show its dependence on location. This is seen to be a two-dimensional Fredholm integral equation of the second kind over the surface S. Once this equation is solved for σ, the disturbance potential φ may be evaluated from equation (12) and the disturbance flow velocities from the derivatives of equation (12) in the coordinate directions.

This method of solution is valid for completely arbitrary bodies. The surface S is not required to be slender, analytic, or simply connected. It is required, however, that the body surface have a continuous normal vector $\hat{n}$. Otherwise the integrand in equation (14) is singular and the right hand side is discontinuous. Thus this method cannot be guaranteed to give correct results for bodies having discontinuities in slope, i.e., corners. This restriction is not of great practical significance, since the corner can be replaced by a small region of large but finite curvature without significantly affecting the flow at other points. Even this, however, is often unnecessary. Experience in applying this method to two-dimensional flows, where analytic solutions for certain bodies with corners are available, has shown that the method gives correct results for cases of true corners if these corners are convex. For concave corners the method fails, and the corner must be rounded in a small region to obtain correct results at other points. These facts often indicate the proper procedure in three-dimensional cases. It appears that the flow around convex corners is calculated correctly, while unrounded concave corners may or may not cause an appreciable error.

The case when the onset flow is not a uniform stream, i.e., when $\vec{V}_\infty$ is not independent of position, is handled in exactly the same way as the uniform stream case. It is simply a matter of defining φ_∞ so that the variable $\vec{V}_\infty$ is its gradient and of using the variable $\vec{V}_\infty$ on the right hand side of equation (14).

7.0 GENERAL DESCRIPTION OF THE METHOD OF SOLUTION

7.1 The Approximation of the Body Surface

There are several possible schemes for the numerical solution of equation (14). In all of them a basic question is how to approximate the body surface. If it were desired to represent this surface exactly by means of analytic expressions, the type of bodies that could be handled would have to be restricted. Since the basic method has no such restriction, it seems undesirable to impose one merely to represent the surface. Moreover, to include all bodies of interest in applications, e.g., wing-fuselages, inlets, ducts, etc., the defining analytic expressions would have to be extremely elaborate. Also, the equation for the source density will have to be solved approximately even if the body is represented exactly.

To allow arbitrary bodies to be considered, it is natural to require the body surface to be specified by a set of points in space. These points are presumably exactly on the body surface and are utilized by the method to obtain an approximation to this surface, which is then used in subsequent calculations. There are two basically different types of approximation. The first uses a single analytic expression or a few such expressions to approximate the surface as a whole. The other uses a large number of analytic expressions, each of which approximates the surface in a small region. While the first of these is more satisfying in many ways, it possesses the undesirable feature described above for exact representations, namely that very elaborate expressions are required.

After the method of approximating the body surface has been decided upon, there are several possible approaches to the numerical solution of equation (14). The equation may be attacked directly as an integral equation using an iterative procedure for the solution of Fredholm integral equations. In this process the integral in (14) is evaluated by numerical means. Alternatively, equation (14) may be replaced by a set of linear algebraic equations. There are various ways of accomplishing this, all of which are equivalent to evaluating the integral in (14) by some quadrature formula in terms of certain unknown values of the source density. These last may be the actual values of

the source density at selected points of the body surface or they may represent
mean values of the source density in some sense over certain regions of the
surface. In any case requiring (14) to hold at a certain number of points
of the surface gives a set of linear equations for the unknown values of the
source density.

The scheme adopted here is as follows. The body surface is approximated
by a large number of small plane elements, which are formed from the original
points defining the body surface. (Figure 3 shows an example of a body surface
that is approximated by plane quadrilateral elements. Although the discussion
of this section is applicable to any kind of plane elements, quadrilaterals
were eventually chosen for this method. This choice is discussed in a sub-
sequent section.) The source density is assumed constant over each of these
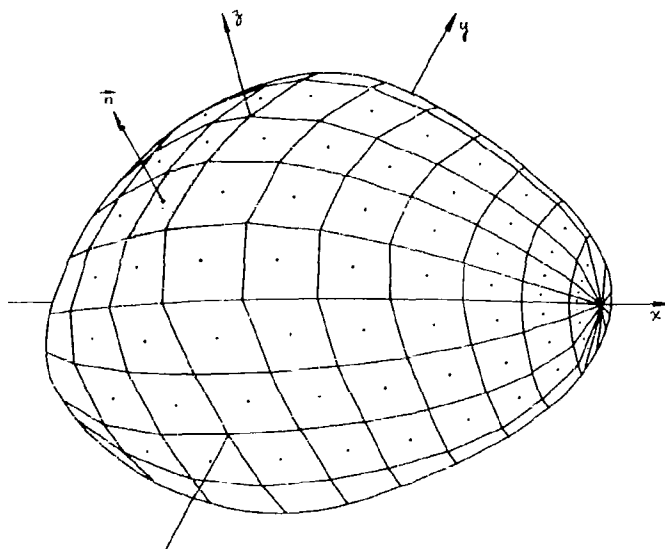
Figure 3. - The approximate representation of the body surface.

elements. This assumption reduces the problem of determining the continuous
function σ to the problem of determining a finite number of values of σ —
one for each of the planar elements. The contribution of each element to the
integral in (14) is obtained by taking the constant but unknown value of σ
on that element out of the integral and then performing the indicated integra-
tion of known geometrical quantities over that element. Thus, requiring
equation (14) to hold at one point p gives a linear relation between the
unknown values of σ on the plane elements. On each element one point is

22

selected where equation (14) is required to hold. This gives a number of linear equations equal to the number of unknown values of σ. Once these are solved, flow velocities may be evaluated at any point by summing the contributions of the plane elements and adding proper components of the onset flow. Flow velocities may be computed at points either on or off the body. If velocities are evaluated on the body, they must be evaluated at the same points where (14) is required to hold, i.e., at the points where the normal velocity is made to vanish. Velocities at other points of the body surface must be obtained through interpolation of these values rather than by direct calculation. This restriction is imposed by the form of the approximation of the body surface. For example, direct calculation by summing the contributions of the plane elements gives an infinite velocity at a point on an edge of one of the elements.

There were three reasons why this relatively crude approach to the solution of equation (14) was adopted. First, it is simpler than any other method that is versatile enough to handle all the body shapes of interest in applications. It seemed logical to first attempt a solution by the simplest means to determine whether or not a more elaborate method is necessary. The chief disadvantage of a simple procedure is that large computation times may be required for high accuracy. The computation times required for this method are indeed large, as is described in a later section, but probably acceptable for most applications. A second reason is that the physical significance of this approximation is evident. This is true both with regard to the degree of approximation to the true body surface afforded by the plane elements and with regard to certain intermediate mathematical results, e.g., the velocities induced by the source elements at points in space. Not only was this fact extremely useful in checking out the method and eliminating errors, but it is of continuing value to users of the method, because it makes clear to a certain extent how the original points defining the body surface should be distributed for best results. The third and most important reason for the selection of this method is that it is the three-dimensional analogue of the method that gave very satisfactory results for two-dimensional and axisymmetric bodies (References 1 and 2).

23

7.2 The Computational Method

7.21 Description of the Method.

This section describes briefly the manner in which this method of solution is carried out on the computing machine.

The body surface is defined by a set of points in three-dimensional space. These will be called the input points. The coordinate system in which these points are given is designated the reference coordinate system. These points should be distributed in such a way that the best representation of the body is obtained with the fewest possible points. In particular, points should be concentrated in regions where the curvature of the body surface is large and in regions where the flow velocity is expected to change rapidly, while points may be distributed sparsely in regions where neither the body geometry nor the flow properties are varying significantly. If the body possesses symmetry planes, only the non-redundant portion of its surface need be specified by input points. The other portions are automatically taken into account by suitably reflecting this portion in the symmetry planes. The symmetry planes are assumed to be coordinate planes of the reference coordinate system.

The body surface is approximated by a set of plane quadrilateral source elements, each of which is formed from four input points. To avoid having to actually input four points for each element, the input points are organized in a certain way, so that they may be associated in groups of four to form elements with each input point being used in the formation of up to four elements. In order to accomplish this, each point is considered to be identified by a pair of integers, one specifying the ''row'' of points to which it belongs and the other specifying the ''column''. The choice of what constitutes a ''row'' or ''column'' is very free. The only restriction is that if all points of each ''column'' are connected by a curve lying in the body surface, no two such curves cross each other, and similarly for ''rows''. It can be seen that these curves connecting all points on the same ''row'' or ''column'' are essentially coordinate curves of a two-dimensional coordinate system lying in the body surface, (see figure 4). The points are input ''column'' by ''column''. The order of a point in a ''column'' determines its ''row'', and

24

the number of points on a "column" may vary. Provision has also been made
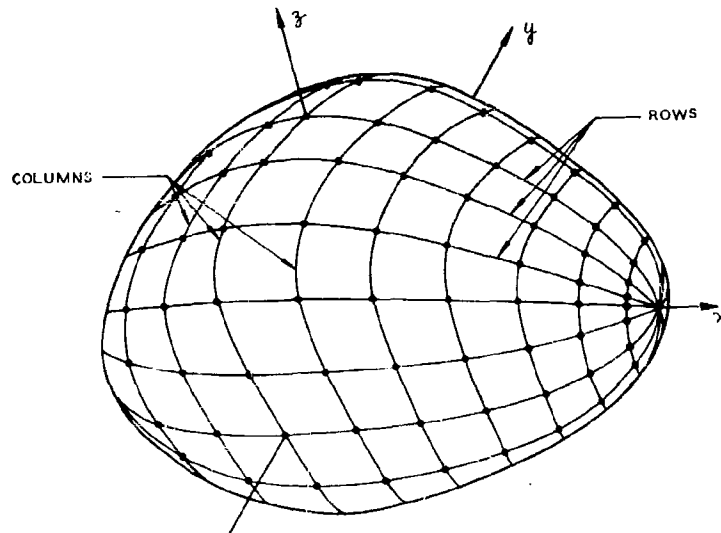
Figure 4. - Organization of input points into "rows" and "columns".

for dividing the body into a certain number of distinct sections, each of which consists of a certain number of ''columns''. This is a natural procedure for many types of bodies, e.g., a wing-fuselage, and permits a great deal of flexibility. For example, it allows points to be concentrated in certain regions very easily. The four points used to form a particular surface element are the two points in one ''column'' in consecutive ''rows'' and the two points in the adjacent ''column'' that are in the same two ''rows''. In general these four points do not lie in a plane.

The plane quadrilateral surface elements (figure 3) are formed from the four appropriate input points as follows. First two vectors are calculated. These are the two ''diagonal'' vectors, each of which is the difference of the position vectors of two points that are neither in the same ''row'' nor in the same ''column''. The cross product of these vectors divided by its own length is taken as the unit normal vector to the plane of the element. The cross product is performed in such a way that it produces an outward normal to the body surface. To completely specify the plane of the element a point in the plane is also required. This point is taken as the point whose coordinates are the averages of the coordinates of the four input points, and it is designated the average point. Four points in the plane are obtained by pro-

25

jecting the input points into the plane along the normal vector. Because of the way in which the plane is defined, all four input points are equidistant from it — the two used to form one ''diagonal'' vector on one side and the other two on the other side. The four points in the plane are the corners of the plane quadrilateral source element, and they are designated corner points. It is these points that are used in all calculations once the complete set of surface elements has been formed, rather than the input points.

It is convenient to derive and to use the formulas for the velocities induced by a quadrilateral source element of uniform strength at points in space assuming the element to lie in a coordinate plane. This necessitates constructing a coordinate system having two of its axes in the plane of the element. Thus three mutually perpendicular unit vectors are required, two of which are in the plane of the element and one of which is normal to it. The unit normal vector has already been found. One of the ''diagonal'' vectors divided by its own length serves as one unit vector in the plane of the element, and the cross product of the unit normal with this vector is the other. This establishes the desired coordinate system, which is designated the element coordinate system. The origin of this system is temporarily taken as the average point. The nine components of the above three unit vectors comprise the elements of the transformation matrix which is used to transform points or vectors between the reference coordinate system and the element coordinate system. In particular, the corner points are transformed immediately into the element coordinate system so that certain geometric properties of the quadrilateral may be computed more easily.

In computing the velocities induced by a plane quadrilateral source element at points in space, it turned out to be very time consuming to use the exact velocity formulas at all points. For this reason, approximate formulas derived from a multipole expansion are employed for points that are sufficiently far from the element for the approximation to be acceptably precise. These approximate formulas require the area of the quadrilateral, the coordinates of the centroid of the area, the second moments of the area, and the length of the maximum diagonal of the quadrilateral. Once computed the centroid replaces the average point as the origin of the element coordinate system.

26

Next it is necessary to select a particular point on each quadrilateral element where the normal velocity will be required to vanish and where the flow velocities will be computed. This point is taken as the point where the quadrilateral induces no velocity in its own plane. It is designated the null point.

At this stage certain of the quantities described above are output from the machine and the calculation terminated. The purpose is to provide a means of finding and eliminating errors in the input data before the lengthy flow calculations are performed. Such errors arise fairly often because of the large amount of input that is required. An examination of the variation of the above geometrical quantities from element to element will often reveal these errors.

Now the velocities induced by the quadrilateral source elements at each other's null points must be computed. This is done under the assumption that the source density on each element is of unit strength. In computing the velocity components induced at a particular null point by a particular element one of three sets of formulas are used depending on the distance between the null point and the centroid of the element. If the ratio of this distance to the maximum diagonal of the element is less than a certain prescribed value, the exact velocity formulas are used. If the ratio is larger than this value, the velocity is calculated by formulas appropriate for either a point source plus a point quadrupole or a point source alone. (The dipole moment is zero since the multipole expansion is based on the centroid.) The choice between these last two possibilities is made by comparing the above ratio to a second prescribed value. The final result of this calculation is the complete set of the velocities induced at each null point by every quadrilateral element, all of which are assumed to have a unit source density. This array may be thought of as a ''matrix of influence coefficients'', the elements of which are vectors in three-dimensional space. A row of this matrix consists of the velocities induced at a single null point by every quadrilateral element, while a column consists of the velocities induced by a single element at every null point. To minimize computing time the various quantities associated with each element that are required to compute the induced velocities are stored simultaneously in the high speed memory of the computing machine and the ''matrix

of influence coefficients'' is calculated row by row. Twenty-eight quantities for each element are required. The result is that the maximum number of elements that may be used to define the body surface is limited by the high speed storage capacity of the machine, which is taxed at this stage of the procedure.

The above paragraph applies to non-symmetric bodies. For bodies having one or more symmetry planes, the procedure is identical to the above except that after the velocity components induced by an element at a particular null point have been calculated, the velocity components induced at the same null point by the image or images of the element are also computed by the same method. Thus, while in the non-symmetric case there is a single set of induced velocity components representing the effect of an element at a null point, there are, respectively, two, four, or eight sets of induced velocity components in cases of one, two, or three planes of symmetry. These are combined in the ways appropriate for use with onset flows in the three coordinate directions. The result is two ''matrices of influence coefficients'' in cases with one symmetry plane and three such matrices in cases with two or three symmetry planes.

To obtain a set of linear algebraic equations for the unknown values of the source density on the elements, the first step is to calculate the normal velocities induced at each null point by the various elements, each of which is still assumed to have a unit source density. This is done by taking the dot product of the induced velocities described above with the normal vectors of the elements at whose null points these velocities were evaluated. The result is a scalar matrix whose elements are the normal velocities induced at the various null points by the various quadrilateral elements with unit source density. This matrix is the coefficient matrix of the required set of linear equations, since multiplying this by the column matrix of the unknown values of the source density on each element evidently gives a column matrix whose elements are the true normal velocities induced at the null points by the entire approximate body surface. A coefficient matrix is formed from each of the ''matrices of influence coefficients'' described above, so there are two such matrices for cases of one plane of symmetry and three such matrices in cases of two or three planes of symmetry. The right hand sides of the linear equations are the negatives of the normal components of the onset flow at the

28

various null points. The method has been constructed so that it will handle three onset flows at one time. Normally, these are unit uniform streams, each one of which is along one of the axes of the reference coordinate system, although they may be any three onset flows for non-symmetric bodies. Each onset flow is used to form a right hand side for use with the appropriate coefficient matrix. In non-symmetric cases the same matrix is used for all onset flows, while in cases of one plane of symmetry one matrix is used for two onset flows (the two in the symmetry plane) and the other matrix is used for the third onset flow. In cases of two or three planes of symmetry a distinct coefficient matrix is used for each onset flow. In any case, three sets of simultaneous linear equations are solved for three complete sets of values of the surface source density. The solutions are effected by a Seidel iterative procedure.

Once the values of the surface source density have been found, the velocity components at each null point are calculated by multiplying the above described induced velocity components (which were calculated assuming a unit source density) by the proper calculated values of the source density and summing all such products that are appropriate for the null point in question. (This summation is thus over all elements of a row of the ''matrix of influence coefficients''.) To the results of this summation must be added the proper components of the onset flow. The resultant velocities and pressures are easily computed from the velocity components. The above quantities and certain others of interest are the final result of the method and comprise the second output of the machine program. There is a complete set of results for each of the three onset flows. If the flow at points off the body surface is desired, these points must be specified, and then velocities and pressures are computed there also. Again there are three sets of results. If results for flow inclinations other than the basic three along the coordinate axes are desired, they can be obtained by a simple combination of these results.

7.22 Discussion of Some Possible Alternatives.

The basic decision underlying this method of solution is described above in Section 7.1 together with some alternative approaches. In implementing this method and constructing a practical calculational procedure, several decisions were made that are not basic to the method. In this section the reasons for

some of these choices are given and alternatives discussed.

It was decided to take the plane source elements that approximate the body surface as quadrilaterals rather than some other plane figures and to organize these elements by the use of a coordinate system in the body surface, i.e., the ''rows'' and ''columns'' described above, despite certain undesirable features of this approach. An objection to the use of quadrilaterals is that adjacent elements do not in general have coincident edges. This is, however, an extremely small effect for normal body shapes. For example, quadrilateral elements can be distributed so that their edges are coincident on any axisymmetric body. The errors from this source are apparently small compared to the errors that result from the basic approximation of the body by plane elements. The organization of the quadrilateral elements by means of a coordinate system in the body surface has the undesirable feature that normally such a coordinate system has a concentration point where one set of coordinate lines comes together. (See figure 4) When this occurs it causes several difficulties related to the element distribution in the neighborhood and in the determination of null points. Moreover, the results of the calculations are generally less accurate near such a point. In practice, concentration points can be avoided for many common types of bodies, e.g., ship hulls, wings, ducts, and inlets. However, the use of ''rows'' and ''columns'' so greatly simplifies the input that their use is judged to be justified in any case. In fact, one of the reasons for choosing quadrilateral elements was that they are most compatible with this organization scheme. This scheme simplifies the input in two ways. First, it permits a given input point to be used in the construction of several elements. Thus in normal cases the required number of input points is only slightly larger than the number of elements. This contrasts with a method where all corner points for each element are input for which the required number of input points is four times the number of elements in the case of quadrilaterals. Reduction of the required input as far as possible is important not only because the possibilities of error are reduced but also because a large amount of required input leads to a reluctance to use the method. Secondly, the organization scheme is easy to visualize and simplifies the input conceptually. It attains its greatest advantage over competing schemes in the frequently occurring case when it is natural to have every point on a ''column'' at the same value of one of the

30

coordinates, e.g., providing input at constant ''chordwise'' or ''spanwise'' stations. This property is not a trivial consideration. It has been found in practice that conceptual difficulties can greatly increase the difficulty of intelligently distributing the input points. Similarly, interpretation of the output is simplified by making the order of points on the output sheet (which is the same order as the order of the input) correspond to physical points in a natural sequence. Triangular elements, whose use is suggested in reference 4, were the only others seriously considered. They have the advantages that the edges of adjacent elements are coincident and that concentration points might be avoided, but there is no apparent way of organizing them to simultaneously obtain a minimum of required input points plus conceptual simplicity. It would be possible to obtain triangular elements from the present organization scheme by dividing the four points associated to form an element into two groups of three, i.e., a sort of ''cutting each quadrilateral in half'' before the input points are projected into a common plane. However, this scheme eliminates many of the advantages of the triangular representation, and introduces certain calculation errors due to the fact that all elements are not constructed in a completely equivalent manner. Triangular elements also have the disadvantage compared to quadrilaterals that the choice of the point on the element where velocities are to be calculated is more critical (see below).

The location of the point on the quadrilateral element where velocities are to be evaluated is a matter of some importance in that it may have an appreciable effect on the accuracy of the calculation. Unfortunately, there is no obvious choice for this point, and indeed there is no way to decide that a particular choice is better than even one other, much less all others. It seems evident that on a rectangular element the proper point is the center. Therefore, the point selected must be defined in such a way that it reduces to the center when the element becomes rectangular. This restriction, however, still allows many possibilities. On most bodies of interest the quadrilateral elements are nearly rectangular over most of the body surface, and thus the final answers do not depend greatly on the point used. However, there are often certain regions of the surface where the elements are not approximately rectangular, and the calculated flow velocities may change appreciably with the choice of this point. Such a region occurs, for example, near the concentration

points discussed above, where the elements usually become triangular (see figure 3). It is felt that this fact is part of the reason why the calculations are normally found to be least accurate near concentration points. The three points considered as possibilities were the null point, the centroid, and the average point. The null point was selected for no better reason than a personal opinion that the choice should tend to minimize errors. A small number of cases that were run with either the centroid or the average point replacing the null point did not indicate that any one of the three is significantly better than the others. It seems evident that this question is in need of further study, but it was decided to postpone this for a while and to use the null point in the meantime. The null point is much more difficult to calculate than either the centroid or the average point and thus a change to either of these would represent a simplification of the method.

There are two further difficulties connected with the use of the null point that were discovered after the machine program had been written. Namely, there are two situations were the iterative procedure used to determine the null point does not converge to the correct point. The first occurs when an element is triangular or nearly triangular (as, for example, may occur near a concentration point). If an element has two long sides and two short ones and is nearly triangular in shape in the sense that either the two long sides are adjacent or one short side is less than about one-fifth the other short side, and if the base to altitude ratio of the triangular shape is less than about one-thirtieth, then the calculated null point lies outside the element. In this case the centroid is used in place of the null point for that element, and the fact is noted on the first output. The second situation occurs when an element has one diagonal much shorter than the other and much shorter than all four sides, e.g., a long, thin, parallelogram. If the ratio of diagonals is less than about one-thirtieth, the iterative procedure does not converge because the induced velocity is very sensitive to position in the vicinity of the null point. In this case the approximate null point obtained in the thirtieth iteration is used and this fact is noted on the first output. (These considerations are discussed further in Section 9.3, which also includes sketches of the unfavorable elements.) Neither of these cases is of much practical significance. A point distribution that leads to elements of such extreme shape is probably not a very good one, and the appearance of

32

either of these situations usually implies that the input points should be re-distributed. In any case the errors arising from the use of these alternatives in place of the null point are probably less than those due to the basic distribution of elements.

In many cases the most time consuming portion of the calculation is the compution of the velocities induced by the quadrilateral elements at each other's null points — the ''matrix of influence coefficients''. Hence the dominant consideration in arranging the calculation of this matrix was the minimization of computation time. As a result, the maximum permissible number of elements that may be used to approximate a body surface is somewhat lower than it would otherwise have been. The most important time reduction came from the replacement of the exact induced velocity formulas by formulas derived from a multipole expansion at distances where the latter are sufficiently accurate. The accuracy of this approximation is described in another section. With the accuracy criterion adopted, the use of the multipole expansion reduces the time of computation of the ''matrix of influence coefficients'' by a factor of about five. The accuracy criterion is arbitrary and can be adjusted so that the exact formulas are used exclusively if desired with a corresponding large increase in computation time. A further reduction in computation time is obtained by computing the induced velocities, except those due to the simple source, in the element coordinate system, with the result that the transformation matrix for the elements must be used to transform velocities and points between the element and reference coordinate systems. Altogether, twenty-eight geometric quantities for each element are used to compute induced velocities, while about half this number would suffice if computation time were not a factor. These numbers are computed only once and saved to avoid unnecessary calculation. If the ''matrix of influence coefficients'' were computed column by column, the velocities induced by a particular element at all null points would be computed consecutively. Thus at any given time only the twenty-eight quantities for a single element would have to be available in the high speed storage of the machine. Since the methods used to solve the linear equations for the source density use the coefficient matrix row by row, this procedure would require transposing the matrix. A large coefficient matrix exceeds the high speed storage capacity of the machine by a factor of about twenty-five, and thus transposing the matrix is rather time

consuming. Therefore, the ''matrix of influence coefficients'' is computed
row by row, and so the twenty-eight quantities for all elements must be
simultaneously available in the high speed memory. The high speed storage
capacity of the machine may thus limit the maximum number of elements that may
be used to define a body surface. This problem was not significant on the
IBM 704 for which this method was originally programmed, because the capacity
of the low speed tape storage was the limiting factor in all cases with
symmetry and permitted only a 25 percent increase in elements over the high
speed storage limit in nonsymmetric cases. Moreover total computing times for
large cases were typically fifteen hours, so an increase in the number of
elements did not seem desirable. However, the IBM 7090, to which the program
has been converted, has available high density tape units that greatly increase
the available low speed storage. The result is that high speed storage capaci-
ty is the limiting factor on this machine for both symmetric and nonsymmetric
bodies and that the limits imposed by low speed storage capacity would permit
a considerable increase in the maximum number of elements. Typical total
computing times for large cases on the IBM 7090 are about four hours, so that
an increase in the number of elements might be desirable.

In taking into account any planes of symmetry that a body might possess,
it is assumed that the elements adjacent to symmetry planes have edges lying
in these planes. Thus flow velocities, which are evaluated at null points,
are not computed at points of the body surface that lie in the symmetry planes.
This seemingly trivial point is often irksome, because velocities at points
in a symmetry plane are frequently desired, and they must be obtained by extra-
polation.

The simultaneous linear equations for the values of the surface source
density on the various elements are solved by one of two alternative forms of
a Seidel iterative procedure. The first of these obtains in each iteration
a complete set of values of the source density from the values in the previous
iteration, while the second always uses the most recently calculated values of
the source density to obtain improved values. The second has proven at least
as fast as the first in all cases and is often much faster. It is, therefore,
employed unless the other is specifically called for. The coefficient matrix
of induced normal velocities is well suited for this relatively simple

34

iterative scheme, because the diagonal elements are much larger than the off-diagonal elements. If a more sophisticated iteration scheme were to be considered, it would require a very careful initial investigation to insure that the solution time would not be increased. In many cases the time required to solve the linear equations is smaller than that required to compute the set of induced velocities, and a reduction of the former would not significantly reduce the total computation time. There are certain kinds of body shapes for which the time required for solution of the linear equations is a large fraction of the total computation time, and a reduction would be quite beneficial. This matter has been investigated, and one very promising means of accelerating the convergence of the iterative procedure has been found. However, it was decided not to incorporate the technique into the method at this time.

The method has been constructed so that it computes flow velocities for three distinct onset flows. Normally, it is desirable to utilize this feature since the elimination of one or two onset flows affects only the time required to solve the linear equations, and thus often does not significantly decrease the total computation time. Any onset flow may be effectively eliminated by specifying a zero vector for that flow, in which case the true zero values of the source density for that flow are simply obtained in the first iteration. This should be done with reluctance, however, since if additional onset flows are required later, the entire computation must be repeated.

8.0 THE VELOCITIES INDUCED BY A PLANE SOURCE QUADRILATERAL

8.1 Exact Expressions for the Induced Velocities

In this section the exact formulas for the velocity components induced at points in space by a plane quadrilateral source element with a unit value of source density are derived. These formulas are the basis of the present method of flow calculation. The derivation is such that the extension to the case of any plane polygonal source element is obvious.

8.11 Formulation of the Problem and Construction of the Fundamental Potential Function for a Side of the Quadrilateral.

Consider a plane quadrilateral source element lying in the xy-plane as shown in figure 5. (Taking the element to lie in the xy-plane is equivalent to working in the element coordinate system.) The value of the surface source
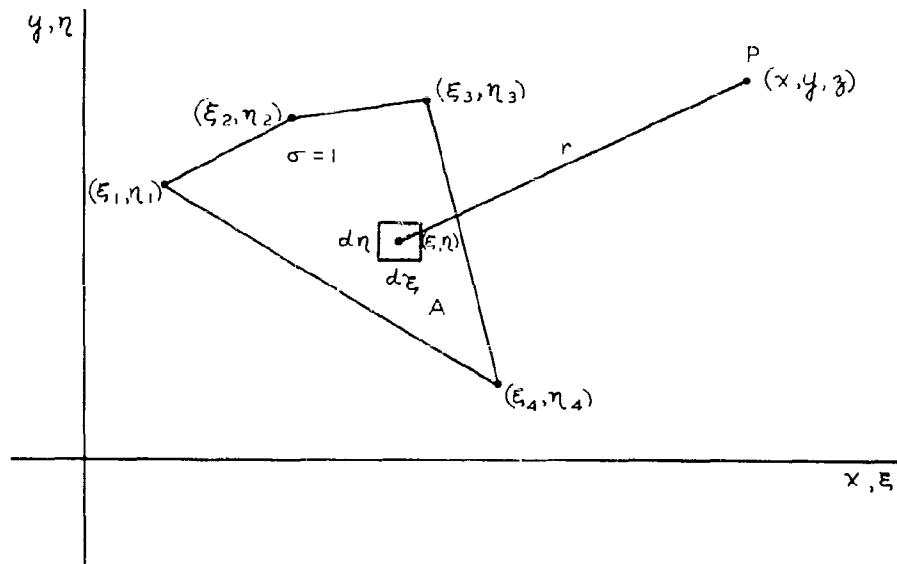
Figure 5. - A plane quadrilateral source element.

density σ on this element is set equal to unity. The xy or $\xi\eta$ coordinates of the four corner points defining the quadrilateral are (ξ_1, η_1), (ξ_2, η_2), (ξ_3, η_3) and (ξ_4, η_4). It is desired to determine the velocity components induced by this source element at a general point P in space with coordinates x, y, z. The potential at the point P is

$$\varphi = \oiint_A \frac{1}{r} \, dA = \oiint_A \frac{d\xi \, d\eta}{\sqrt{(x - \xi)^2 + (y - \eta)^2 + z^2}} \tag{15}$$

where r is the distance from P to a point on the quadrilateral with coordinates $(\xi, \eta, 0)$, and the range of integration is the area A of the quadrilateral. The velocity components at P are given by

$$V_x = -\frac{\partial \varphi}{\partial x} = \oiint_A \frac{(x - \xi) \, d\xi \, d\eta}{r^3} \tag{16}$$

$$V_y = -\frac{\partial \varphi}{\partial y} = \oiint_A \frac{(y - \eta) \, d\xi \, d\eta}{r^3} \tag{17}$$

$$V_z = -\frac{\partial \varphi}{\partial z} = \oiint_A \frac{z \, d\xi \, d\eta}{r^3} \tag{18}$$

It is convenient to divide the effect of the entire quadrilateral into a sum of functions, each of which depends only on one side of the quadrilateral. This division also allows the results to be generalized to the case of any polygonal source element. To accomplish this one of the corner points is taken as the initial corner point and the others are numbered in the order they are encountered in traversing the perimeter of the element with the exterior of the area on the left; see figure 5. For each side of the element a right and a left can then be defined with respect to the direction of traversal of the side from a lower numbered end point to a higher numbered endpoint. The area of the element is on the right. Now a fundamental potential function for each side is constructed as the sum of the potentials of two semi-infinite source strips whose boundaries consist of the side of the quadrilateral and semi-infinite lines parallel to one of the coordinate axes. The strip on the right of the side has a value of source density $\sigma = + 1/2$, while the strip on the left has $\sigma = - 1/2$. The semi-infinite boundaries of the strips may be parallel to either coordinate axis, but they must all be parallel to the same one. These strips, which are now taken parallel to the y-axis, are shown in figure 6 for the four sides of the quadrilateral sketched in figure 5. It can be seen that if the sides shown in figure 6 are put together to form the quadrilateral of figure 5, the source densities on the strips cancel outside

37
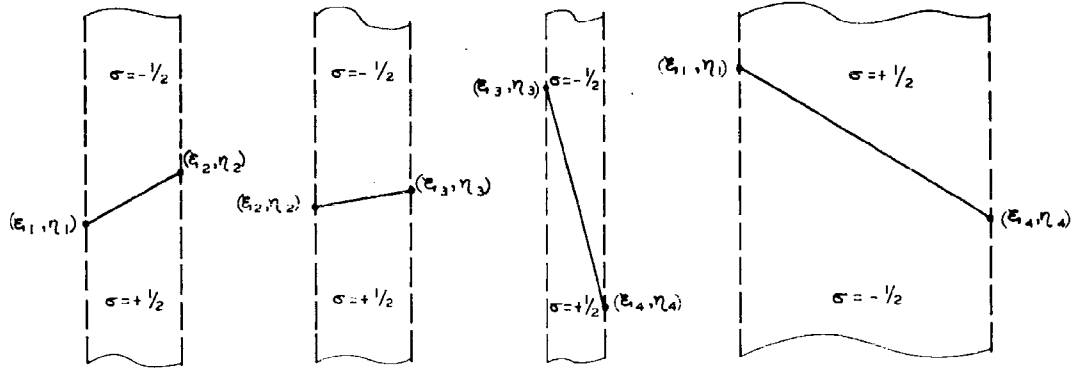
Figure 6. - Fundamental potentials for sides of a quadrilateral.

the quadrilateral and add inside to give a unit value. Thus the potential
and velocity due to the quadrilateral are sums of the potentials and veloci-
ties due to the four pairs of semi-infinite source strips shown in figure 6.
It can readily be verified that this statement is true regardless of the re-
lative positions of the corner points and moreover that it is true for poly-
gons of any number of sides.

(a)   (b)
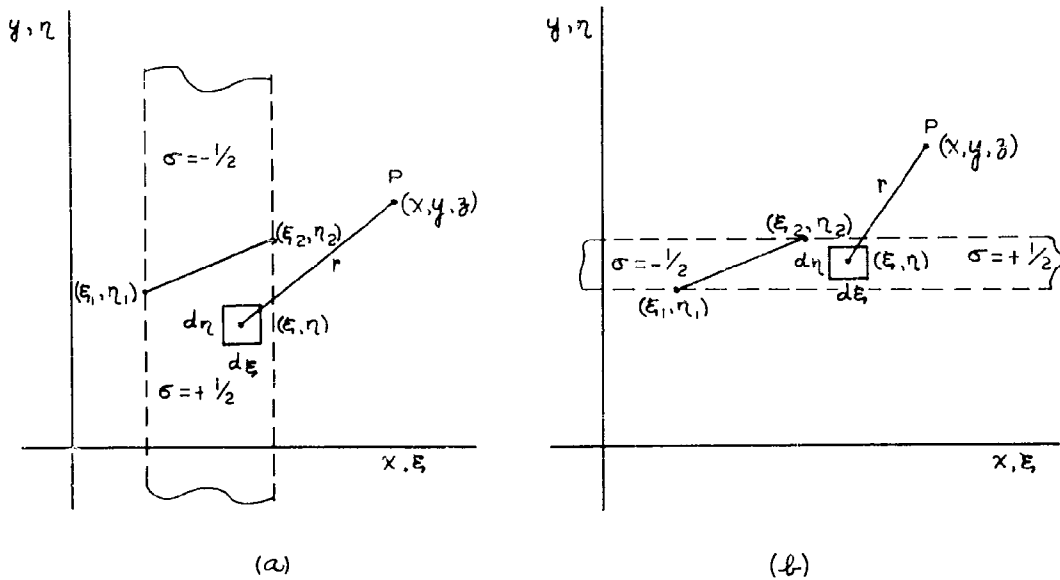
Figure 7. - Two possibilities for the fundamental potential of a side.

The problem of finding the velocities induced by the quadrilateral is thus reduced to the problem of finding the velocities induced by the pair of semi-infinite strips associated with one side. For definiteness the side between (ξ_1, η_1) and (ξ_2, η_2) is selected. A fundamental potential function may be constructed using semi-infinite strips that are parallel to either coordinate axis, and the two possibilities are shown in figure 7.

8.12 Derivation of the Induced Velocity Components Parallel to the Plane of the Quadrilateral.

The induced velocity component V_x is most conveniently obtained using for a fundamental potential function the potential of a pair of strips parallel to the x-axis as shown in figure 7b, while the component V_y is obtained more conveniently using a fundamental potential function due to strips parallel to the y-axis as shown in figure 7a. The latter component will be calculated first.

The velocity V_y due to the pair of strips shown in figure 7a is obtained as an integral of the form (17) carried out over the total area of the strips and using the proper values of σ. Specifically,

$$V_{y_{12}} = \frac{1}{2} \int_{\xi_1}^{\xi_2} d\xi \left\{ \int_{-\infty}^{\eta_{12}} - \int_{\eta_{12}}^{\infty} \right\} \frac{(y - \eta)\, d\eta}{\left[(x - \xi)^2 + (y - \eta)^2 + z^2\right]^{3/2}} \qquad (19)$$

where η_{12} is being used to denote the η coordinate of a point on the line between (ξ_1, η_1) and (ξ_2, η_2). This is the correct form if $\xi_2 > \xi_1$. If $\xi_1 > \xi_2$, the signs of the integrals with respect to η are reversed, and the sign of the integral with respect to ξ is also effectively reversed. The final result is valid for either sign of $\xi_2 - \xi_1$, as may be verified. The integral with respect to η in (19) is a standard form. When the integration is performed, the contributions of the infinite limits cancel, while the contributions of the finite limits add. The result is

$$V_{y_{12}} = \int_{\xi_1}^{\xi_2} \frac{d\xi}{\sqrt{(x - \xi)^2 + (y - \eta_{12})^2 + z^2}} = \int_{\xi_1}^{\xi_2} \frac{d\xi}{r} \qquad (20)$$

39

where r is the distance from the point P to a point on the line between (ξ_1, η_1) and (ξ_2, η_2). The integration variable in (20) may be changed to the arc length s along the line between (ξ_1, η_1) and (ξ_2, η_2) by means of the substitution

$$\frac{d\xi}{ds} = \frac{\xi_2 - \xi_1}{\sqrt{(\xi_2 - \xi_1)^2 + (\eta_2 - \eta_1)^2}} = \frac{\xi_2 - \xi_1}{d_{12}} \tag{21}$$

where d_{12} is the length of the side. Then (20) becomes

$$V_{y_{12}} = \frac{\xi_2 - \xi_1}{d_{12}} \int_0^{d_{12}} \frac{ds}{r} \tag{22}$$

The integral in (22) is seen to be the potential at P due to a finite line source of unit linear source density coincident with the side of the quadrilateral. The integration is most conveniently performed by working in the plane containing the point P and the line between (ξ_1, η_1) and (ξ_2, η_2) as shown in figure 8. In this figure, r_1 and r_2 denote the distance from the point P to the points (ξ_1, η_1) and (ξ_2, η_2), respectively, while s_1 and s_2 are the components of these distances along the side of the quadrilateral. With this notation (22) becomes
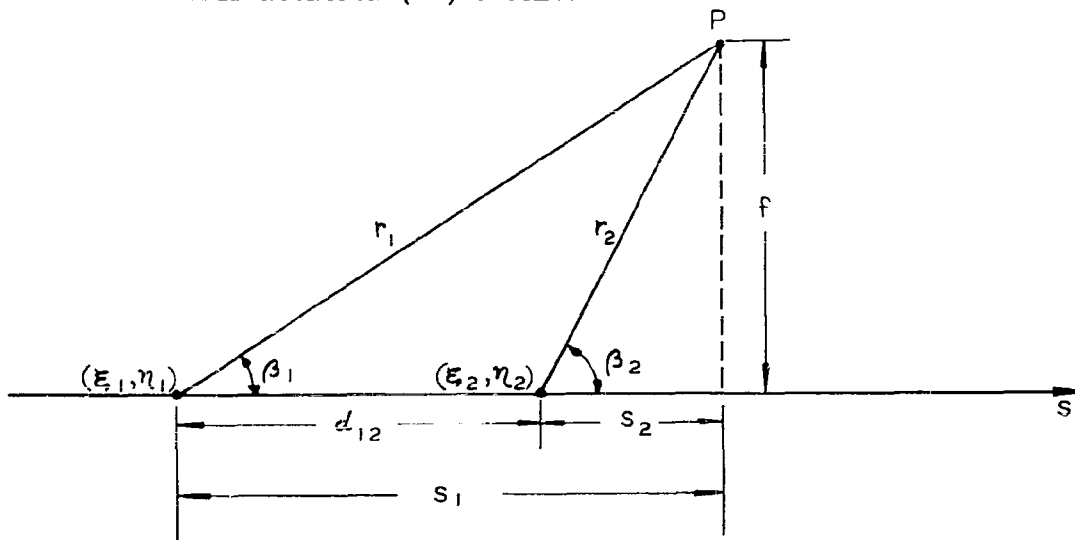
Figure 8. - The potential due to a finite line source.

40

$$V_{y_{12}} = \frac{\xi_2 - \xi_1}{d_{12}} \int_0^{d_{12}} \frac{ds}{\sqrt{s^2 - 2s_1 s + s_1^2 + f^2}}$$

$$= \frac{\xi_2 - \xi_1}{d_{12}} \log \frac{r_2 + d_{12} - s_1}{r_1 - s_1} = \frac{\xi_2 - \xi_1}{d_{12}} \log \frac{r_2 - s_2}{r_1 - s_1} \qquad (23)$$

$$= \frac{\xi_2 - \xi_1}{d_{12}} \log \frac{r_2}{r_1} \left(\frac{1 - \cos \beta_2}{1 - \cos \beta_1} \right)$$

This result is indeterminate when $\beta_1 = \beta_2 = 0$, i.e., on the extension of the side of the quadrilateral. The difficulty can be removed in the following way. From the law of cosines

$$\cos \beta_1 = \frac{r_1^2 - r_2^2 + d_{12}^2}{2 r_1 d_{12}} \qquad (24)$$

$$\cos \beta_2 = \frac{r_1^2 - r_2^2 - d_{12}^2}{2 r_2 d_{12}}$$

So,

$$\frac{r_2}{r_1} \frac{1 - \cos \beta_2}{1 - \cos \beta_1} = \frac{2 r_2 d_{12} - r_1^2 + r_2^2 + d_{12}^2}{2 r_1 d_{12} - r_1^2 + r_2^2 - d_{12}^2}$$

$$= \frac{(r_2 + d_{12})^2 - r_1^2}{(r_2 + d_{12} - r_1)(r_2 + r_1 - d_{12})} \qquad (25)$$

$$= \frac{r_1 + r_2 + d_{12}}{r_1 + r_2 - d_{12}}$$

The argument of the logarithm in (23) can accordingly be written in terms of the distances r_1, r_2 and d_{12}. These distances can be expressed in terms of the original coordinate system. Thus finally the y-component of velocity

41

at the point P with coordinates x, y, z due to the fundamental potential function of the side between (ξ_1, η_1) and (ξ_2, η_2) can be written

$$V_{y_{12}} = \frac{\xi_1 - \xi_2}{d_{12}} \, \log \left(\frac{r_1 + r_2 - d_{12}}{r_1 + r_2 + d_{12}} \right) \tag{26}$$

where

$$r_1 = \sqrt{(x - \xi_1)^2 + (y - \eta_1)^2 + z^2} \tag{}$$

$$r_2 = \sqrt{(x - \xi_2)^2 + (y - \eta_2)^2 + z^2} \tag{27}$$

$$d_{12} = \sqrt{(\xi_2 - \xi_1)^2 + (\eta_2 - \eta_1)^2} \tag{}$$

The x component of velocity is obtained by integrating over strips whose semi-infinite sides are parallel to the x-axis, with order of integration reversed. The procedure is the same as that used above for the y-component. The result is

$$V_{x_{12}} = \frac{\eta_2 - \eta_1}{d_{12}} \, \log \frac{r_1 + r_2 - d_{12}}{r_1 + r_2 + d_{12}} \tag{28}$$

where the quantities r_1, r_2, and d_{12} are again given by (27).

8.13 Derivation of the Induced Velocity Component Normal to the Plane of the Quadrilateral.

To obtain the component V_z of the velocity at the point P, the fundamental potential function for the side of the quadrilateral between (ξ_1, η_1) and (ξ_2, η_2) is constructed using semi-infinite strips parallel to the y-axis as was done for V_y. The region of integration is thus the one shown in figure 7a and the velocity component is given by an integral of the form (18) with the same integration limits as for equation (19). Specifically,

42

$$V_{z_{12}} = \frac{z}{2} \int_{\xi_1}^{\xi_2} d\xi \left\{ \int_{-\infty}^{\eta_{12}} - \int_{\eta_{12}}^{\infty} \right\} \frac{d\eta}{\left[(x-\xi)^2 + (y-\eta)^2 + z^2 \right]^{3/2}} \tag{29}$$

The integral with respect to η is a standard form. Again the contributions of the infinite limits cancel, while the contributions of the finite limits add. The result is

$$V_{z_{12}} = -z \int_{\xi_1}^{\xi_2} \frac{(y-\eta_{12})\, d\xi}{\left[(x-\xi)^2 + z^2 \right] \sqrt{(x-\xi)^2 + (x-\eta_{12})^2 + z^2}} \tag{30}$$

There is no obvious physical interpretation of equation (30) as there was for the analogous equation (20), and so it will be integrated directly. Recall that η_{12} denotes a variable point on the line between (ξ_1, η_1) and (ξ_2, η_2). Thus η_{12} can be expressed as a function of ξ in the form

$$\eta_{12} = m_{12}\xi + b_{12} \tag{31}$$

where

$$m_{12} = \frac{\eta_2 - \eta_1}{\xi_2 - \xi_1} \tag{32}$$

is the slope of the side of the quadrilateral and

$$b_{12} = \frac{\xi_2 \eta_1 - \xi_1 \eta_2}{\xi_2 - \xi_1} \tag{33}$$

Also define the quantities

$$q_{12} = y - b_{12} - m_{12}x \tag{34}$$

$$u = x - \xi \tag{35}$$

In terms of these variables equation (30) becomes

43

$$V_{z_{12}} = z \int_{x-\xi_1}^{x-\xi_2} \frac{(m_{12}u + q_{12})du}{(u^2+z^2)\sqrt{u^2+(m_{12}u+q_{12})^2+z^2}} \qquad (36)$$

By the methods of Hardy (reference 5)

$$\int \frac{(m_{12}u + q_{12})\,du}{(u^2+z^2)\sqrt{u^2+(m_{12}u+q_{12})^2+z^2}} = \qquad (37)$$

$$= -\frac{1}{z}\tan^{-1}\left\{ \frac{q_{12}\sqrt{q_{12}^2+m_{12}^2 z^2}\left[m_{12}^2 z^2 - m_{12}q_{12}u\right]}{z\sqrt{q_{12}^2\left[m_{12}^2 z^2 - m_{12}q_{12}u\right]^2 + \left[q_{12}^2 + m_{12}q_{12}u\right]^2\left[(1+m_{12}^2)z^2+q_{12}^2\right]m_{12}^2}} \right\}$$

After some algebraic manipulation, the cancellation of common terms in the numerator and denominator, and the use of equations (31) and (34), the above result can be written

$$\int \frac{(m_{12}u + q_{12})\,du}{(u^2+z^2)\sqrt{u^2+(m_{12}u+q_{12})^2+z^2}} = -\frac{1}{z}\tan^{-1}\left\{ \frac{m_{12}z^2 - q_{12}u}{z\sqrt{u^2+z^2+\left[q_{12}+m_{12}u\right]^2}} \right\} \qquad (38)$$

$$= -\frac{1}{z}\tan^{-1}\left\{ \frac{m_{12}(u^2+z^2)-(y-\eta_{12})u}{z\sqrt{u^2+(y-\eta_{12})^2+z^2}} \right\}$$

Using the integration limits of equation (36) with equation (38) gives as the z-component of velocity at the point P with coordinates x, y, z due to the fundamental potential function of the side between (ξ_1, η_1) and (ξ_2, η_2)

$$V_{z_{12}} = \tan^{-1}\left(\frac{m_{12}e_1 - h_1}{z\,r_1}\right) - \tan^{-1}\left(\frac{m_{12}e_2 - h_2}{z\,r_2}\right) \qquad (39)$$

44

where

$$e_1 = z^2 + (x - \xi_1)^2 \qquad\qquad e_2 = z^2 + (x - \xi_2)^2 \tag{40}$$

$$h_1 = (y - \eta_1)(x - \xi_1) \qquad\qquad h_2 = (y - \eta_2)(x - \xi_2) \tag{41}$$

and where m_{12} is given by (32) and r_1 and r_2 by (27).

8.14 Summary of the Exact Induced Velocity Formulas for a Quadrilateral Source Element.

The velocity components induced by any polygonal source element of unit source density are obtained by adding terms of the form derived in the previous section. For each velocity component there is one term of the above form for each side of the polygon. The terms for the other sides are obtained from those for the side between (ξ_1, η_1) and (ξ_2, η_2) by a cyclic permutation of the corner points. Since quadrilateral source elements are the ones of interest for this method, the induced velocity formulas for this case are written down explicitly here.

A quadrilateral source element of unit density lying in the xy-plane with corner points (ξ_1, η_1), (ξ_2, η_2), (ξ_3, η_3), and (ξ_4, η_4) as shown in figure 5 induces the following velocity components at a point P with coordinates x, y, z:

$$V_x = \frac{\eta_2 - \eta_1}{d_{12}} \log\left(\frac{r_1 + r_2 - d_{12}}{r_1 + r_2 + d_{12}}\right) + \frac{\eta_3 - \eta_2}{d_{23}} \log\left(\frac{r_2 + r_3 - d_{23}}{r_2 + r_3 + d_{23}}\right)$$
$$+ \frac{\eta_4 - \eta_3}{d_{34}} \log\left(\frac{r_3 + r_4 - d_{34}}{r_3 + r_4 + d_{34}}\right) + \frac{\eta_1 - \eta_4}{d_{41}} \log\left(\frac{r_4 + r_1 - d_{41}}{r_4 + r_1 + d_{41}}\right) \tag{42}$$

$$V_y = \frac{\xi_1 - \xi_2}{d_{12}} \log\left(\frac{r_1 + r_2 - d_{12}}{r_1 + r_2 + d_{12}}\right) + \frac{\xi_2 - \xi_3}{d_{23}} \log\left(\frac{r_2 + r_3 - d_{23}}{r_2 + r_3 + d_{23}}\right)$$
$$+ \frac{\xi_3 - \xi_4}{d_{34}} \log\left(\frac{r_3 + r_4 - d_{34}}{r_3 + r_4 + d_{34}}\right) + \frac{\xi_4 - \xi_1}{d_{41}} \log\left(\frac{r_4 + r_1 - d_{41}}{r_4 + r_1 + d_{41}}\right) \tag{43}$$

$$V_z = \tan^{-1}\left(\frac{m_{12}e_1 - h_1}{z\ r_1}\right) - \tan^{-1}\left(\frac{m_{12}e_2 - h_2}{z\ r_2}\right)$$

$$+ \tan^{-1}\left(\frac{m_{23}e_2 - h_2}{z\ r_2}\right) - \tan^{-1}\left(\frac{m_{23}e_3 - h_3}{z\ r_3}\right)$$

$$+ \tan^{-1}\left(\frac{m_{34}e_3 - h_3}{z\ r_3}\right) - \tan^{-1}\left(\frac{m_{34}e_4 - h_4}{z\ r_4}\right) \tag{44}$$

$$+ \tan^{-1}\left(\frac{m_{41}e_4 - h_4}{z\ r_4}\right) - \tan^{-1}\left(\frac{m_{41}e_4 - h_1}{z\ r_1}\right)$$

where

$$d_{12} = \sqrt{(\xi_2 - \xi_1)^2 + (\eta_2 - \eta_1)^2}$$

$$d_{23} = \sqrt{(\xi_3 - \xi_2)^2 + (\eta_3 - \eta_2)^2}$$

$$d_{34} = \sqrt{(\xi_4 - \xi_3)^2 + (\eta_4 - \eta_3)^2} \tag{45}$$

$$d_{41} = \sqrt{(\xi_1 - \xi_4)^2 + (\eta_1 - \eta_4)^2}$$

where

$$m_{12} = \frac{\eta_2 - \eta_1}{\xi_2 - \xi_1} \qquad\qquad m_{23} = \frac{\eta_3 - \eta_2}{\xi_3 - \xi_2}$$

$$m_{34} = \frac{\eta_4 - \eta_3}{\xi_4 - \xi_3} \qquad\qquad m_{41} = \frac{\eta_1 - \eta_4}{\xi_1 - \xi_4} \tag{46}$$

and

$$r_k = \sqrt{(x - \xi_k)^2 + (y - \eta_k)^2 + z^2} \qquad , k = 1,\ 2,\ 3,\ 4 \tag{47}$$

$$e_k = z^2 + (x - \xi_k)^2 \qquad\qquad , k = 1,\ 2,\ 3,\ 4 \tag{48}$$

$$h_k = (y - \eta_k)(x - \xi_k) \qquad\qquad , k = 1,\ 2,\ 3,\ 4 \tag{49}$$

These are the basic formulas of the method.

In actually evaluating these expressions V_x and V_y cause no trouble. They become infinite on the edges of the quadrilateral, but in practice they are never evaluated there. The component V_z requires special handling in certain cases. As $z \to 0$, $V_z \to 0$ if the point P is approaching a point in the plane outside the boundaries of the quadrilateral. If P approaches a point within the quadrilateral $V_z \to 2\pi$ (sgn z) as $z \to 0$. These facts may be verified from equation (44). In the course of this method of flow calculation it is required to evaluate V_z at points in the plane of the quadrilateral elements. In particular, the null point of each element is in the plane of that element and within the quadrilateral. At such a point V_z should equal $+ 2\pi$, since the case of interest is that for which $z \to 0$ through positive values, rather than through negative values, i.e., the field point approaches the body surface from the exterior flow field rather than from the interior of the body. It may also be required to evaluate induced velocity components at points in the plane of a quadrilateral outside the boundaries of the quadrilateral, for example, at the null points of other elements if the body surface has a flat region. Points in the plane of a quadrilateral element should have $z = 0$, but, because of round-off error, they may have small values of z with either sign. Thus, for points inside the quadrilateral, equation (44) may give 2π with either sign. To avoid this error, the absolute value of z is tested before velocities are computed, and if it is less than some small prescribed number, which is nevertheless large compared to the expected round-off error, it is set equal to plus zero and each inverse tangent of equation (44) is set equal to $\pi/2$ with the sign of the numerator of its argument. This gives $V_z = 0$ for points outside the quadrilateral and $V_z = +2\pi$ for points inside the quadrilateral. Another situation that may cause trouble in the computing machine is when the slope of a side of the quadrilateral is infinite, i.e., when a side is parallel to the y-axis. It is evident from equation (44) that in this case the two inverse tangents corresponding to that side cancel each other. To avoid difficulties each of the quantities $(\xi_2 - \xi_1)$, $(\xi_3 - \xi_2)$, $(\xi_4 - \xi_3)$, and $(\xi_1 - \xi_4)$ are tested to determine whether they are zero, and if any one of them is zero, the two inverse tangents corresponding to that side are set equal to zero. Finally, it should be mentioned that the inverse tangents in equation (44) are evaluated in the normal range $- \pi/2$ to $+ \pi/2$. It is tempting to combine

some of the inverse tangents in this equation using the tangent addition law, but if this is done, great care must be exercised with regard to the range in which the resulting inverse tangents should be evaluated.

8.15 An Example of the Velocity Induced by a Quadrilateral Element.

In addition to their basic use, formulas (42), (43), and (44) are of some interest by themselves. These formulas were used to compute induced velocity components for a variety of quadrilateral shapes. The results for two of the shapes, the square and the isosceles right triangle are used in a subsequent section to evaluate the accuracy of the multipole expansion. In this section a single example is given. Figure 9 shows curves of constant velocity magnitude due to a unit source density on the quadrilateral shown in the figure. Figure 9a shows the velocity in the plane of the element, $z = 0$, while figure 9b shows the velocity in a plane above the element, $z = 1$. In figure 9a the velocity magnitude is computed from x and y components only. The velocity normal to the plane of the elements, which is non-zero inside the element, is neglected. In this figure it can be seen that there is a single point inside the quadrilateral where the velocity is zero. It is the null point discussed elsewhere. In the $z = 1$ plane (figure 9b), there is no point where the velocity is zero. Instead, there is a point of maximum velocity. As can be seen in the figure, the maximum velocity magnitude in the plane $z = 1$ is 2.14.

8.2 Approximation of the Induced Velocities by a Multipole Expansion

The evaluation of the induced velocity components by the exact formulas, equations (42) through (49), is quite time-consuming. To reduce computing time approximate expressions are used instead of these formulas wherever possible. In this section approximate expressions are derived by means of a multipole expansion.
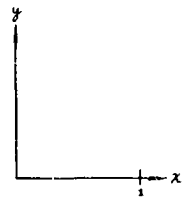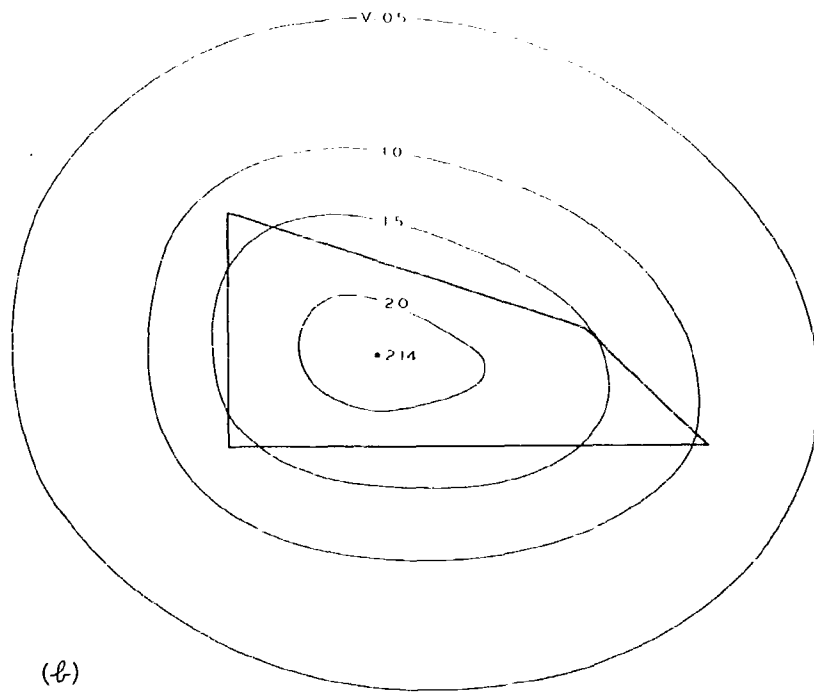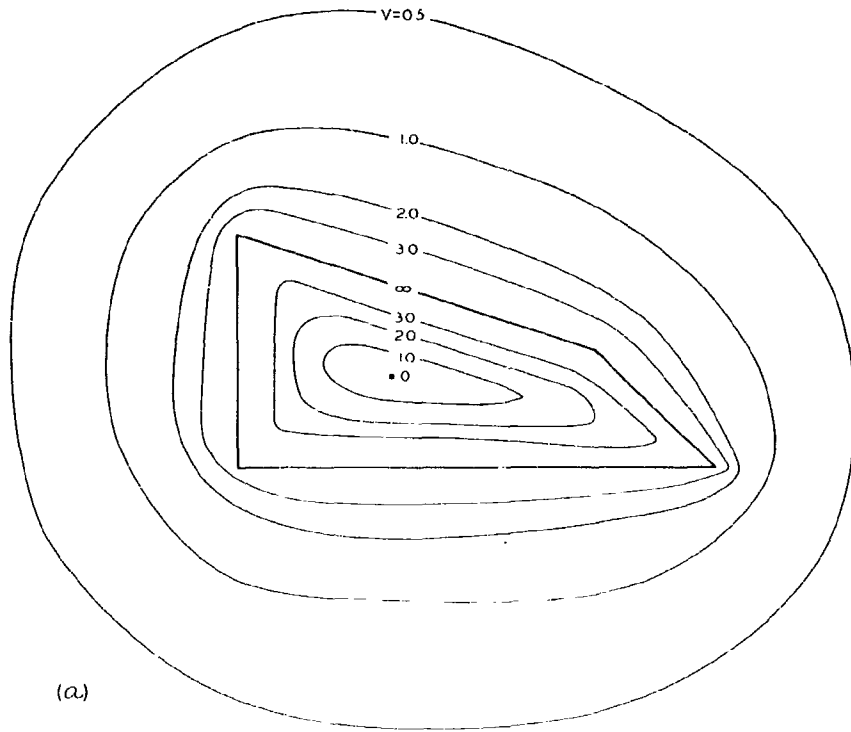
Figure 9. - Velocity magnitudes induced by a typical quadrilateral. (a) $z = 0$, (b) $z = 1.0$

8.21 Derivation of Approximate Formulas for the Induced Velocity Components.

Consider again the potential at a point P with coordinates x, y, z due to a quadrilateral element of unit source density in the xy-plane. The origin of the coordinate system is taken as a point inside the quadrilateral as shown in figure 10. (This is actually not necessary for the validity of the expansion, but it is the only case of interest in the present application.)
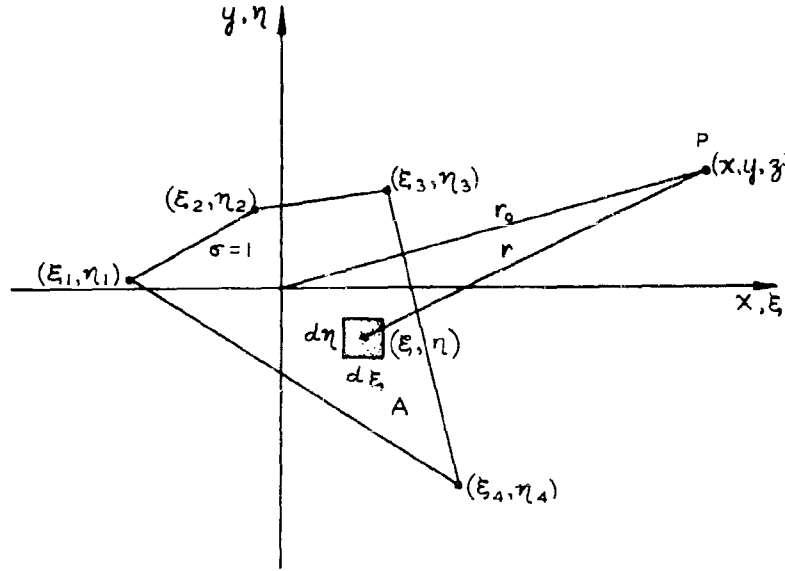
Figure 10. - The multipole expansion.

The potential at P is, as before

$$\varphi = \oiint_A \frac{1}{r} \, dA = \oiint_A \frac{d\xi \, d\eta}{\sqrt{(x - \xi)^2 + (y - \eta)^2 + z^2}} \tag{50}$$

Now in the multipole expansion the integrand in equation (50), i.e., $1/r$, is expanded in a power series in ξ and η about the origin. When that is done, each term of the series contains a certain derivative of $1/r$ evaluated at $\xi = \eta = 0$ multiplied by certain powers of ξ and η. The first of these depends only on x, y, z and may thus be taken out of the integral. The result is that the potential may be expressed as a series of terms each of which is a product of a function of x, y, z, which is independent of the shape of the quadrilateral, and an integral of certain powers of ξ and η,

which depends only on the shape of the quadrilateral and is independent of the point where the potential is being evaluated. First define

$$r_o = \sqrt{x^2 + y^2 + z^2} \tag{51}$$

$$w = \frac{1}{r_o} \tag{52}$$

Then through terms of second order the expansion of equation (50) is

$$\varphi = A w - (M_x w_x + M_y w_y) + \frac{1}{2} (I_{xx} w_{xx} + 2 I_{xy} w_{xy} + I_{yy} w_{yy}) + \cdots \tag{53}$$

where

$$A = \oiint_A d\xi \, d\eta \tag{54}$$

$$M_x = \oiint_A \xi \, d\xi \, d\eta \qquad\qquad M_y = \oiint_A \eta \, d\xi \, d\eta \tag{55}$$

$$I_{xx} = \oiint_A \xi^2 d\xi \, d\eta \qquad I_{xy} = \oiint_A \xi \, \eta \, d\xi \, d\eta \qquad I_{yy} = \oiint_A \eta^2 \, d\xi \, d\eta \tag{56}$$

and where subscripts x and y used on w denote partial derivatives with respect to those variables. The designation of multipole expansion arises from the fact that the various terms in the expansion (53) can be interpreted as the potentials of point singularities of various orders, each of which is constructed by the confluence of two singularities of the next lowest order. For example, the first term of equation (53) is the potential of a point source of strength A located at the origin. The second term is the sum of the potentials of a dipole of strength M_x oriented along the x-axis and a dipole of strength M_y oriented along the y-axis, both of which are located at the origin. The third term is the sum of the potentials of the three independent quadrupoles at the origin with strengths proportional to I_{xx}, I_{xy}, and I_{yy}. Such a multipole expansion can be shown to converge for all points sufficiently far from the origin. In the present application convergence is not a problem. The multipole expansion is used here only at points sufficiently far from the element so that the expansion not only converges but converges rapidly enough

51

so that terms of higher order than second may be neglected. A more general discussion of the multipole expansion can be found in any electrodynamics text, for example reference 6.

Equations (54), (55), and (56) show the geometrical significance of the strengths of the various singularities. The source strength A is the area of the quadrilateral, the dipole strengths, M_x and M_y are the first moments of the area about the origin, and the quadrupole strengths, I_{xx} , I_{xy} , and I_{yy} are the second moments or "moments of inertia" of the area about the origin. In the present application the origin of the coordinate system in which the quadrilateral lies in the xy-plane, i.e., the element coordinate system discussed elsewhere, is taken as the centroid of the area of the quadrilateral. With this choice of origin the first moments, M_x and M_y , vanish, and there are no dipole terms.

The approximate equations for the induced velocity components are obtained by truncating equation (53) after the second order terms shown and differentiating with $M_x = M_y = 0$. The results are

$$
V_x = - \frac{\partial \varphi}{\partial x} = - \left[Aw_x + \frac{1}{2} I_{xx} w_{xxx} + I_{xy} w_{xxy} + \frac{1}{2} I_{yy} w_{xyy} \right] \tag{57}
$$

$$
V_y = - \frac{\partial \varphi}{\partial y} = - \left[Aw_y + \frac{1}{2} I_{xx} w_{xxy} + I_{xy} w_{xyy} + \frac{1}{2} I_{yy} w_{yyy} \right] \tag{58}
$$

$$
V_z = - \frac{\partial \varphi}{\partial z} = - \left[Aw_z + \frac{1}{2} I_{xx} w_{xxz} + I_{xy} w_{xyz} + \frac{1}{2} I_{yy} w_{yyz} \right] \tag{59}
$$

In these equations A , I_{xx} , I_{xy} , and I_{yy} are the geometrical quantities discussed above, while the derivatives of w are

$$
w_x = - x \, r_o^{-3}
$$

$$
w_y = - y \, r_o^{-3} \tag{60}
$$

$$
w_z = - z \, r_o^{-3}
$$

52

$$
\left.
\begin{aligned}
w_{xxx} &= 3x(3p + 10x^2)\, r_o^{-7} \\[4pt]
w_{xxy} &= 3y\, p\, r_o^{-7} \\[4pt]
w_{xyy} &= 3x\, q\, r_o^{-7} \\[4pt]
w_{yyy} &= 3y(3q + 10y^2)\, r_o^{-7} \\[4pt]
w_{xxz} &= 3z\, p\, r_o^{-7} \\[4pt]
w_{xyz} &= -15xyz\, r_o^{-7} \\[4pt]
w_{yyz} &= 3z\, q\, r_o^{-7}
\end{aligned}
\right\}
\tag{61}
$$

where r_o is given by (51) and where

$$
\begin{aligned}
p &= y^2 + z^2 - 4x^2 \\[4pt]
q &= x^2 + z^2 - 4y^2
\end{aligned}
\tag{62}
$$

8.22 Comparison of the Exact and Approximate Induced Velocity Formulas.

The approximate induced velocity formulas, (57), (58) and (59) are used in two forms. In one they are used exactly as they stand, which is equivalent to replacing the quadrilateral element by a point source and a point quadrupole. In the second, only the first term in each equation is retained, which is equivalent to replacing the quadrilateral by a point source alone. The velocity components computed by these formulas are seriously in error if they are used at points near the quadrilateral element, but they are quite accurate if the point where the velocities are being evaluated is sufficiently far from the quadrilateral. The criterion used to decide when the use of either form of the approximate equations is valid for a particular point is the ratio of the distance between that point and the centroid of the quadrilateral to some characteristic dimension of the quadrilateral. If this ratio is larger than a certain prescribed number, the quadrilateral is replaced by a source and quadrupole, unless the ratio is also larger than a second prescribed number, in which case the quadrilateral is replaced by a source alone. The characteristic dimension of the quadrilateral used to form this ratio is a quantity called the maximum diagonal of the quadrilateral. This quantity, which is denoted by the symbol t, is defined following equation (84) in Section 9.2. For most quadrilateral elements it is just what its name implies, i.e., the maximum dimension of the quadrilateral. For certain kinds of elements this is

not true. In particular for triangular elements, the maximum diagonal may turn out to be the length of the second longest side. In any case of interest it is, however, within a factor of two of the largest dimension.

Comparisons were made between velocities computed by the exact and approximate formulas for a variety of quadrilateral shapes having unit source density to determine values of the ratio of distance between field point and centroid to maximum diagonal that insure sufficient accuracy in the induced velocity computation. The results of some of these comparisons for two quadrilateral shapes are presented here. The first quadrilateral is a square whose maximum diagonal is just the common length of its diagonals. Figure 11 shows velocity magnitudes computed by the exact formulas, together with the absolute values of the errors in the velocity magnitudes computed by the source-quadrupole formulas and the source formulas. For clarity of presentation, the two error curves have been multiplied by ten. Each set of curves represents velocities computed at points along a particular line. As shown in the sketches on the figure, two such lines are in the plane of the square — one intersecting the square at a corner (figure 11a) and one at the midpoint of a side (figure 11b) —, while the other two lines are normal to the plane of the square — one intersecting this plane at the centroid (figure 11c) and one at a corner (figure 11d). In all cases except that shown in figure 11c the velocity magnitude computed by the exact formulas becomes infinite at a finite distance from the centroid, i.e., on the edge of the quadrilateral, so that the error curves in these cases have vertical asymptotes. The locations of the asymptotes can be inferred from the sketches. The axis is a vertical asymptote for the error curves of figure 11c, since both sets of approximate formulas give infinite values of the velocity magnitude at the centroid while the exact formulas give a finite value. The square is a particularly favorable case for the multipole expansion and it can be seen that the approximate formulas are quite accurate even very near the square. As a measure of the absolute size of these velocities, it might be recalled that the normal velocity at points on the square is 2π. The second quadrilateral shape chosen is the isosceles right triangle. The maximum diagonal is taken as the length of one of the legs of the triangle. Figure 12 shows velocity magnitudes computed by the exact formulas, together with the absolute values of the errors in the velocity magnitudes computed by the two sets of approximate formulas. Again,
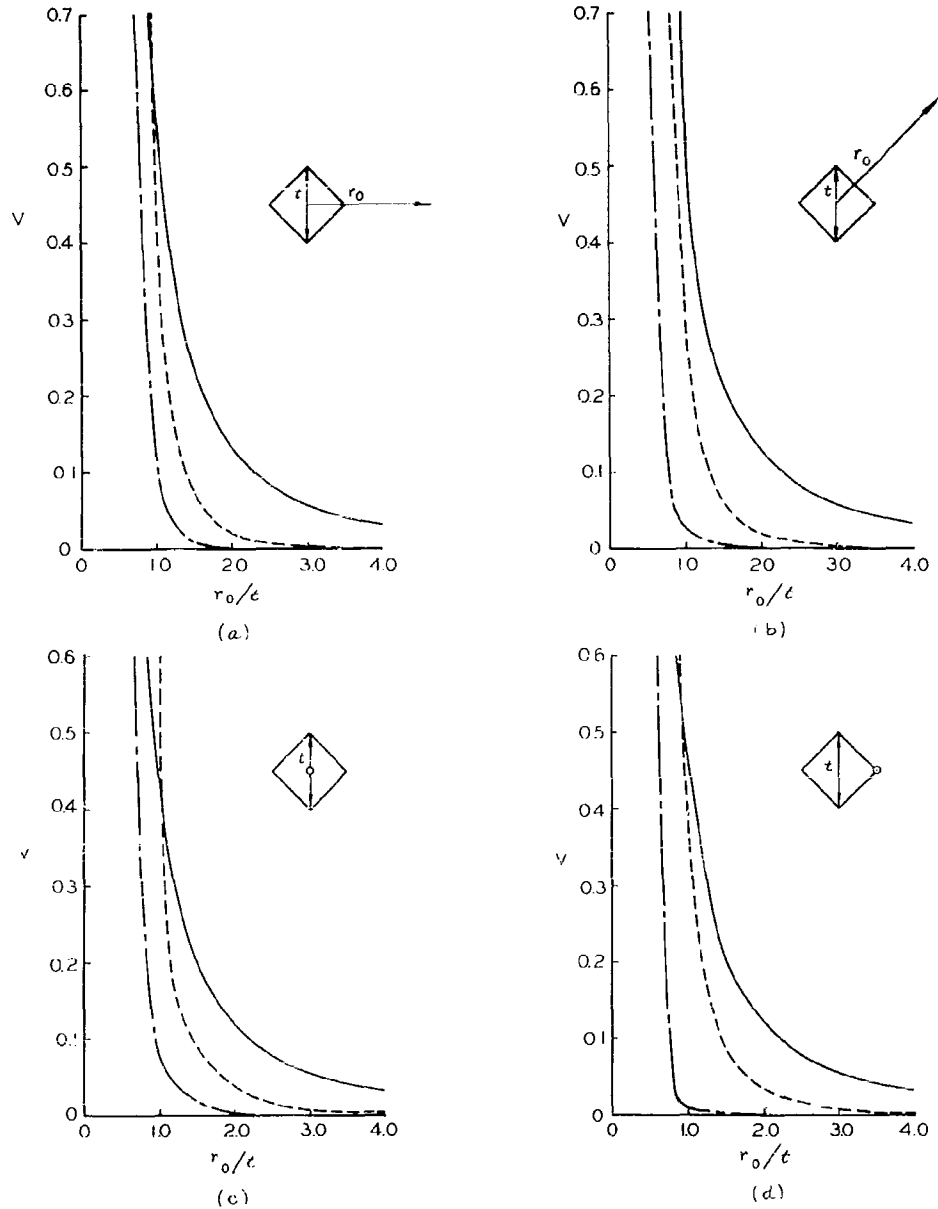
Figure 11. - Errors in the velocity magnitudes computed by the source and source-quadrupole formulas for a square element. In parts (a) and (b) the velocities are evaluated at points along lines in the plane of the element as shown in the sketches. In parts (c) and (d) the velocities are evaluated at points along lines perpendicular to the plane of the element. The intersections of these lines with the plane of the element are shown in the sketches. In all cases the abscissa represents the distance between the centroid of the element and the point where the velocity is evaluated.

55

Figure 12. - Errors in the velocity magnitudes computed by the source and source -quadrupole formulas for an isosceles right triangle element. In parts (a) and (b) the velocities are evaluated at points along lines in the plane of the element as shown in the sketches. In parts (c) and (d) the velocities are evaluated at points along lines perpendicular to the plane of the element. The intersections of these lines with the plane of the element are shown in the sketches. In all cases the abscissa represents the distance between the centroid of the element and the point where the velocity is evaluated.

56

the error curves have been multiplied by ten. As was done for the square, the points where the velocity is evaluated are distributed on four lines: two in the plane of the triangle, one of which intersects the triangle at a corner (figure 12a) and one at the midpoint of a side (figure 12b), and two normal to the plane of the triangle, one of which intersects the triangle at its centroid (figure 12c) and one at a corner (figure 12d). As before, the abscissa of these plots is the ratio of the distance of a point from the centroid of the triangle to the maximum diagonal. The error curves for the triangle have vertical asymptotes at various locations as was explained above for the square. The isosceles right triangle is a relatively unfavorable case for the multipole expansion, but still the approximate formulas give accurate values of the velocity at some distance from the centroid.

Comparisons similar to the above were made for a variety of quadrilateral shapes and for the individual velocity components as well as the velocity magnitude. It was decided that the simple source formulas are sufficiently accurate if the point where the velocity is being evaluated has a distance from the centroid of the quadrilateral element of at least 4 times the length of the maximum diagonal of the element. The source-quadrupole formulas are sufficiently accurate if this distance is at least $\sqrt{6} = 2.45$ times the length of the maximum diagonal. If these values are used, the maximum error in any velocity component due to using the approximate formulas is less than 0.001 in the worst case.

9.0   THE EXPLICIT COMPUTATION METHOD

The manner in which this flow computation method has been implemented for the computing machine is explained in detail in the various parts of this section.

9.1   Input Scheme

9.11   General Input Procedure.

The way in which a body surface is input to the machine program is explained below together with certain restrictions. The information will probably be of interest only to those who intend to use the method.

The input to this program consists of the coordinates of a number of points. These points define the surface of the three-dimensional body around which the flow is to be computed. Their coordinates are given in the reference coordinate system. For the purpose of organizing these points for computation, each point is assigned a pair of integers, m and n. These integers need not be input, but their use must be understood to insure the correctness of the input and to facilitate the interpretation of the output.

For each point, n identifies the ''column'' of points to which it belongs, while m identifies its position in the ''column'', i.e., the ''row''. The first point of a ''column'' always has $m = 1$. To insure that the program will compute outward normal vectors, the following condition must be satisfied by the input points. If an observer is located in the flow and is oriented so that locally he sees points on the surface with m values increasing upward, he must also see n values increasing toward the right. Examples of correct and incorrect input are shown in figure 13. In this figure the flow field lies above the paper, while the interior of the body lies below the paper. Occasionally, it happens that despite all care a body is input incorrectly. If the entire body is input incorrectly — not some sections correctly and some incorrectly —, the difficulty can be remedied by changing the sign of one coordinate of all the input points. This trick will give a correctly input body of the proper shape at perhaps a peculiar location. Otherwise, the input will have to be done over.

Quadrilateral elements are computed from groups of four neighboring points. Two of these points are on one ''column'' or n-line and have consecutive values of m. The other two are on the next highest n-line at the same values of m, respectively, as the first two. An element is identified by a pair of integers that are the same as those used to identify the point with the lowest values of m and n of the four used to form the element. The element identified by the integers m, n is formed from the points corresponding to: m, n; m + 1, n; m, n + 1; and m + 1, n + 1.

Figure 13. - Examples of correct and incorrect input.

The body surface is imagined divided into sections, which may be actual physical divisions or may be selected for convenience. A section is defined as consisting of a certain number of n-lines, say N_T, and this number, which must be at least two, must be specified on the input at the beginning of the section. Within each section the n-lines are input in order of increasing n. On each n-line the points are input in order of increasing m. The number of points on each n-line, say M_n, must be specified on the input at the beginning of each n-line. The first n-line of the first section is n = 1. From then on the n-lines are numbered consecutively through all sections, i.e., the numbering is not begun over at the beginning of each section. Elements will be formed that are associated with points on every n-line except those that are last in their respective sections. Points on these latter n-lines are used only to form elements associated with points on the next lowest n-lines.

The logic of the computation proceeds as follows. Suppose the program is ready to compute the elements associated with the points on a particular n-line, say the line n. To do this it uses the points on the line n and the

line n + 1. Let the number of points on the line n be M_n and the number on the line n + 1 be M_{n+1}. The difference $\Delta M_n = M_{n+1} - M_n$ is computed. If this is non-negative, the program computes the $M_n - 1$ elements associated with the points m = 1, 2, ..., $M_n - 1$ on the line n. The last point on the line is skipped, and the program proceeds to the next point which is the first point on the line n + 1, and prepares to compute the elements associated with the points on the latter line. If the difference ΔM_n is negative, the program computes the $M_{n+1} - 1$ elements associated with the points m = 1, 2, ..., $M_{n+1} - 1$ on the line n. The next $|\Delta M_n| + 1$ points are skipped, and the program proceeds to the $(|\Delta M_n| + 2)$th point after that, which is the first point on the line n + 1, and prepares to compute the elements associated with the points on the latter line. When the first point on the last n-line of a section is reached, say the line N_T, the program skips all M_{N_T} points on that line and proceeds to the first point on the first n-line of the new section. This process continues until elements have been computed for all sections.

To illustrate this procedure, consider the plan view of a body shown in figure 14.
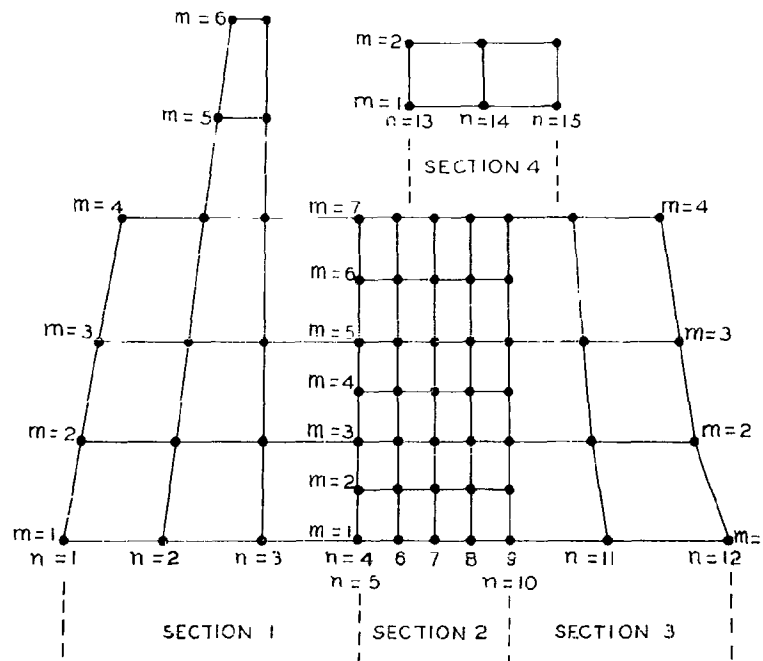
Figure 14. - Plan view of the input points on a body divided into sections.

This body has been divided into four sections. The first section contains four n-lines, n = 1, 2, 3, 4; the second, five n-lines, n = 5, 6, 7, 8, 9; the third three n-lines, n = 10, 11, 12; and the fourth, three n-lines, n = 13, 14, 15. In the first section the number of points on each n-line is:

$$n = 1 \quad 2 \quad 3 \quad 4$$

$$M_n = 4 \quad 6 \quad 6 \quad 4$$

The program finds $\Delta M_1 = 6 - 4 = 2 > 0$, so it computes $M_1 - 1 = 3$ elements for this line corresponding to the points $m = 1, 2, 3$. It skips the point $m = 4$, $n = 1$ and proceeds to the next point, which is $m = 1$, $n = 2$. Since $\Delta M_2 = 6 - 6 = 0$, $M_2 - 1 = 5$ elements are computed for this line corresponding to the points $m = 1, 2, 3, 4, 5$. The point $m = 6$, $n = 2$ is skipped, and the program proceeds to the next point, which is $m = 1$, $n = 3$. Here it finds $\Delta M_3 = 4 - 6 = -2 < 0$, so it computes $M_4 - 1 = 3$ elements for this line corresponding to the points $m = 1, 2, 3$. Now $|\Delta M_3| + 1 = 3$ points, i.e., $m = 4, 5, 6$, are skipped, and the program proceeds to the point $m = 1$, $n = 4$. Notice that the line $n = 4$ has only four points, the points $m = 1, 2, 3, 4$ in the m-grid of section 1, which is listed in the figure along the $n = 1$ and $n = 2$ lines. It is these points that are used to form the elements associated with the points of line $n = 3$. When the program reaches the point $m = 1$, $n = 4$, it realizes it has attained the fourth and last n-line of section 1, so it skips $M_4 = 4$ points and proceeds to point $m = 1$, $n = 5$, the first point of section 2. Notice that this point is identical with the point $m = 1$, $n = 4$ that the program just left, and indeed the lines $n = 4$ and $n = 5$ are physically identical. Some of the points on the two lines are physically identical but correspond to different values of m. This is of no consequence. In this scheme sections are completely independent. The program determines that it has entered a new section with five n-lines and proceeds to compute. Since $M_n = 7$, $\Delta M_n = 0$ for all n-lines in this section, $M_n - 1 = 6$ elements, corresponding to the points $m = 1, 2, 3, 4, 5, 6$, are computed for each of the lines $n = 5, 6, 7, 8$. The fifth n-line of section 2, $n = 9$, is skipped and the program proceeds to the first point of section 3, $m = 1$, $n = 10$. Again notice that lines $n = 9$ and $n = 10$ are physically identical. Now three elements are computed for each of the lines $n = 10$ and $n = 11$ of section 3, and the program skips to the physically isolated section 4. Notice

61

that the n = 13 line of this section is aligned with the n = 7 line of
section 2 and that the points for which m = 2 are aligned with the m = 6
points of section 1. These facts are irrelevant because of the independence
of the sections. After one element is computed for each of the lines n = 13
and n = 14, the program realizes it has completed the last section and goes on
to other computations. Notice that no elements were computed corresponding
to points on lines n = 4, 9, 12, 15.
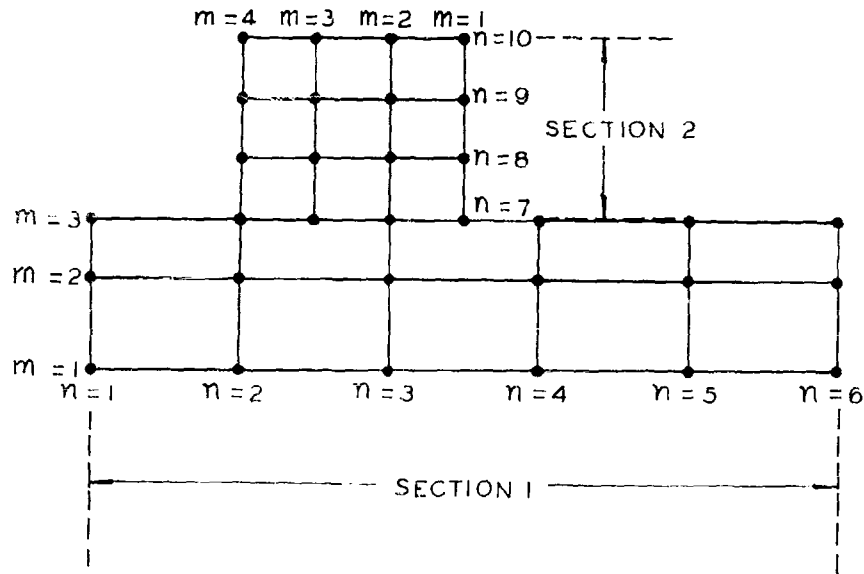
Figure 15. - Another possible division into sections.

There is no restriction that the m and n lines of different sections
have to be roughly parallel. The arrangement shown in figure 15 is per-
missible.

Bending the n-lines at their ends to form triangular or nearly triangular
elements is sometimes useful in cases of thin bodies of rounded planform.
Figure 16 shows an example of a triangular element. Notice that the point
m + 1, n may be located anywhere on the line between points m, n and m + 1,
n + 1 without changing the element. In particular, it may be taken coincident
with either m, n or m + 1, n + 1. An example of the use of this device to
fit a rounded planform is shown in figure 17. Notice that the number of points
on each n-line is increasing by one per line on the left portion of the body
and decreasing by one per line on the right portion.
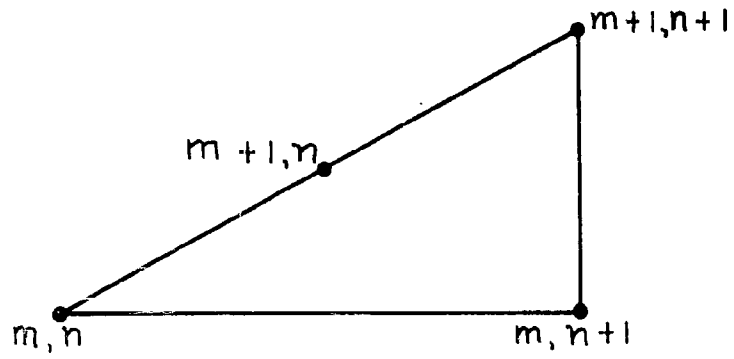
Figure 16. - The location of input points to form a triangular element.
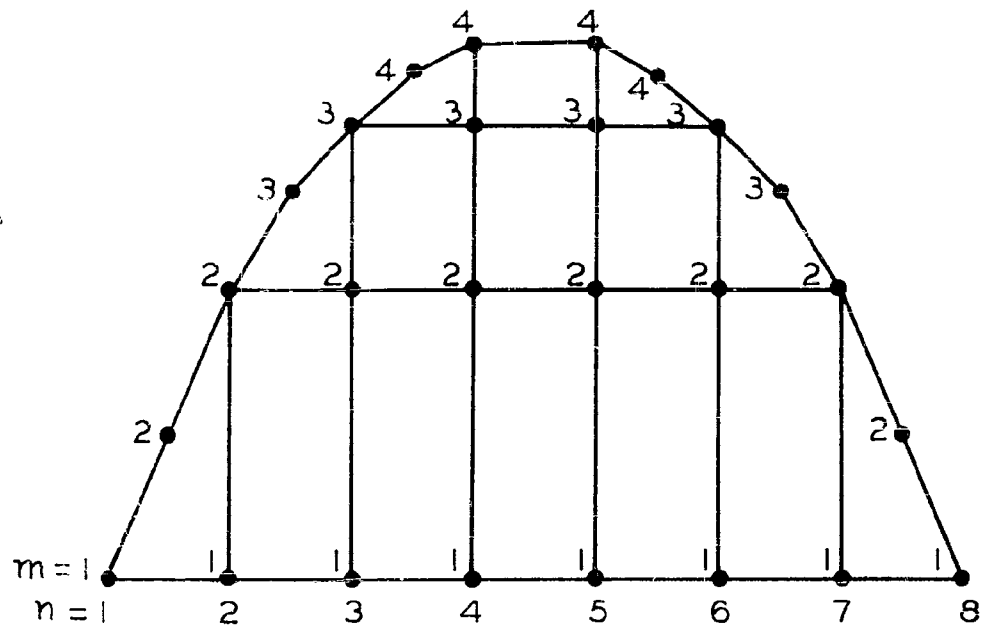
Figure 17. - The use of nearly triangular elements on a thin body of rounded planform.

63
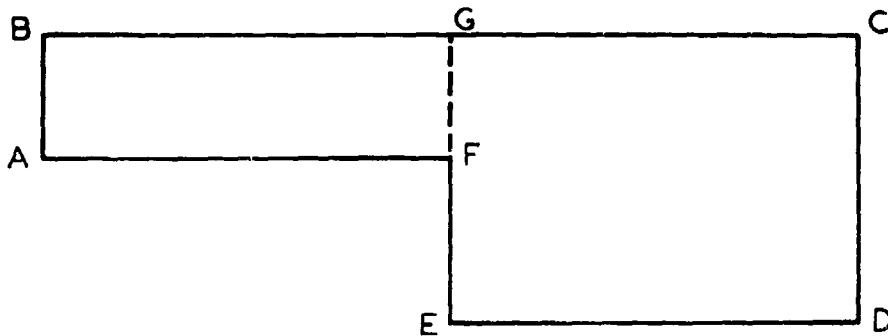
Figure 18. - A restriction on the division of the body into sections.

As a final example, consider the planform in figure 18. The first point on every n-line must be m = 1. Neither line AF nor line ED can correspond to m = 1 unless the body is divided into sections, e.g., along FG. A single section may be used by letting line CD correspond to m = 1 with n increasing from D to C or by letting line BC correspond to m = 1 with n increasing from C to B.

If it is desired to compute flow velocities at points off the body surface, the coordinates of these points, which are designated off-body points, must also be input. The order in which off-body points are input is immaterial. For good accuracy, the distance from an off-body point to the body surface should be at least twice the characteristic dimension of the elements on that portion of the surface. The flow properties at points nearer the surface should be obtained by interpolation between the off-body points and the null points. The interpolation is simpler, and the basic calculational accuracy is higher, if the off-body points near the surface are located along normals to the surface that intersect the surface at null points. Off-body points located near the edges of elements are particularly susceptible to error because of the infinite velocities occurring at these edges.

9.12 Bodies with Symmetry Planes.

If the body surface possesses planes of symmetry, the fact may be noted in the input to the program and only the non-redundant portion need be specified by input points. The other portions are automatically taken into account. The

64

symmetry planes are assumed to be coordinate planes of the reference coordinate system. To facilitate the calculations the choice of which coordinate planes are symmetry planes for a given body is not left open. Particular coordinate planes are selected once and for all as symmetry planes, and the body surface must be input to conform with this selection, or the calculated flow velocities will be meaningless. The assumptions for the symmetry planes are listed below.

If a body has one plane of symmetry this plane must be the xz-plane of the reference coordinate system. The y-coordinates of all input points must have the same sign — either positive or negative. If the body is closed, i.e., if it intersects its symmetry plane, the points in the symmetry plane, i.e., the points having y = 0, must be included among the input points. Usually, the points in the symmetry plane are taken as on a common m-line or n-line.

If a body has two planes of symmetry, these planes must be the xz-plane and the xy-plane of the reference coordinate system. The z coordinates of all input points must have the same sign, and similarly for the y coordinates. They may be of either sign; and the sign need not be the same for the y-coordinates as it is for the z-coordinates. If the body intersects its symmetry planes (or plane), the points in these planes, i.e., the points having y = 0 or z = 0, must be included among the input points.

If a body has three planes of symmetry, these must be the three coordinate planes of the reference coordinate system. The x-coordinates of all input points must have the same sign, and similarly for the y and z coordinates. Any coordinate may have either sign. If the body intersects its symmetry planes, the points in these planes, i.e., points having zero value of a coordinate, must be included among the input points.

Thus with the usual orientation of coordinate axes, a body may have a ''right and left'' symmetry, a ''right and left'' and ''up and down'' symmetry, or a ''right and left'', ''up and down'', and ''fore and aft'' symmetry. In some cases this may not be the most natural way to specify the body, but the resulting inconvenience should be minor. Any direction of the onset flow may

65

be specified for all cases.

Off-body points in cases with symmetry planes are handled the same way as was described previously.

9.2 Formation of the Plane Quadrilateral Surface Element.

Suppose now that the stage of the calculation has been reached at which it is required to form a plane surface element from the four points whose identifying integers are m, n; $m + 1$, n; $m + 1$, $n + 1$; and m, $n + 1$. Since only one element is considered here, it is convenient to identify the points by the subscripts 1, 2, 3, and 4 respectively. See figure 19. Notice that the points are numbered consecutively around the elements as was illustrated in figure 5. Let these points have input coordinates in the reference coordinate system as follows:
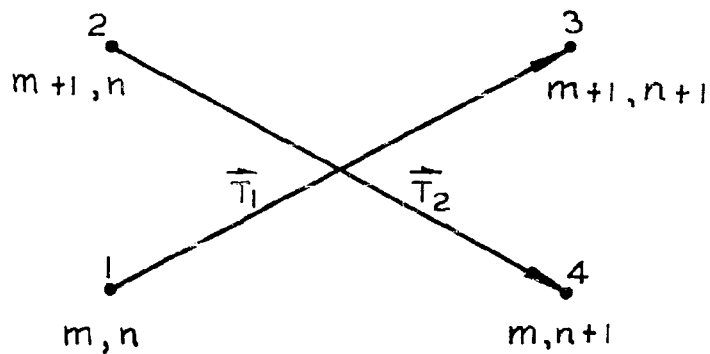
Figure 19. - The formation of an element from four input points.

$$1 \; : \; x_1^i \quad y_1^i \quad z_1^i$$

$$2 \; : \; x_2^i \quad y_2^i \quad z_2^i$$

$$3 \; : \; x_3^i \quad y_3^i \quad z_3^i \tag{63}$$

$$4 \; : \; x_4^i \quad y_4^i \quad z_4^i$$

The superscript i identifies the coordinates as input coordinates. Now the two ''diagonal'' vectors are formed — the vector $\vec{T}_1$ from point 1 to point 3 and the vector $\vec{T}_2$ from point 2 to point 4: In general these vectors are not orthogonal. Their components are:

$$T_{1x} = x_3^i - x_1^i \qquad T_{1y} = y_3^i - y_1^i \qquad T_{1z} = z_3^i - z_1^i$$

$$T_{2x} = x_4^i - x_2^i \qquad T_{2y} = y_4^i - y_2^i \qquad T_{2z} = z_4^i - z_2^i \tag{64}$$

The vector $\vec{N}$ is taken as the cross product of these, i.e., $\vec{N} = \vec{T}_2 \times \vec{T}_1$. Its components are:

$$N_x = T_{2y} T_{1z} - T_{1y} T_{2z}$$

$$N_y = T_{1x} T_{2z} - T_{2x} T_{1z} \tag{65}$$

$$N_z = T_{2x} T_{1y} - T_{1x} T_{2y}$$

The unit normal vector, $\vec{n}$, to the plane of the element is taken as $\vec{N}$ divided by its own length N, i.e.,

$$n_x = \frac{N_x}{N}$$

$$n_y = \frac{N_y}{N} \tag{66}$$

$$n_z = \frac{N_z}{N}$$

where

$$N = \sqrt{N_x^2 + N_y^2 + N_z^2} \tag{67}$$

The plane of the element is now completely determined if a point in this plane is specified. This point is taken as the point whose coordinates $\bar{x}, \bar{y}, \bar{z}$ are the averages of the coordinates of the four input points, i.e.,

$$\bar{x} = \frac{1}{4}\left[x_1^i + x_2^i + x_3^i + x_4^i\right]$$

$$\bar{y} = \frac{1}{4}\left[y_1^i + y_2^i + y_3^i + y_4^i\right] \tag{68}$$

$$\bar{z} = \frac{1}{4}\left[z_1^i + z_2^i + z_3^i + z_4^i\right]$$

Now the input points will be projected into the plane of the element along the normal vector. The resulting points are the corner points of the quadrilateral element. The signed distance of the k-th input point (k = 1, 2, 3, 4) from the plane is

$$d_k = n_x(\bar{x} - x_k^i) + n_y(\bar{y} - y_k^i) + n_z(\bar{z} - z_k^i) \qquad k = 1, 2, 3, 4 \tag{69}$$

It turns out that, due to the way in which the plane was generated from the input points, all the d_k's have the same magnitude, those for points 1 and 3 having one sign and those for points 2 and 4 having the opposite sign. Symbolically,

$$d_k = (-1)^{k-1} d_1 \qquad k = 1, 2, 3, 4 \tag{70}$$

The magnitude of the common projection distance is called d, i.e.,

$$d = |d_1| \tag{71}$$

The coordinates of the corner points in the reference coordinate system are given by

$$x_k' = x_k^i + n_x d_k$$

$$y_k' = y_k^i + n_y d_k \qquad k = 1, 2, 3, 4 \tag{72}$$

$$z_k' = z_k^i + n_z d_k$$

Now the element coordinate system must be constructed. This requires the components of three mutually perpendicular unit vectors, one of which points along each of the coordinate axes of the system, and also the coordinates of the

68

origin of the coordinate system. All these quantities must be given in terms of the reference coordinate system. The unit normal vector is taken as one of the unit vectors, so two perpendicular unit vectors in the plane of the element are needed. Denote these unit vectors $\vec{t}_1$ and $\vec{t}_2$. The vector $\vec{t}_1$ is taken as $\vec{T}_1$ divided by its own length T_1, i.e.,

$$t_{1x} = \frac{T_{1x}}{T_1}$$

$$t_{1y} = \frac{T_{1y}}{T_1}$$

$$t_{1z} = \frac{T_{1z}}{T_1}$$

(73)

where

$$T_1 = \sqrt{T_{1x}^2 + T_{1y}^2 + T_{1z}^2}$$

(74)

The vector $\vec{t}_2$ is defined by $\vec{t}_2 = \vec{n} \times \vec{t}_1$, so that its components are

$$t_{2x} = n_y t_{1z} - n_z t_{1y}$$

$$t_{2y} = n_z t_{1x} - n_x t_{1z}$$

$$t_{2z} = n_x t_{1y} - n_y t_{1x}$$

(75)

The vector $\vec{t}_1$ is the unit vector parallel to the x or ξ axis of the element coordinate system, while $\vec{t}_2$ is parallel to the y or η axis, and $\vec{n}$ is parallel to the z or ζ axis of this coordinate system.

To transform the coordinates of points and the components of vectors between the reference coordinate system and the element coordinate system, the transformation matrix is required. The elements of this matrix are the components of the three basic unit vectors, $\vec{t}_1$, $\vec{t}_2$, and $\vec{n}$. To make the notation uniform define

$$a_{11} = t_{1x} \qquad a_{12} = t_{1y} \qquad a_{13} = t_{1z}$$

$$a_{21} = t_{2x} \qquad a_{22} = t_{2y} \qquad a_{23} = t_{2z} \qquad (76)$$

$$a_{31} = n_x \qquad a_{32} = n_y \qquad a_{33} = n_z$$

The transformation matrix is thus the array

$$
\begin{array}{ccc}
a_{11} & a_{12} & a_{13} \\
a_{21} & a_{22} & a_{23} \\
a_{31} & a_{32} & a_{33}
\end{array} \qquad (77)
$$

To transform the coordinates of points from one system to the other, the coordinates of the origin of the element coordinate system in the reference coordinate system are required. Let these be denoted x_o, y_o, z_o. Then if a point has coordinates x', y', z' in the reference coordinate system and coordinates x, y, z in the element coordinate system, the transformation from the reference to the element system is

$$x = a_{11}(x' - x_o) + a_{12}(y' - y_o) + a_{13}(z' - z_o)$$

$$y = a_{21}(x' - x_o) + a_{22}(y' - y_o) + a_{23}(z' - z_o) \qquad (78)$$

$$z = a_{31}(x' - x_o) + a_{32}(y' - y_o) + a_{33}(z' - z_o)$$

while the transformation from the element to the reference system is

$$x' = x_o + a_{11}x + a_{21}y + a_{31}z$$

$$y' = y_o + a_{12}x + a_{22}y + a_{32}z \qquad (79)$$

$$z' = z_o + a_{13}x + a_{23}y + a_{33}z$$

Vectors are transformed in a similar way. If a vector has components V_x, V_y, V_z in the element coordinate system and components V_x', V_y', V_z', in the

70

reference coordinate system, these are related by equations (78) and (79), where V_x, V_y, V_z replace x, y, z, respectively, in these equations and V'_x, V'_y, V'_z replace $(x' - x_o)$, $(y' - y_o)$, $(z' - z_o)$. The origin is temporarily taken as the point whose coordinates are the averages of those of the four input points, i.e., the point with coordinates $\bar{x}$, $\bar{y}$, $\bar{z}$ in the reference system.

The corner points are now transformed into the element coordinate system based on the average point as origin. These points have coordinates x'_k, y'_k, z'_k in the reference coordinate system. Their coordinates in the element coordinate system with this origin are denoted by ξ^*_k, η^*_k, 0. Because they lie in the plane of the element, they have a zero z or ζ coordinate in the element coordinate system. Also, because the vector $\bar{t}_1$, which defines the x or ξ axis of the element coordinate system, is a multiple of the "diagonal" vector from point 1 to point 3, the coordinate η^*_1 and the coordinate η^*_3 are equal. This is illustrated in figure 20. Using the above transformation these coordinates are explicitly
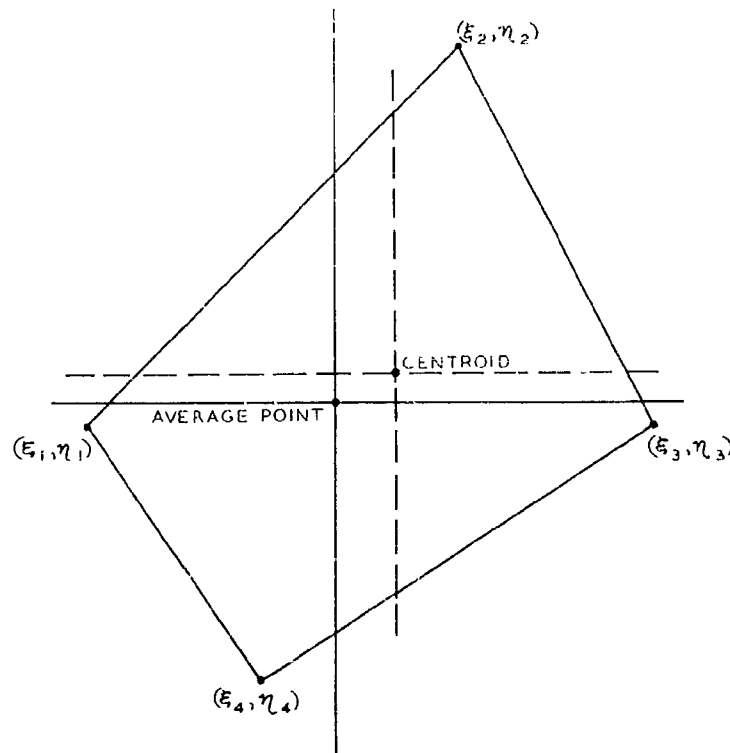
.Figure 20. - A plane quadrilateral element. Transfer of origin from average point to null point.

71

$$\xi_k^* = a_{11}(x_k' - \bar{x}) + a_{12}(y_k' - \bar{y}) + a_{13}(z_k' - \bar{z})$$
$$\eta_k^* = a_{21}(x_k' - \bar{x}) + a_{22}(y_k' - \bar{y}) + a_{23}(z_k' - \bar{z}) \qquad k = 1, 2, 3, 4 \qquad (80)$$

These corner points are taken as the corners of a plane quadrilateral which is the fundamental source element employed in this method.

The origin of the element coordinate system is now transferred to the centroid of the area of the quadrilateral. With the average point as origin the coordinates of the centroid in the element coordinate system are:

$$\xi_0 = \frac{1}{3} \frac{1}{\eta_2^* - \eta_4^*} \left[\xi_4^*(\eta_1^* - \eta_2^*) + \xi_2^*(\eta_4^* - \eta_1^*) \right]$$

$$\eta_0 = -\frac{1}{3} \eta_1^* \qquad (81)$$

These are subtracted from the coordinates of the corner points in the element coordinate system based on the average point as origin to obtain the coordinates of the corner points in the element coordinate system based on the centroid as origin (see figure 20). Accordingly, these latter coordinates are

$$\xi_k = \xi_k^* - \xi_0$$
$$\eta_k = \eta_k^* - \eta_0 \qquad k = 1, 2, 3, 4 \qquad (82)$$

Since the centroid is to be used as the origin of the element coordinate system, its coordinates in the reference coordinate system are required for use with the transformation matrix. These coordinates are

$$x_0 = \bar{x} + a_{11}\xi_0 + a_{21}\eta_0$$
$$y_0 = \bar{y} + a_{12}\xi_0 + a_{22}\eta_0 \qquad (83)$$
$$z_0 = \bar{z} + a_{13}\xi_0 + a_{23}\eta_0$$

Since in all subsequent transformations between the reference coordinate system and the element coordinate system the centroid is used as origin of the latter, its coordinates are denoted x_0, y_0, z_0 to conform with the notation of equations (78) and (79). The coordinates of the average point are no longer needed. The change in origin of the element coordinate system of course has no effect on the coordinates of the corner points in the reference coordinate system.

The lengths of the two diagonals of the quadrilateral, t_1 and t_2, are computed from

$$t_1^2 = (\xi_3 - \xi_1)^2$$

$$t_2^2 = (\xi_4 - \xi_2)^2 + (\eta_4 - \eta_2)^2 \tag{84}$$

The larger of these is selected and designated the maximum diagonal, t.

The coefficients of the zeroth and second order terms in the multipole expansion of the velocity induced by a quadrilateral element consist of the area of the quadrilateral and the three second moments of the area (see Section 8.21). In terms of the coordinates of the corner points, the area of the quadrilateral is

$$A = \frac{1}{2} (\xi_3 - \xi_1)(\eta_2 - \eta_4) \tag{85}$$

while the second moments are

$$I_{xx} = \frac{1}{12} (\xi_3 - \xi_1) \Big[\eta_1(\xi_4 - \xi_2)(\xi_1 + \xi_3 + \xi_2 + \xi_4) +$$
$$+ (\eta_2 - \eta_4)(\xi_1^2 + \xi_1 \xi_3 + \xi_3^2) + \tag{86}$$
$$+ \xi_2 \eta_2(\xi_1 + \xi_3 + \xi_2) - \xi_4 \eta_4(\xi_1 + \xi_3 + \xi_4) \Big]$$

$$I_{xy} = \frac{1}{24}(\xi_3 - \xi_1) \Big[2\xi_4(\eta_1^2 - \eta_4^2) - 2\xi_2(\eta_1^2 - \eta_2^2) +$$
$$+ (\xi_1 + \xi_3)(\eta_2 - \eta_4)(2\eta_1 + \eta_2 + \eta_4) \Big] \tag{87}$$

73

$$I_{yy} = \frac{1}{12}(\xi_3 - \xi_1)(\eta_2 - \eta_4)\left[(\eta_1 + \eta_2 + \eta_4)^2 - \eta_1(\eta_2 + \eta_4) - \eta_2\eta_4\right] \tag{88}$$

In obtaining these formulas use has been made of the fact that $\eta_1 = \eta_3$.

9.3 Determination of the Null Point

The point of the quadrilateral element at which induced velocities are to be computed is the so-called null point, i.e., the point where the element itself induces no velocity in its own plane. The x and y coordinates of this point in the element coordinate system are obtained as the solution of two simultaneous non-linear equations. These equations are

$$V_x(x, y) = 0$$
$$V_y(x, y) = 0 \tag{89}$$

where the expressions for V_x and V_y are those given in equations (42) and (43) with $z = 0$ and the ξ_k, η_k, $k = 1, 2, 3, 4$, set equal to the coordinates of the corner points which were obtained in the previous section.

These equations are solved by means of an iterative procedure, which utilizes analytic expressions for the derivatives of V_x and V_y. With the notation $(\ )_x = \partial/\partial x$, $(\ )_y = \partial/\partial y$, these derivatives can be written

$$(V_x)_x = \frac{\eta_2 - \eta_1}{D_{12}}(r_1 + r_2)_x + \frac{\eta_3 - \eta_2}{D_{23}}(r_2 + r_3)_x + \frac{\eta_4 - \eta_3}{D_{34}}(r_3 + r_4)_x + \frac{\eta_1 - \eta_4}{D_{41}}(r_4 + r_1)_x$$

$$(V_x)_y = \frac{\eta_2 - \eta_1}{D_{12}}(r_1 + r_2)_y + \frac{\eta_3 - \eta_2}{D_{23}}(r_2 + r_3)_y + \frac{\eta_4 - \eta_3}{D_{34}}(r_3 + r_4)_y + \frac{\eta_1 - \eta_4}{D_{41}}(r_4 + r_1)_y$$

$$(V_y)_x = \frac{\xi_1 - \xi_2}{D_{12}}(r_1 + r_2)_x + \frac{\xi_2 - \xi_3}{D_{23}}(r_2 + r_3)_x + \frac{\xi_3 - \xi_4}{D_{34}}(r_3 + r_4)_x + \frac{\xi_4 - \xi_1}{D_{41}}(r_4 + r_1)_x$$

$$(V_y)_y = \frac{\xi_1 - \xi_2}{D_{12}}(r_1 + r_2)_y + \frac{\xi_2 - \xi_3}{D_{23}}(r_2 + r_3)_y + \frac{\xi_3 - \xi_4}{D_{34}}(r_3 + r_4)_y + \frac{\xi_4 - \xi_1}{D_{41}}(r_4 + r_1)_y$$

$$\tag{90}$$

where

$$(r_1 + r_2)_x = \frac{x - \xi_1}{r_1} + \frac{x - \xi_2}{r_2}$$

$$(r_2 + r_3)_x = \frac{x - \xi_2}{r_2} + \frac{x - \xi_3}{r_3}$$

$$(r_3 + r_4)_x = \frac{x - \xi_3}{r_3} + \frac{x - \xi_4}{r_4} \tag{91}$$

$$(r_4 + r_1)_x = \frac{x - \xi_4}{r_4} + \frac{x - \xi_1}{r_1}$$

$$(r_1 + r_2)_y = \frac{y - \eta_1}{r_1} + \frac{y - \eta_2}{r_2}$$

$$(r_2 + r_3)_y = \frac{y - \eta_2}{r_2} + \frac{y - \eta_3}{r_3}$$

$$(r_3 + r_4)_y = \frac{y - \eta_3}{r_3} + \frac{y - \eta_4}{r_4} \tag{92}$$

$$(r_4 + r_1)_y = \frac{y - \eta_4}{r_4} + \frac{y - \eta_1}{r_1}$$

and

$$2\, D_{12} = (r_1 + r_2)^2 - d_{12}^{\,2}$$

$$2\, D_{23} = (r_2 + r_3)^2 - d_{23}^{\,2}$$

$$2\, D_{34} = (r_3 + r_4)^2 - d_{34}^{\,2} \tag{93}$$

$$2\, D_{41} = (r_4 + r_1)^2 - d_{41}^{\,2}$$

These derivatives can be evaluated very quickly. The time required for their computation is much less than that required for the computation of V_x and V_y. Since the velocity is the negative gradient of a potential function φ, it is true that $(V_x)_y = (V_y)_x$. However, it was found convenient to calculate each separately and to use this fact as a check on the correctness of the programming.

The iterative procedure is as follows. Let x_p and y_p denote the p-th approximation to the x and y coordinates of the null point, and let the notation $[\ ]^{(p)}$ denote the quantity in brackets evaluated at $x = x_p$, $y = y_p$. Once the p-th approximation has been found, the (p + 1)-th approximation is obtained by solving the following pair of linear algebraic equations for x_{p+1}, y_{p+1}.

$$\left[(V_x)_x\right]^{(p)}(x_{p+1} - x_p) + \left[(V_x)_y\right]^{(p)}(y_{p+1} - y_p) = -\left[V_x\right]^{(p)}$$

$$\left[(V_y)_x\right]^{(p)}(x_{p+1} - x_p) + \left[(V_y)_y\right]^{(p)}(y_{p+1} - y_p) = -\left[V_y\right]^{(p)}$$

(94)

The first approximation is $x = y = 0$, i.e., the centroid of the quadrilateral. The iterative procedure is terminated when the induced velocity components at the approximate null point are both less in absolute value than a prescribed value. This value is set at 0.0001.

This iterative procedure is thus a gradient method in that the non-linear equations (89) are replaced by the linear equations (94), whose coefficients are the derivatives of the non-linear functions. The corrections to the values of x_p and y_p computed from (94) are correct to first order and are in error by terms proportional to the second derivatives of V_x and V_y. The method is seen to be the two-dimensional analogue of the Newton-Raphson procedure for a single non-linear equation. Usually the convergence is fairly rapid - three or four iterations. This is partly due to the fact that for most quadrilaterals the centroid is quite close to the null point.

There is one case where the procedure converges to the wrong point. This occurs for quadrilateral elements that are approximately long thin triangles. More precisely, the unfavorable case occurs when an element has two sides that are much longer than the other two and either the long sides are adjacent, as shown in figure 21a or one of the short sides is large compared to the other, as shown in figure 21b. As can be seen in figure 21, in both these cases the quadrilaterals are approximately triangles with a large ''altitude'' to ''base'' ratio. The iterative procedure fails if this ratio is larger than about thirty.
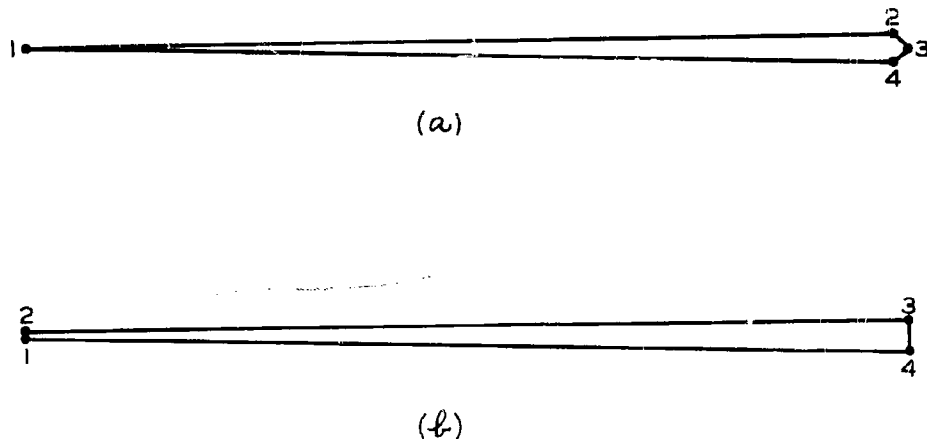
Figure 21. - Elements for which the calculated null point is outside.

For such elements the induced velocity is a slowly varying function of position along the long dimension of the element and the first correction obtained from (94) using the centroid is such that the next approximation is a point outside the element. From then on successive approximations are points further and further away from the element as the procedure seeks out the ''null point'' at infinity, where the induced velocity is obviously zero. While an iteration scheme could probably be devised that converged in such cases, it has not been done. Instead, after the iterative procedure has converged, the distance between the computed null point and the centroid is computed. (It is just the distance of the null point from the origin since the calculation is performed in the element coordinate system.) If the distance is smaller than the maximum diagonal of the element as defined following equation (84), the calculation proceeds normally, for the true null point is the only point this near the centroid where the induced velocity components are sufficiently small for the iterative procedure to converge. If this distance is larger than the maximum diagonal, the computed null point is outside the element, and it is discarded. In this case the centroid replaces the null point in all subsequent calculations.

There is another type of element for which the procedure does not converge, namely an element having one diagonal much shorter than any side as shown in figure 22. For such elements the induced velocity varies rapidly with distance along the short dimension. Successive approximations to the null point form a non-convergent sequence, all of which are quite close to the

77
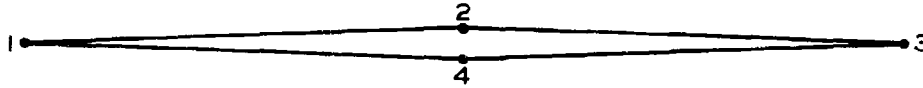
, Figure 22. - An element for which the null point iterative procedure does not converge. ,

true null point. The procedure is simply terminated after thirty iterations and the last approximation used in subsequent computations.

It should be mentioned that no systematic study of the convergence of this iterative procedure was conducted, but difficulties were remedied as they occurred in the actual calculation of potential flows. There may be other types of elements for which the null point cannot be calculated in this manner, but if so they have not been encountered in almost a year of using this method for a variety of body shapes. In fact, it is intuitively clear that if any of the above types of elements occur in practice, it implies that the points used to define the body surface were not intelligently distributed.

If either of the above substitutes for the null point are used rather than the null point itself, this fact is noted on the first output from the machine as described in the next section. In any event a point on the element is selected at which induced velocities are to be evaluated, and this point will subsequently be referred to as the null point regardless of what it actually is. The coordinates of this point in the element coordinate system are denoted x_{np}, y_{np}. These are transformed into the reference coordinate system by means of the transformation matrix as shown in equation (79) to obtain the coordinates, x'_{np}, y'_{np}, z'_{np}, of the null point in the reference coordinate system.

Finally, to illustrate the location of the null point, calculations were performed for a series of isosceles triangles of various altitude to base ratios. The results are given in figure 23. It can be seen that for very small altitude to base ratios the null point occurs at half the altitude, while for large values of this ratio it approaches the base of the triangle.

78
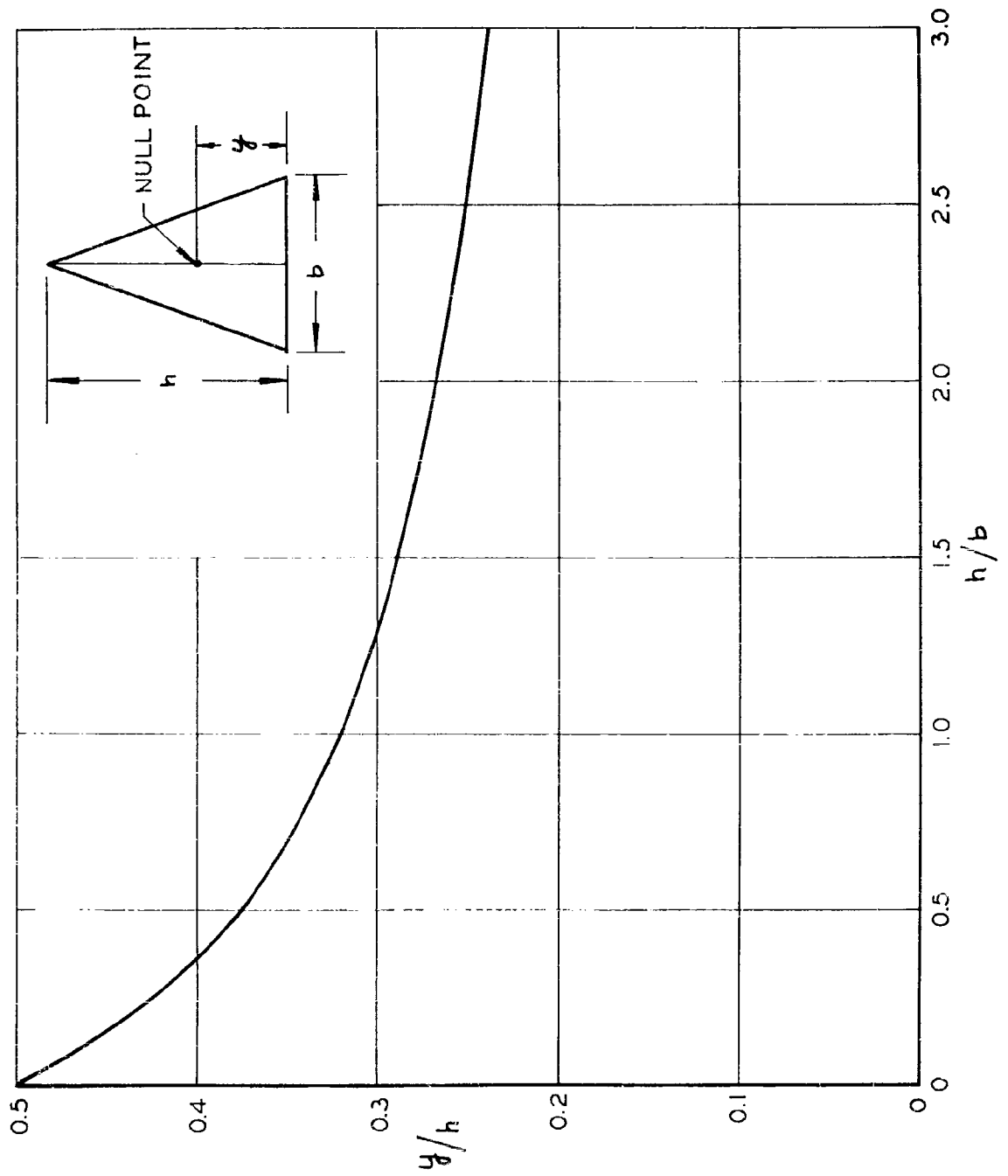
Figure 23. - Location of the null point on isosceles triangles.

The null point coincides with the centroid when the triangle is equilateral, i.e., $y = \frac{1}{3} h$ for an altitude to base ratio of 0.866.

9.4 The First Output

After the quantities described in the previous sections have been computed for all the quadrilateral elements formed from the input points, certain geometrical properties of the elements are output from the machine. The order in which the elements are listed is the order in which they were formed as described above. Recall that each element is associated with one of the input points used to construct it and is designated by the same pair of integers, m and n, used to identify the input point. The elements are listed n-line by n-line, starting with the first and continuing through all sections. On each n-line the elements are listed in order of increasing m. The tabulated information for each element occupies three lines of printing. The quantities listed are: the identifying integers m and n, the coordinates of the four input points used to form the element, the components of the unit normal vector, the coordinates of the null point in the reference coordinate system, the common projection distance d of the four input points into the plane of the element, the maximum diagonal t, and the area of the quadrilateral. The format of this listing is as follows:

$$
\begin{array}{cccccccc}
n & m & x_1^i & x_2^i & x_3^i & x_4^i & n_x & x'_{np} & d & (1 \text{ or } 2) \\
& & y_1^i & y_2^i & y_3^i & y_4^i & n_y & y'_{np} & t \\
& & z_1^i & z_2^i & z_3^i & z_4^i & n_z & z'_{np} & A
\end{array}
$$

The designation 1 or 2 on the extreme right identifies elements for which the null point iterative procedure failed as discussed above and is absent for normal elements. A symbol 1 denotes that the computed null point was outside the element and thus that the listed null point is actually the centroid. A symbol 2 denotes that the iterative procedure did not converge and thus that the listed null point is only approximate. In both exceptional cases the listed value of d is incorrect.

The main purpose of this output is to enable errors in the input points to be discovered before the lengthy flow calculations are performed. Errors in the input points occur fairly often because of the large amount of input required. Usually, these are simply errors of transcription such as misplaced decimal points or transposed digits, but they are often difficult to find. If the flow computations are performed with an incorrect input point, they must be completely redone. There is no provision for saving those parts of the computation that might be correct. The computation time up to the first output is usually a fraction of one percent of the total computation time for the case, and if an error can be discovered at this stage, a great saving results. Experience to date indicates that about half the input errors are discovered by examining the first output. Thus its use has proved very worthwhile.

Unfortunately, there are no precise rules for discovering input errors by means of the first output. It is a technique that must be learned from experience. Moreover, there is a considerable individual variation. Different people will find a given error in different ways. The one general principle is that all quantities should vary systematically from element to adjoining element. Thus, in particular, there should be a systematic variation along an n-line, which is readily verified on the first output. There should also be a systematic variation along m-lines, which cannot be conveniently checked on the first output.

The first output is also the only listing of the input points produced by the program and provides the only convenient method of associating input points with elements, if this should be desired.

9.5 Formation of the Vector Matrix of Influence Coefficients.
The Induced Velocities

9.51 Organization of the Elements.

It is now required to compute the velocities induced by the quadrilateral elements at each other's null points. All elements are assumed to have unit source density. In this and succeeding calculations, some of the quantities

81

used to form the elements are superfluous and are discarded. Subsequently, an element is thought of as being defined by the following quantities: the coordinates of the null point and the centroid, which is the origin of the element coordinate system, in the reference coordinate system, the elements of the transformation matrix, the coordinates of the four corner points in the element coordinate system, the maximum diagonal and the area and second moments of the quadrilateral. Thus the following twenty-eight quantities are required for each element:

$$
\begin{array}{ccc}
x'_{np} & y'_{np} & z'_{np} \\[4pt]
x_o & y_o & z_o \\[4pt]
a_{11} & a_{12} & a_{13} \\[4pt]
a_{21} & a_{22} & a_{23} \\[4pt]
a_{31} & a_{32} & a_{33}
\end{array}
$$

$$
\begin{array}{cccc}
\xi_1 & \eta_1 & \xi_2 & \eta_2 \\[4pt]
\xi_3 & \eta_3 & \xi_4 & \eta_4
\end{array}
$$

$$
\begin{array}{cc}
t & A
\end{array}
$$

$$
\begin{array}{ccc}
I_{xx} & I_{xy} & I_{yy}
\end{array}
$$

The components of the unit normal vector are also needed but by equation (76) these are given by the last row of the transformation matrix. To minimize computing time these are computed only once and saved.

The elements are now considered to be ordered in the sequence in which they were listed on the first output. That is, the elements on the first n - line are listed in order of increasing m, followed by the elements of the second n-line in order of increasing m, and similarly for all n-lines. (This, indeed, is the way they are stored in the machine.) Thus each element may be designated by a single identifying integer, i or j, which represents its position in this sequence. This identifying integer never appears on the input or the output of the method, but is basic to the logic of all the

82

computations to follow. The total number of elements is denoted N.

The basic calculation described in this section is the computation of the velocity components induced at the null point of the i-th element by a unit source density distribution on the j-th element. This calculation requires the coordinates of the null point of the i-th element and may require any of the above-listed twenty-eight quantities associated with the j-th element except the coordinates of the null point. To avoid complication these quantities will not at first be subscripted i and j in the explanation to follow. It need only to be kept in mind that the null point is always that of the i-th element where velocity components are being evaluated, while all other quantities correspond to the j-th element, which is inducing the velocity.

The method calculates the velocity components induced at one particular null point by all N elements in turn and repeats this procedure for each null point. Thus the induced velocity matrix or ''matrix of influence co-efficients'' is computed row by row, each row being put into the low speed storage of the machine as it is completed. The computation of each row requires the above list of twenty-eight quantities for all elements, and to minimize computation time these must all be in the high-speed storage of the machine simultaneously. If these were computed as needed or obtained from low speed storage, the process would have to be repeated N^2 times, which is very time consuming. The result is that high speed storage capacity is often the limiting factor in the number of elements that may be employed. If the matrix were computed column by column, i.e., if the velocity components induced by one particular element were calculated at each null point in turn, and the process repeated for each element, this storage limit would not exist. Only one set of twenty-eight numbers are needed for each column. These could be computed as needed, since this would require only N such calculations — a trivial matter. Since the matrix is eventually used row by row, this latter method would require transposing the matrix, which is a time consuming procedure, and the method employed was chosen to avoid it.

9.52 Non-symmetric Bodies.

The first step in computing the velocity components induced at the null point of the i-th element by the j-th element is to compute the distance r_o between this null point and the origin of the j-th element coordinate system. This is

$$r_o = \sqrt{(x'_{np} - x_o)^2 + (y'_{np} - y_o)^2 + (z'_{np} - z_o)^2} \tag{95}$$

where, as mentioned above, subscripts i and j are omitted. This distance is now compared with the product of the maximum diagonal of the j-th element and a prescribed number ρ_2, which is customarily set equal to 4, but may have any desired value. If

$$r_o \geq \rho_2 \, t \tag{96}$$

the j-th element is approximated by a point source at the origin of its co-ordinate system. (This approximation is equivalent in accuracy to a point source plus a point dipole, since the dipole moments of the quadrilateral with respect to its origin are zero.) The velocity components are computed by formulas equivalent to those obtained from equations (57), (58), and (59) by retaining only the first terms. These equations, however, are expressed in the element coordinate system. To avoid transforming the null point into the element coordinate system, which in this case would be a significant fraction of the computation time, the velocity components are evaluated directly in the reference coordinate system by well-known formulas that are easily ob-tained from these. Specifically, if equation (96) is satisfied, the velocity components in the reference coordinate system are given by

$$V'_x = A \, r_o^{-3} \, (x'_{np} - x_o)$$

$$V'_y = A \, r_o^{-3} \, (y'_{np} - y_o) \tag{97}$$

$$V'_z = A \, r_o^{-3} \, (z'_{np} - z_o)$$

If, on the other hand,

$$r_o < \rho_2 \, t \tag{98}$$

the coordinates of the i-th null point x'_{np}, y'_{np}, z'_{np} are transformed into the j-th element coordinate system obtaining x_{np}, y_{np}, z_{np}. This allows the formulas of Section 8.0 to be employed. The transformation is accomplished by means of equation (78). Now r_o is compared with the product of the maximum diagonal t and a second prescribed number ρ_1, which is set equal to $\sqrt{6} = 2.45$ unless otherwise specified. If

$$r_o \gtrless \rho_1 t \tag{99}$$

the j-th element is approximated by a point source plus a point quadrupole at the origin of its coordinate system. The velocity components at the i-th null point are computed by equations (57), (58), and (59) using equations (60), (61), and (62). The coordinates of the i-th null point in the j-th coordinate system, x_{np}, y_{np}, z_{np}, replace x, y, z, respectively, in the equations, while the value of r_o used is that already computed by equation (95) using coordinates in the reference coordinate system. If r_o were computed using x_{np}, y_{np}, z_{np} in (51), the same value would of course be obtained. The velocity components V_x, V_y, V_z thus obtained are in terms of the element coordinate system.

If, instead

$$r_o < \rho_1 t \tag{100}$$

the velocity components are evaluated from the exact formulas for a quadrilateral, i.e., from equations (42), (43), and (44) using equations (45) through (49). Again x_{np}, y_{np}, z_{np} replace x, y, z in these formulas, while ξ_k, η_k, $k = 1, 2, 3, 4$, are the coordinates of the corner points of the j-th element. In the evaluation of these formulas attention must be paid to the discussion following equation (49) with regard to certain limiting cases, in particular the case $i = j$ where the null point is on the element in question. As above, the velocity components V_x, V_y, V_z thus obtained are in terms of the element coordinate system.

In the last two cases, the induced velocity components V_x, V_y, V_z in the element coordinate system must be transformed to obtain the components V'_x, V'_y, V'_z in the reference coordinate system. This is done using the form

of equation (79) appropriate for vectors as is discussed immediately below the equation. Thus finally in one of three ways the components V'_x, V'_y, V'_z of the velocity components induced at the i-th null point by the j-th element are obtained.

The notation is now changed to bring in i and j explicitly. Define the vector $\vec{V}_{ij}$ as the vector velocity induced at the null point of the i-th element by a unit source density on the j-th element. Let the components of this vector in the reference coordinate system be X_{ij}, Y_{ij}, Z_{ij}, so that the change of notation may be expressed symbolically as

$$X_{ij} = V'_x$$

$$Y_{ij} = V'_y \qquad \qquad (101)$$

$$Z_{ij} = V'_z$$

The complete set of $\vec{V}_{ij}$ for all i and j comprise the vector elements of the ''matrix of influence coefficients'' for non-symmetric bodies.

The normal velocity induced at the null point of the i-th element by a unit source density on the j-th element is obtained by taking the dot product of $\vec{V}_{ij}$ with the unit normal vector of the i-th element $\hat{n}_i$. This induced normal velocity is denoted A_{ij}. It is given by

$$A_{ij} = \hat{n}_i \cdot \vec{V}_{ij} = n_{ix} X_{ij} + n_{iy} Y_{ij} + n_{iz} Z_{ij} \qquad (102)$$

The complete set of A_{ij} form the coefficient matrix for the set of linear equations for the values of the surface source density on the quadrilateral elements. For non-symmetric bodies the matrices $\vec{V}_{ij}$ and A_{ij} are used for all onset flows.

9.53 Bodies with One Symmetry Plane.

If a body has one plane of symmetry, only the non-redundant portion of the body need be input. The other half of the body is generated by reflecting the half that is input in the symmetry plane. As stated above, the symmetry plane is the xz-coordinate plane of the reference coordinate system. Figure 24
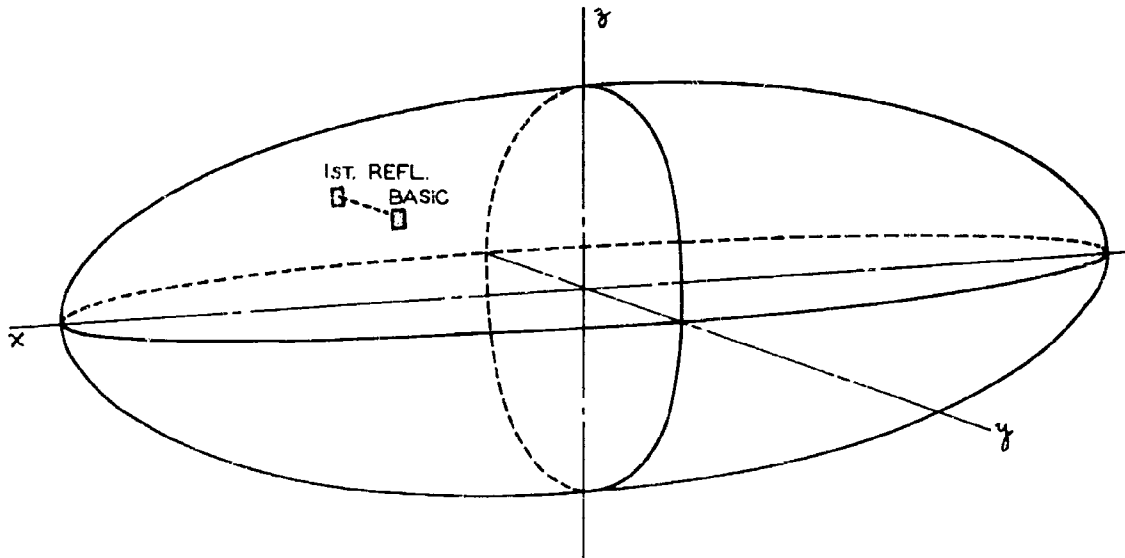
Figure 24. - A body with one symmetry plane.

is a sketch of a typical body with one symmetry plane. Input points define
the half of the body surface on one side of the xz-plane. Elements are formed
from these points in the manner described above, and such elements are denoted
basic elements. The other half of the body is taken into account by being
covered with elements that are the reflections of the basic elements in the
symmetry plane. These latter are denoted reflected elements, and thus refer-
ence will be made to the j-th basic element and the j-th reflected element.

Because of the symmetry of the body surface, the value of the surface
source density on any reflected element is related to the value of the source
density on the corresponding basic element in a very simple way, and thus only
the latter need be calculated. The relation between the values of source
density on a basic and reflected element depends on the direction of the
uniform onset flow. By inspection of figure 24, it is clear that if the onset
flow is parallel to the x or z axis of the reference coordinate system,
the source density on a reflected element is equal in value to the source
density on the corresponding basic element. (This is true in fact for any
onset flow in the xz-plane.) If the onset flow is parallel to the y-axis of
the reference coordinate system, the source densities on corresponding basic

87

and reflected elements are equal in magnitude but of opposite sign. The relation is more complicated for other flow inclinations, but these are not considered, since the results for such inclinations may be obtained by a simple combination of the cases mentioned above.

The calculational procedure is identical to the nonsymmetric case until the stage is reached at which the matrix of induced velocities is to be computed. That is, the basic elements are formed from the input points in the same way to obtain the twenty-eight defining quantities for each element that are listed in Section 9.51. Also, the velocity induced at the null point of the i-th basic element by a unit source density on the j-th basic element is calculated in the way described in Section 9.52. Immediately after this, the velocity induced at the null point of the i-th basic element by the j-th reflected element must be calculated. Thus the twenty-eight quantities defining the j-th basic element are required.

Since a reflected element is the mirror image of the corresponding basic element in the xz-plane of the reference coordinate system, its twenty-eight defining quantities are identical to those for the basic element except that the signs of the y reference coordinates of all points and the y-components of all vectors are changed. Referring to the list in Section 9.51, this means that the signs of the following quantities must be changed:

$$y'_{np} \qquad y_o \qquad a_{12} \qquad a_{22} \qquad a_{32}$$

However, since velocities are not evaluated at the null points of reflected elements, the sign of y'_{np} need not be changed. Moreover, the reflection has made the element coordinate system left-handed. To make the coordinate system of the reflected element right-handed, the sign of the unit normal vector, i.e., the third row of the transformation matrix, is reversed. This means that the signs of a_{31} and a_{33} are changed, while the sign of a_{32} goes back to what it was originally. Thus finally, a reflected element is obtained from a basic element by changing the signs of five of the twenty-eight defining quantities. The five whose signs are changed are:

$$y_o \qquad a_{12} \qquad a_{22} \qquad a_{31} \qquad a_{33}$$

For the purposes of this method the reflection of an element in the xz-plane may be defined as the change of these five signs. The velocity components induced by the j-th reflected element at the null point of the i-th basic element are then computed by the method of 9.52. When this is completed, the signs of the above quantities are returned to their original values.

Suppose that the above calculations have been completed. Let $\vec{V}_{ij}$ be the vector velocity induced at the null point of the i-th basic element by the j-th basic element, and let $\vec{V}_{ij}^{(r)}$ be the velocity induced there by the j-th reflected element. These vectors have components X_{ij}, Y_{ij}, Z_{ij} and $X_{ij}^{(r)}$, $Y_{ij}^{(r)}$, $Z_{ij}^{(r)}$, respectively, in the reference coordinate system. These vectors are now combined in two ways. Define the vector

$$\vec{V}_{ij}^{(1)} = \vec{V}_{ij} + \vec{V}_{ij}^{(r)} \tag{103}$$

with components

$$X_{ij}^{(1)} = X_{ij} + X_{ij}^{(r)}$$

$$Y_{ij}^{(1)} = Y_{ij} + Y_{ij}^{(r)} \tag{104}$$

$$Z_{ij}^{(1)} = Z_{ij} + Z_{ij}^{(r)}$$

and the vector

$$\vec{V}_{ij}^{(2)} = \vec{V}_{ij} - \vec{V}_{ij}^{(r)} \tag{105}$$

with components

$$X_{ij}^{(2)} = X_{ij} - X_{ij}^{(r)}$$

$$Y_{ij}^{(2)} = Y_{ij} - Y_{ij}^{(r)} \tag{106}$$

$$Z_{ij}^{(2)} = Z_{ij} - Z_{ij}^{(r)}$$

The vector $\vec{V}_{ij}^{(1)}$ is thus the velocity induced at the null point of the i-th basic element by the j-th basic and reflected elements when these latter two have equal values of source density. Similarly the vector $\vec{V}_{ij}^{(2)}$ is the velocity induced at the null point of the i-th basic element by the j-th basic and reflected elements when these latter two have source densities equal in

value but of opposite sign. The complete sets of $\vec{V}_{ij}^{(1)}$ and $\vec{V}_{ij}^{(2)}$ are accordingly the vector ''matrices of influence coefficients'' for bodies with one plane of symmetry. The second of these is appropriate for use with an onset flow parallel to the y-axis of the reference coordinate system, i.e., flow normal to the symmetry plane, while the first is appropriate for use with onset flows parallel to the x or z axes of the reference coordinate system, i.e., flows in the symmetry plane. These matrices are N x N, where N is the number of basic elements only.

Taking the dot products of the vectors $\vec{V}_{ij}^{(1)}$ and $\vec{V}_{ij}^{(2)}$ with the unit normal vector of the i-th basic element gives the induced normal velocities $A_{ij}^{(1)}$ and $A_{ij}^{(2)}$ in a manner similar to that shown in equation (102) for the non-symmetric case. The complete sets of $A_{ij}^{(1)}$ and $A_{ij}^{(2)}$ form the coefficient matrices for the sets of linear equations for the values of the surface source density on the basic elements.

9.54 Bodies with Two Symmetry Planes.

Bodies with two planes of symmetry are handled by an obvious extension of the procedure of the previous section. Only one-fourth of the body surface is specified by input points, while the other three-fourths is taken into account by reflections. As before elements formed from input points are designated basic elements. To each basic element there now correspond three reflected elements, which are obtained by successive reflections in the symmetry planes. The two symmetry planes are the xz and xy coordinate planes of the reference coordinate system. Figure 25 shows a sketch of a typical body with two planes of symmetry and the relation of the basic and reflected elements. The first reflected element is obtained by reflecting the basic element in the xz-plane; the second reflected element is obtained by reflecting the first reflected element in the xy-plane; and the third reflected element is obtained by reflecting the second reflected element in the xz-plane. The basic element may be obtained from the third reflected element by a reflection in the xy-plane.

If the onset flow is parallel to one of the coordinate axes, the values of the source density on a basic element and the three corresponding reflected elements are all equal in magnitude. The signs of these source densities
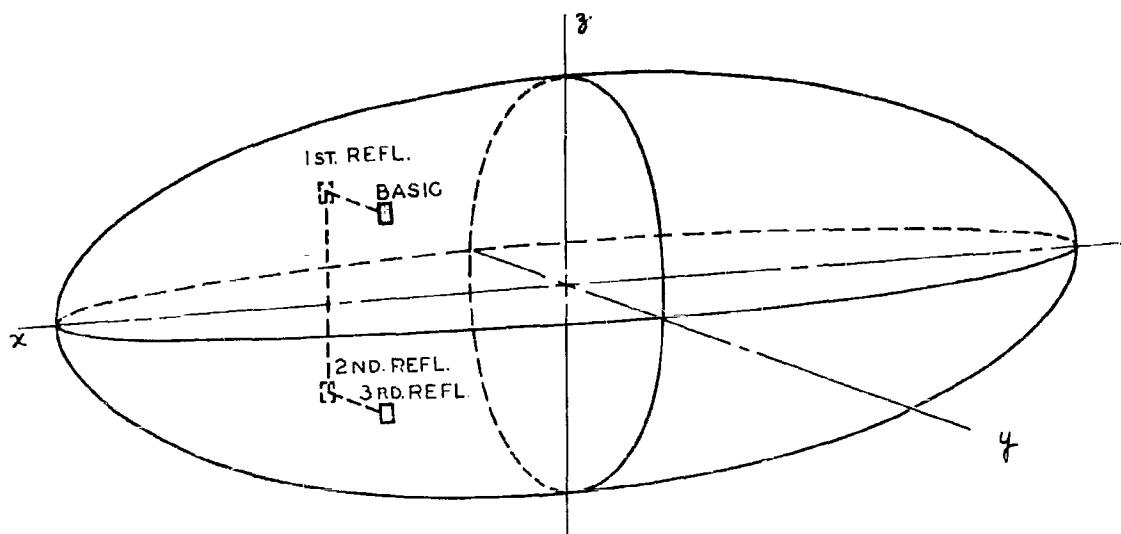
Figure 25. - A body with two symmetry planes.

depend on the direction of the onset flow. Inspection of figure 25 shows that:
if the onset flow is parallel to the x-axis, the signs of the source densities
on all three reflected elements are the same as that on the basic element;
if the onset flow is parallel to the y-axis, the sign of the source density on
the third reflected element is the same as that on the basic element, while
the source densities on the first and second reflected elements have the
opposite sign; if the onset flow is parallel to the z-axis, the sign of the
source density on the first reflected element is the same as that on the basic
element, while the source densities on the second and third reflected ele-
ments have opposite sign.

The calculation method for bodies with two symmetry planes is identical
to that for non-symmetric bodies through the first output, and the basic
elements are formed from the input points in the usual way. The first differ-
ence occurs during the computation of the ''matrices of influence coefficients''.
After the velocity induced at the null point of the i-th basic element by a
unit source density on the j-th basic element has been calculated, the com-
putation is repeated three more times to obtain the velocities induced at this
null point by the j-th reflected elements. All induced velocities are com-
puted by the method of section 9.52 and thus all that this calculation re-
quires is the set of twenty-eight defining quantities for each of the reflected

elements. In the previous section, the reflection of an element in the xz-plane was discussed and it turned out that twenty-three of the defining quantities are unchanged, while the following five are changed in sign:

$$y_o \qquad a_{12} \qquad a_{22} \qquad a_{31} \qquad a_{33}$$

A reflection in the xy-plane is acomplished in a similar way except that it is the z-components of vectors and coordinates of points whose signs are changed rather than the y-components and coordinates. After each reflection the signs of the components of the normal vector are changed to make the element coordinate system right-handed. The result is that the reflection of an element in the xy-plane is accomplished by changing the signs of the following five quantities:

$$z_o \qquad a_{13} \qquad a_{23} \qquad a_{31} \qquad a_{32}$$

It is convenient to show the relations between the basic and reflected elements by means of the following table.

Element	Origin	Transformation Matrix			Signs Changed from Previous Element	
Basic	x_o	a_{11}	a_{12}	a_{13}		
	y_o	a_{21}	a_{22}	a_{23}		
	z_o	a_{31}	a_{32}	a_{33}		
First Reflected	x_o	a_{11}	$-a_{12}$	a_{13}	y_o	
	$-y_o$	a_{21}	$-a_{22}$	a_{23}	a_{12}	a_{22}
	z_o	$-a_{31}$	a_{32}	$-a_{33}$	a_{31}	a_{33}
Second Reflected	x_o	a_{11}	$-a_{12}$	$-a_{13}$	z_o	
	$-y_o$	a_{21}	$-a_{22}$	$-a_{23}$	a_{13}	a_{23}
	$-z_o$	a_{31}	$-a_{32}$	$-a_{33}$	a_{31}	a_{32}
Third Reflected	x_o	a_{11}	a_{12}	$-a_{13}$	y_o	
	y_o	a_{21}	a_{22}	$-a_{23}$	a_{12}	a_{22}
	$-z_o$	$-a_{31}$	$-a_{32}$	a_{33}	a_{31}	a_{33}
Basic	x_o	a_{11}	a_{12}	a_{13}	z_o	
	y_o	a_{21}	a_{22}	a_{23}	a_{13}	a_{23}
	z_o	a_{31}	a_{32}	a_{33}	a_{31}	a_{32}

The signs of any of the twenty-eight defining quantities not listed in this table are the same for all corresponding elements. After all four induced velocities have been computed, the basic element is obtained again in the manner shown in the table.

Suppose now the velocities induced at the null point of the i-th basic element by the j-th basic, first reflected, second reflected, and third reflected elements have been computed. Let these be designated $\vec{V}_{ij}$, $\vec{V}_{ij}^{(1r)}$, $\vec{V}_{ij}^{(2r)}$, $\vec{V}_{ij}^{(3r)}$, respectively. The components of these vectors in the reference coordinate system are:

$$\vec{V}_{ij} \quad : \quad X_{ij} \qquad Y_{ij} \qquad Z_{ij}$$

$$\vec{V}_{ij}^{(1r)} \quad : \quad X_{ij}^{(1r)} \qquad Y_{ij}^{(1r)} \qquad Z_{ij}^{(1r)}$$

$$\vec{V}_{ij}^{(2r)} \quad : \quad X_{ij}^{(2r)} \qquad Y_{ij}^{(2r)} \qquad Z_{ij}^{(2r)}$$

$$\vec{V}_{ij}^{(3r)} \quad : \quad X_{ij}^{(3r)} \qquad Y_{ij}^{(3r)} \qquad Z_{ij}^{(3r)}$$

These are now combined in the proper ways for use with onset flows parallel to the coordinate axes. Define the vector

$$\vec{V}_{ij}^{(1)} = \vec{V}_{ij} + \vec{V}_{ij}^{(1r)} + \vec{V}_{ij}^{(2r)} + \vec{V}_{ij}^{(3r)} \tag{107}$$

with components

$$X_{ij}^{(1)} = X_{ij} + X_{ij}^{(1r)} + X_{ij}^{(2r)} + X_{ij}^{(3r)}$$

$$Y_{ij}^{(1)} = Y_{ij} + Y_{ij}^{(1r)} + Y_{ij}^{(2r)} + Y_{ij}^{(3r)} \tag{108}$$

$$Z_{ij}^{(1)} = Z_{ij} + Z_{ij}^{(1r)} + Z_{ij}^{(2r)} + Z_{ij}^{(3r)}$$

the vector

$$\vec{V}_{ij}^{(2)} = \vec{V}_{ij} - \vec{V}_{ij}^{(1r)} - \vec{V}_{ij}^{(2r)} + \vec{V}_{ij}^{(3r)} \tag{109}$$

with components

$$X_{ij}^{(2)} = X_{ij} - X_{ij}^{(1r)} - X_{ij}^{(2r)} + X_{ij}^{(3r)}$$

$$Y_{ij}^{(2)} = Y_{ij} - Y_{ij}^{(1r)} - Y_{ij}^{(2r)} + Y_{ij}^{(3r)} \tag{110}$$

$$Z_{ij}^{(2)} = Z_{ij} - Z_{ij}^{(1r)} - Z_{ij}^{(2r)} + Z_{ij}^{(3r)}$$

and the vector

$$\vec{V}_{ij}^{(3)} = \vec{V}_{ij} + \vec{V}_{ij}^{(1r)} - \vec{V}_{ij}^{(2r)} - \vec{V}_{ij}^{(3r)} \tag{111}$$

with components

$$X_{ij}^{(3)} = X_{ij} + X_{ij}^{(1r)} - X_{ij}^{(2r)} - X_{ij}^{(3r)}$$

$$Y_{ij}^{(3)} = Y_{ij} + Y_{ij}^{(1r)} - Y_{ij}^{(2r)} - Y_{ij}^{(3r)} \tag{112}$$

$$Z_{ij}^{(3)} = Z_{ij} + Z_{ij}^{(1r)} - Z_{ij}^{(2r)} - Z_{ij}^{(3r)}$$

The complete sets of $\vec{V}_{ij}^{(1)}$, $\vec{V}_{ij}^{(2)}$, and $\vec{V}_{ij}^{(3)}$ are thus the vector ''matrices of influence coefficients'' for bodies with two planes of symmetry. They are suitable for use with onset flows parallel to the x, y, and z coordinate axes, respectively. Each matrix is $N \times N$, where N is the number of basic elements.

As before, the dot products of the vectors $\vec{V}_{ij}^{(1)}$, $\vec{V}_{ij}^{(2)}$, and $\vec{V}_{ij}^{(3)}$ with the unit normal vector of the i-th basic element are performed to obtain the induced normal velocities $A_{ij}^{(1)}$, $A_{ij}^{(2)}$, and $A_{ij}^{(3)}$, in a manner similar to that shown in equation (102). The complete sets of these induced normal velocities form the coefficient matrices for the sets of linear algebraic equations for the values of the surface source density on the basic elements.

94

9.55 Bodies with Three Symmetry Planes.

Bodies with three planes of symmetry are handled by carrying the procedure of the previous section one step further. One-eighth of the body surface is specified by input points while the other seven-eighths is taken into account by reflections. To each basic element, which is formed from input points, there correspond seven reflected elements, which are designated first reflected element, second reflected element, etc. The symmetry planes are the coordinate planes of the reference coordinate system. Figure 26 shows a sketch of a typical body with three planes of symmetry and the position of the various reflected elements.
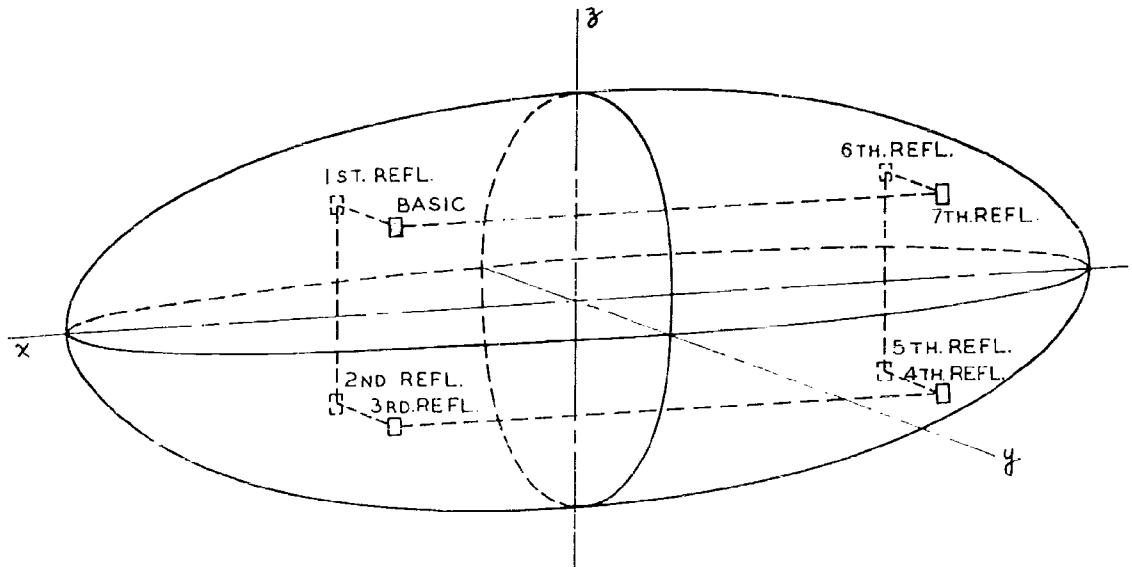
Figure 26. - A body with three symmetry planes.

The relationships of the reflected elements, which are obtained by successive reflections of the basic element in the symmetry planes, are shown in the table below:

This Element is Reflected	In This Plane	To Obtain This Element
Basic	x-z	1st Reflected
1st Reflected	x-y	2nd Reflected
2nd Reflected	x-z	3rd Reflected
3rd Reflected	y-z	4th Reflected
4th Reflected	x-z	5th Reflected
5th Reflected	x-y	6th Reflected
6th Reflected	x-z	7th Reflected
7th Reflected	y-z	Basic

If the onset flow is parallel to one of the coordinate axes, the values of the source density on a basic element and the seven corresponding reflected elements are all equal in magnitude. The sign of the source densities depends on the direction of the onset flow. The relation of these signs are given in the table below, which may be verified by inspection of figure 26:

Direction of Onset Flow	Reflected Elements With Same Sign as Basic			Reflected Elements with Opposite Sign to Basic			
x-axis	1st	2nd	3rd	4th	5th	6th	7th
y-axis	3rd	4th	7th	1st	2nd	5th	6th
z-axis	1st	6th	7th	2nd	3rd	4th	5th

The calculation method proceeds in the usual way through formation of the basic elements and the first output. To compute the ''matrices of influence coefficients'' it is necessary to compute the velocity induced at the null point of the i-th basic element by the j-th basic element and by all seven of the j-th reflected elements. The induced velocities are computed by the method of Section 9.52, and the twenty-eight defining quantities for each reflected element are required. In this case, in addition to reflections in the xz and xy coordinate planes as was done in the previous section, reflections in the yz-plane are also performed. After a line of reasoning similar to that used for the other symmetry planes, it turns out that an element is reflected in the yz-plane by changing the sign of the following five quantities:

$$x_o \qquad a_{11} \qquad a_{21} \qquad a_{32} \qquad a_{33}$$

As before, this reflection includes a reversal of sign of the unit normal vector to make the element coordinate system right-handed.

The relations between the basic and reflected elements are shown in the following table.

Element	Origin	Transformation Matrix			Signs Changed From Previous Element		
Basic	x_0	a_{11}	a_{12}	a_{13}			
	y_0	a_{21}	a_{22}	a_{23}			
	z_0	a_{31}	a_{32}	a_{33}			
First Reflected	x_0	a_{11}	$-a_{12}$	a_{13}		y_0	
	$-y_0$	a_{21}	$-a_{22}$	a_{23}	a_{12}		a_{22}
	z_0	$-a_{31}$	a_{32}	$-a_{33}$	a_{31}		a_{33}
Second Reflected	x_0	a_{11}	$-a_{12}$	$-a_{13}$		z_0	
	$-y_0$	a_{21}	$-a_{22}$	$-a_{23}$	a_{13}		a_{23}
	$-z_0$	a_{31}	$-a_{32}$	$-a_{33}$	a_{31}		a_{32}
Third Reflected	x_0	a_{11}	a_{12}	$-a_{13}$		y_0	
	y_0	a_{21}	a_{22}	$-a_{23}$	a_{12}		a_{22}
	$-z_0$	$-a_{31}$	$-a_{32}$	a_{33}	a_{31}		a_{33}
Fourth Reflected	$-x_0$	$-a_{11}$	a_{12}	$-a_{13}$		x_0	
	y_0	$-a_{21}$	a_{22}	$-a_{23}$	a_{11}		a_{21}
	$-z_0$	$-a_{31}$	a_{32}	$-a_{33}$	a_{32}		a_{33}
Fifth Reflected	$-x_0$	$-a_{11}$	$-a_{12}$	$-a_{13}$		y_0	
	$-y_0$	$-a_{21}$	$-a_{22}$	$-a_{23}$	a_{12}		a_{22}
	$-z_0$	a_{31}	a_{32}	a_{33}	a_{31}		a_{33}
Sixth Reflected	$-x_0$	$-a_{11}$	$-a_{12}$	a_{13}		z_0	
	$-y_0$	$-a_{21}$	$-a_{22}$	a_{23}	a_{13}		a_{23}
	z_0	$-a_{31}$	$-a_{32}$	a_{33}	a_{31}		a_{32}
Seventh Reflected	$-x_0$	$-a_{11}$	a_{12}	a_{13}		y_0	
	y_0	$-a_{21}$	a_{22}	a_{23}	a_{12}		a_{22}
	z_0	a_{31}	$-a_{32}$	$-a_{33}$	a_{31}		a_{33}
Basic	x_0	a_{11}	a_{12}	a_{13}		x_0	
	y_0	a_{21}	a_{22}	a_{23}	a_{11}		a_{21}
	z_0	a_{31}	a_{32}	a_{33}	a_{32}		a_{33}

The signs of any of the twenty-eight quantities not listed in this table are the same for all corresponding elements. After all eight induced velocities have been computed, the basic element is obtained again as shown in the table.

Suppose now the vector velocities induced at the null point in the i-th basic element by the j-th basic element and its seven reflected elements have been computed. Let these vectors and their components in the reference coordinate system be denoted:

$$\vec{V}_{ij} \quad : \quad X_{ij} \qquad Y_{ij} \qquad Z_{ij}$$

$$\vec{V}_{ij}^{(1r)} \quad : \quad X_{ij}^{(1r)} \qquad Y_{ij}^{(1r)} \qquad Z_{ij}^{(1r)}$$

. . . .

. . . .

$$\vec{V}_{ij}^{(7r)} \quad : \quad X_{ij}^{(7r)} \qquad Y_{ij}^{(7r)} \qquad Z_{ij}^{(7r)}$$

These are now combined in the proper ways for use with onset flows parallel to the coordinate axes. Define the vector

$$\vec{V}_{ij}^{(1)} = \vec{V}_{ij} + \vec{V}_{ij}^{(1r)} + \vec{V}_{ij}^{(2r)} + \vec{V}_{ij}^{(3r)} - \vec{V}_{ij}^{(4r)} - \vec{V}_{ij}^{(5r)} - \vec{V}_{ij}^{(6r)} - \vec{V}_{ij}^{(7r)} \quad (113)$$

with components

$$X_{ij}^{(1)} = X_{ij} + X_{ij}^{(1r)} + X_{ij}^{(2r)} + X_{ij}^{(3r)} - X_{ij}^{(4r)} - X_{ij}^{(5r)} - X_{ij}^{(6r)} - X_{ij}^{(7r)}$$

$$Y_{ij}^{(1)} = Y_{ij} + Y_{ij}^{(1r)} + Y_{ij}^{(2r)} + Y_{ij}^{(3r)} - Y_{ij}^{(4r)} - Y_{ij}^{(5r)} - Y_{ij}^{(6r)} - Y_{ij}^{(7r)} \quad (114)$$

$$Z_{ij}^{(1)} = Z_{ij} + Z_{ij}^{(1r)} + Z_{ij}^{(2r)} + Z_{ij}^{(3r)} - Z_{ij}^{(4r)} - Z_{ij}^{(5r)} - Z_{ij}^{(6r)} - Z_{ij}^{(7r)}$$

the vector

$$\vec{V}_{ij}^{(2)} = \vec{V}_{ij} - \vec{V}_{ij}^{(1r)} - \vec{V}_{ij}^{(2r)} + \vec{V}_{ij}^{(3r)} + \vec{V}_{ij}^{(4r)} - \vec{V}_{ij}^{(5r)} - \vec{V}_{ij}^{(6r)} + \vec{V}_{ij}^{(7r)} \quad (115)$$

with components

$$X_{ij}^{(2)} = X_{ij} - X_{ij}^{(1r)} - X_{ij}^{(2r)} + X_{ij}^{(3r)} + X_{ij}^{(4r)} - X_{ij}^{(5r)} - X_{ij}^{(6r)} + X_{ij}^{(7r)}$$

$$Y_{ij}^{(2)} = Y_{ij} - Y_{ij}^{(1r)} - Y_{ij}^{(2r)} + Y_{ij}^{(3r)} + Y_{ij}^{(4r)} - Y_{ij}^{(5r)} - Y_{ij}^{(6r)} + Y_{ij}^{(7r)} \qquad (116)$$

$$Z_{ij}^{(2)} = Z_{ij} - Z_{ij}^{(1r)} - Z_{ij}^{(2r)} + Z_{ij}^{(3r)} + Z_{ij}^{(4r)} - Z_{ij}^{(5r)} - Z_{ij}^{(6r)} + Z_{ij}^{(7r)}$$

and the vector

$$\vec{V}_{ij}^{(3)} = \vec{V}_{ij} + \vec{V}_{ij}^{(1r)} - \vec{V}_{ij}^{(2r)} - \vec{V}_{ij}^{(3r)} - \vec{V}_{ij}^{(4r)} - \vec{V}_{ij}^{(5r)} + \vec{V}_{ij}^{(6r)} + \vec{V}_{ij}^{(7r)} \qquad (117)$$

with components

$$X_{ij}^{(3)} = X_{ij} + X_{ij}^{(1r)} - X_{ij}^{(2r)} - X_{ij}^{(3r)} - X_{ij}^{(4r)} - X_{ij}^{(5r)} + X_{ij}^{(6r)} + X_{ij}^{(7r)}$$

$$Y_{ij}^{(3)} = Y_{ij} + Y_{ij}^{(1r)} - Y_{ij}^{(2r)} - Y_{ij}^{(3r)} - Y_{ij}^{(4r)} - Y_{ij}^{(5r)} + Y_{ij}^{(6r)} + Y_{ij}^{(7r)} \qquad (118)$$

$$Z_{ij}^{(3)} = Z_{ij} + Z_{ij}^{(1r)} - Z_{ij}^{(2r)} - Z_{ij}^{(3r)} - Z_{ij}^{(4r)} - Z_{ij}^{(5r)} + Z_{ij}^{(6r)} + Z_{ij}^{(7r)}$$

The complete sets of $\vec{V}_{ij}^{(1)}$, $\vec{V}_{ij}^{(2)}$, and $\vec{V}_{ij}^{(3)}$, are the vector ''matrices of influence coefficients'' for bodies with three planes of symmetry. They are suitable for use with onset flows parallel to the x, y, and z coordinate axes respectively. Each matrix is $N \times N$, where N is the number of basic elements.

As before, the dot products of the vectors $\vec{V}_{ij}^{(1)}$, $\vec{V}_{ij}^{(2)}$, and $\vec{V}_{ij}^{(3)}$ with the unit normal vector of the i-th basic element are performed as shown in equation (102) to obtain the induced normal velocities $A_{ij}^{(1)}$, $A_{ij}^{(2)}$, and $A_{ij}^{(3)}$. The complete sets of these induced normal velocities form the coefficient matrices for the sets of linear algebraic equations for the values of the surface source density on the basic elements.

9.56 Summary, Unification of Notation, and Designation of Onset Flows.

The results of the calculations of the previous parts of Section 9.5 may be described in a unified form applicable to all body surfaces, whatever the symmetry condition. It may be said that in all cases three vector ''matrices of influence coefficients'' are obtained, each of which is appropriate for use with an onset flow parallel to one of the coordinate axes. These three matrices are identical for non-symmetric cases, while the first and third are identical for cases of one plane of symmetry. The vector elements of these matrices, $\vec{V}_{ij}^{(1)}$, $\vec{V}_{ij}^{(2)}$, and $\vec{V}_{ij}^{(3)}$, are the vector velocities induced at the null point of the i-th element (or the i-th basic element in cases of symmetry) by a unit source density on the j-th element (or j-th basic element and its corresponding reflected elements in cases of symmetry). In particular, the actual velocities induced at the null point of the i-th element (or i-th basic element) by the j-th element (or j-th basic and reflected elements) is obtained by multiplying these velocities by the true value of the source density on the j-th element (or j-th basic element).

The sets of induced velocities $\vec{V}_{ij}^{(1)}$, $\vec{V}_{ij}^{(2)}$, and $\vec{V}_{ij}^{(3)}$, are appropriate for use with onset flows parallel to the x, the y, and the z coordinate axes, respectively. The method has been constructed to handle these three onset flows simultaneously. That is, in normal cases three onset flow vectors are input. These are: the vector $\vec{V}_{\infty}^{(1)}$, with components

$$V_{\infty x}^{(1)} = 1 \qquad V_{\infty y}^{(1)} = 0 \qquad V_{\infty z}^{(1)} = 0 \qquad (119)$$

the vector $\vec{V}_{\infty}^{(2)}$ with components

$$V_{\infty x}^{(2)} = 0 \qquad V_{\infty y}^{(2)} = 1 \qquad V_{\infty z}^{(2)} = 0 \qquad (120)$$

and the vector $\vec{V}_{\infty}^{(3)}$ with components

$$V_{\infty x}^{(3)} = 0 \qquad V_{\infty y}^{(3)} = 0 \qquad V_{\infty z}^{(3)} = 1 \qquad (121)$$

The notation may be made more compact by introducing the integer superscript (s), where s = 1, 2, 3. Then the set of induced vector velocities $\vec{V}_{ij}^{(s)}$

and induced normal velocities $A_{ij}^{(s)}$ is used for the onset flow $\vec{V}_{\infty}^{(s)}$ to compute a complete set of source densities and flow velocities. The onset flows $\vec{V}_{\infty}^{(s)}$, s = 1, 2, 3, are given by equations (119), (120), and (121). Thus normally three complete flow calculations are performed.

There are two cases where the onset flows need not be the three unit vectors given in equations (119), (120), (121). For non-symmetric body surfaces there is only one distinct ''matrix of influence coefficients'', i.e.,

$$\vec{V}_{ij}^{(1)} = \vec{V}_{ij}^{(2)} = \vec{V}_{ij}^{(3)} = \vec{V}_{ij} \tag{122}$$

Thus this matrix is suitable for use with any onset flow and the three onset flow vectors $\vec{V}_{\infty}^{(s)}$, s = 1, 2, 3, may be unit uniform streams of arbitrary inclination. Also, for body surfaces with one plane of symmetry, two of the ''matrices of influence coefficients'' are identical, i.e.,

$$\vec{V}_{ij}^{(1)} = \vec{V}_{ij}^{(3)} \tag{123}$$

Thus the onset flows $\vec{V}_{\infty}^{(1)}$ and $\vec{V}_{\infty}^{(3)}$ may be any unit uniform streams in the xz-plane, i.e., in the plane of symmetry.

For the other cases, i.e., all flows for body surfaces with two or three symmetry planes and $\vec{V}_{\infty}^{(2)}$ for body surfaces with one plane of symmetry, the onset flows must be as shown in equations (119), (120), and (121), and in all cases the onset flows must be uniform streams of unit magnitude. If less than three onset flows are desired, the others may be input with all components zero. This however will not affect the computation of the ''matrices of influence coefficients''.

9.6 The Linear Algebraic Equations for the Values
of the Surface Source Density

9.61 Formulation of the Equations.

Now the values of the surface source density on the elements will be obtained as the solution of a set of linear algebraic equations. Recall that the source density is assumed constant on each quadrilateral element. Thus

there are N unknown values of the source density, where N is the number of elements formed from the input points (basic elements in cases of symmetry). The total normal velocity is required to vanish at the null point of each element formed from the input points and thus there are N equations for the N unknown values of the source density.

For any onset flow $\vec{V}_{\infty}^{(s)}$ (see Section 9.56 for notation) the normal velocity induced at the null point of the i-th element by a unit source density on the j-th element is $A_{ij}^{(s)}$. (For bodies with symmetry the designations ''i-th basic element'' and ''j-th basic and reflected elements'' should be used in the previous statement, but the extension to cases of symmetry is obvious with the notation of 9.56, and subsequently explicit mention of cases of symmetry will be omitted.) Thus the actual normal velocity induced at the i-th null point by the j-th element may be written $A_{ij}^{(s)} \cdot \sigma_{j}^{(s)}$, where $\sigma_{j}^{(s)}$ denotes the constant value of the source density on the j-th element for the onset flow $\vec{V}_{\infty}^{(s)}$. The total normal velocity induced at the i-th null point by all quadrilateral elements is accordingly,

$$N_{i}^{(s)} = \sum_{j=1}^{N} A_{ij}^{(s)} \sigma_{j}^{(s)} \tag{124}$$

The normal component of the onset flow at the i-th null point is the dot product of the onset flow vector and the unit normal vector of the i-th element, i.e.,

$$V_{\infty n_{i}}^{(s)} = \vec{n}_{i} \cdot \vec{V}_{\infty}^{(s)} = n_{ix} V_{\infty x}^{(s)} + n_{iy} V_{\infty y}^{(s)} + n_{iz} V_{\infty z}^{(s)} \tag{125}$$

The total normal velocity at the i-th null point is the sum of (124) and (125). Thus the requirement that the normal velocity vanish at all null points gives the following set of linear equations for the values of the source density

$$\sum_{j=1}^{N} A_{ij}^{(s)} \sigma_{j}^{(s)} = - V_{\infty n_{i}}^{(s)} \qquad i = 1, 2, \ldots, N \tag{126}$$

By successively taking $s = 1, 2, 3$ in (126), a complete set of source densities is obtained for each onset flow.

9.62 Solution of the Equations.

The numerical solution of equations (126) is a major portion of the total calculation. In typical cases the coefficient matrix $A_{ij}^{(s)}$ has an order N of 500 - 800, and so solution by direct elimination is not feasible. Of many possibilities, the only ones actually programmed are two forms of the Seidel iterative procedure. This procedure has the advantage of being extremely simple so that the time per iteration is minimized, although the number of iterations required to obtain a sufficiently accurate solution may be larger than for a more sophisticated procedure. The coefficient matrix $A_{ij}^{(s)}$ is rather well suited to this procedure since for most bodies its diagonal elements are much larger than any off-diagonal elements.

In the first form of the iterative procedure the (p + 1)st approximation to the solution $\sigma_i^{(s)(p+1)}$ is obtained from the p-th approximation $\sigma_i^{(s)(p)}$ by the relation

$$\sigma_i^{(s)(p+1)} = -\frac{1}{A_{ii}^{(s)}}\left[\sum_{\substack{j=1 \\ j\neq i}}^{N} A_{ij}^{(s)} \sigma_j^{(s)(p)} + V_\infty^{(s)} n_i\right] \qquad i = 1, 2,\ldots,N \tag{127}$$

With the definition

$$\delta\sigma_i^{(s)(p)} = \sigma_i^{(s)(p+1)} - \sigma_i^{(s)(p)} \tag{128}$$

this may be put in the following form, which is more convenient for calculation,

$$\delta\sigma_i^{(s)(p)} = -\frac{1}{A_{ii}^{(s)}}\left[\sum_{j=1}^{N} A_{ij}^{(s)} \sigma_j^{(s)(p)} + V_\infty^{(s)} n_i\right] \qquad i = 1, 2,\ldots,N \tag{129}$$

In this form the entire set of $\sigma_i^{(s)(p+1)}$ is calculated from the values of the previous approximation $\sigma_i^{(s)(p)}$.

In the other form of the iteration the most recently calculated approximations to the $\sigma_i^{(s)}$ are used in the right-hand side of (129). Specifically, the $\sigma_i^{(s)(p+1)}$ are obtained from the $\sigma_i^{(s)(p)}$ by the relation

$$\delta \sigma_i^{(s)(p)} = -\frac{1}{A_{ii}^{(s)}} \left[\sum_{j=1}^{i-1} A_{ij}^{(s)} \sigma_j^{(s)(p+1)} + \sum_{j=1}^{N} A_{ij}^{(s)} \sigma_j^{(s)(p)} + V_{\infty n_i}^{(s)} \right] \quad (130)$$

In either case the iteration (129) or (130) is repeated until the maximum value of $|\delta \sigma_i^{(s)(p)}|$ for a particular p is less than a certain prescribed number. This number has been set at 0.0001.

The initial values of the $\sigma_i^{(s)}$ are taken as zero in both forms of the iterations. In practice three sets of equations are solved simultaneously — one for each value of s. An iteration is performed for each set of equations in turn, and this procedure is repeated until one set of $\sigma_i^{(s)}$ has converged to within the prescribed accuracy. Then iterations are performed in turn for the remaining two sets of equations until one of these sets of $\sigma_i^{(s)}$ converges. Finally the last set of equations is iterated by itself until convergence is attained. If less than three onset flows are desired, the other onset flows may be set equal to zero. It is evident from the form of (129) and (130) that for such onset flows convergence to zero is obtained immediately, and some saving in computation time results.

The second form of the iteration (130) always converges at least as rapidly as the first form (129) and almost always converges considerably faster. Generally, the form (129) requires from 7 to 60 iterations for convergence, with typical cases requiring 30 to 40. The form (130) requires 7 to 40 iterations for convergence, with typical cases requiring 15 to 25. Thus the form (130) is always used in practice. The other is presented here for completeness. The order in which the elements are considered may affect the rate of convergence for the second form of the iteration, while for the first form it cannot. This, however, has never been a factor in the speed of the solution.

One method of accelerating the convergence of either (129) or (130) that has been investigated but not programmed is based on the fact that after a certain number of iterations the ratio

$$\rho_i^{(s)(p)} = \frac{\delta \sigma_i^{(s)(p)}}{\delta \sigma_i^{(s)(p-1)}} \tag{131}$$

is practically independent of p (and also practically independent of i, although this fact is not particularly useful). If this were exactly true, i.e., if

$$\rho_i^{(s)(p)} = \rho_i^{(s)} \tag{132}$$

then the final value of $\sigma_i^{(s)(p)}$, say $\sigma_i^{(s)(\infty)}$ could be written

$$\sigma_i^{(s)(\infty)} = \sigma_i^{(s)(p)} + \delta \sigma_i^{(s)(p)} + \delta \sigma_i^{(s)(p+1)} + \delta \sigma_i^{(s)(p+2)} + \ldots \tag{133}$$

$$= \sigma_i^{(s)(p)} + \delta \sigma_i^{(s)(p)} \left[1 + \left(\rho_i^{(s)} \right) + \left(\rho_i^{(s)} \right)^2 + \ldots \right]$$

or, by summing the geometric series

$$\sigma_i^{(s)(\infty)} = \sigma_i^{(s)(p)} + \frac{\delta \sigma_i^{(s)(p)}}{1 - \rho_i^{(s)}} \tag{134}$$

In many cases, after a relatively small number of iterations $\rho_i^{(s)(p)}$ becomes sufficiently independent of p for the use of (134) to give a considerable improvement in the accuracy of the approximation. In such cases the use of (134) at a particular stage or stages of the iterative procedure (129) or (130) can significantly reduce the number of iterations required for convergence. The inclusion of this feature in the method of solution of the linear equations is primarily a matter of designing tests on the size of $\delta \sigma_i^{(s)(p)}$ and $\left[\rho_i^{(s)(p)} - \rho_i^{(s)(p-1)} \right]$ so that (134) will be applied at the proper stage of the iterative procedure.

9.7 Calculation of Total Flow Velocities. The Second Output.

9.71 Velocities and Pressures on the Body Surface.

Once the values of the surface source density on all elements have been determined, the actual flow velocities at the null points are calculated by multiplying the elements of the ''matrices of influence coefficients'',(which were calculated assuming a unit value for all source densities) by the corresponding true values of the source densities, summing, and adding the onset flow. Recall that the velocity induced at the null point of the i-th element by a unit source density on the j-th element is the vector $\vec{v}_{ij}^{(s)}$ with components $X_{ij}^{(s)}$, $Y_{ij}^{(s)}$, and $Z_{ij}^{(s)}$, where s identifies the corresponding onset flow $\vec{V}_{\infty}^{(s)}$. Let the total flow velocity at the null point of the i-th element be denoted by the vector $\vec{V}_{i}^{(s)}$ with components $v_{ix}^{(s)}$, $v_{iy}^{(s)}$, $v_{iz}^{(s)}$. These components are given by

$$v_{ix}^{(s)} = \sum_{j=1}^{N} X_{ij}^{(s)}\, \sigma_{j}^{(s)} + v_{\infty x}^{(s)}$$

$$v_{iy}^{(s)} = \sum_{j=1}^{N} Y_{ij}^{(s)}\, \sigma_{j}^{(s)} + v_{\infty y}^{(s)} \qquad (135)$$

$$v_{iz}^{(s)} = \sum_{j=1}^{N} Z_{ij}^{(s)}\, \sigma_{j}^{(s)} + v_{\infty z}^{(s)}$$

Equations (135) are evaluated for all values of i, i.e., for every null point, and for s = 1, 2, 3 to give flow velocities for all three onset flows. The velocity components given by (135) are the basic results of this computation method. For convenience certain other quantities of interest are computed from the velocity components. These are the velocity magnitude

$$V_{i}^{(s)} = \sqrt{\left(v_{ix}^{(s)}\right)^2 + \left(v_{iy}^{(s)}\right)^2 + \left(v_{iz}^{(s)}\right)^2} \qquad (136)$$

the pressure coefficient

$$c_{p_i}^{(s)} = 1 - \left(v_{i}^{(s)}\right)^2 \qquad (137)$$

106

and the direction cosines of the total flow velocity vector

$$\gamma_{ix}^{(s)} = V_{ix}^{(s)} \Big/ V_i^{(s)}$$

$$\gamma_{iy}^{(s)} = V_{iy}^{(s)} \Big/ V_i^{(s)} \tag{138}$$

$$\gamma_{iz}^{(s)} = V_{iz}^{(s)} \Big/ V_i^{(s)}$$

It might be mentioned in passing that if the onset flow is input as a uniform stream of other than unit magnitude, all calculated quantities are correct except the pressure coefficient. Finally, as a measure of the accuracy of the solution, the total normal velocity at each null point is computed from

$$V_{ni}^{(s)} = \sum_{j=1}^{N} A_{ij}^{(s)} \sigma_j^{(s)} + V_{\infty n_i}^{(s)} \tag{139}$$

The second output of the method has a format similar to that of the first output, and the elements are listed in the same order. The quantities tabulated are: the identifying integers m and n, the coordinates of the null point in the reference coordinate system, the components of the total flow velocity at the null point, the magnitude of this velocity and the square of this magnitude, the pressure coefficient, the direction cosines of the total flow velocity vector, the components of the unit normal vector, the total normal velocity, and the value of the surface source density on the element. The format of this listing is as follows:

n	m	x_{np}'	$V_i^{(s)}$	$V_{ix}^{(s)}$	$\gamma_{ix}^{(s)}$	n_x	$V_{ni}^{(s)}$
		y_{np}'	$\left(V_i^{(s)}\right)^2$	$V_{iy}^{(s)}$	$\gamma_{iy}^{(s)}$	n_y	$\sigma_i^{(s)}$
		z_{np}'	$c_{p_i}^{(s)}$	$V_{iz}^{(s)}$	$\gamma_{iz}^{(s)}$	n_z	

In the above listing the notation of the earlier sections has been followed and the subscript i omitted from the coordinates of the null point and the components of the normal vector. The above information is listed for every

null point, and there is one complete output for each onset flow, i.e., for every value of s.

9.72 Velocities and Pressures at Points off the Body Surface.

The velocity may also be computed at points off the body surface. Such points are designated off-body points. The coordinates of the off-body points in the reference coordinate system, are input to the machine at the beginning of the program along with the input points, but they are not used until this stage of the calculation.

The off-body points are identified by the integer subscript ν, which denotes the order in which they were input. The coordinates of the ν-th off-body point in the reference coordinate system are denoted $x'_{ob\nu}$, $y'_{ob\nu}$, $z'_{ob\nu}$. Each off-body point is inserted into the portion of the program that computes the vector "matrices of influence coefficients" and treated exactly like a null point. That is, for the ν-th off-body point a set of $X^{(s)}_{\nu j}$, $Y^{(s)}_{\nu j}$, $Z^{(s)}_{\nu j}$, $j = 1, \ldots, N$, $s = 1, 2, 3$, is computed by the methods of Section 9.5 using the coordinates of the off-body point in place of the coordinates of a null point in the formulas of that section. The $X^{(s)}_{\nu j}$, $Y^{(s)}_{\nu j}$, $Z^{(s)}_{\nu j}$ are the velocity components induced at the off-body point by a unit source density on the j-th element (or by the j-th basic and reflected elements in cases of symmetry). The velocity components at each off-body point are then calculated from

$$V^{(s)}_{\nu x} = \sum_{j=1}^{N} X^{(s)}_{\nu j} \sigma^{(s)}_{j} + V^{(s)}_{\infty x}$$

$$V^{(s)}_{\nu y} = \sum_{j=1}^{N} Y^{(s)}_{\nu j} \sigma^{(s)}_{j} + V^{(s)}_{\infty y} \qquad (140)$$

$$V^{(s)}_{\nu z} = \sum_{j=1}^{N} Z^{(s)}_{\nu j} \sigma^{(s)}_{j} + V^{(s)}_{\infty z}$$

Equations (140) are evaluated for $s = 1, 2, 3$ to give velocity components for all three onset flows. These velocity components are combined in a

manner similar to equations (136), (137), and (138) to give velocity magnitude $V_v^{(s)}$, pressure coefficient $c_{pv}^{(s)}$ and the direction cosines of the velocity vector $\gamma_{vx}^{(s)}$, $\gamma_{vy}^{(s)}$, $\gamma_{vz}^{(s)}$. These quantities are listed on separate output. The format of this listing is as follows:

$$
\begin{array}{ccccc}
\nu & x_{obv}' & V_v^{(s)} & V_{vx}^{(s)} & \gamma_{vx}^{(s)} \\[2ex]
& y_{obv}' & \left(V_v^{(s)}\right)^2 & V_{vy}^{(s)} & \gamma_{vy}^{(s)} \\[2ex]
& z_{obv}' & c_{pv}^{(s)} & V_{vz}^{(s)} & \gamma_{vz}^{(s)}
\end{array}
$$

There is of course a complete listing for each onset flow.

9.8 Storage Limits. The Maximum Number of Elements

The maximum number of elements that may be used to approximate a body surface is dictated by the storage capacity of the computing machine. The method utilizes both the high speed core storage of the machine and the low speed tape storage. The capacity of either type of storage may be the limiting factor on the number of elements. These two types of storage limits are discussed below for the two computing machines for which this method has been programmed — the IBM 704 and the IBM 7090. The high speed storage capacity of the machine is taxed during the calculation of the sets of induced velocities or ''matrices of influence coefficients'', described in Section 9.5. During this computation the twenty-eight quantities defining each element must be in the core. Also, since the induced velocity matrices are transferred to tape storage one row at a time, there must be a provision for storing a complete row of the induced velocity matrices. Thus for each element a set of the quantities $X_{ij}^{(s)}$, $Y_{ij}^{(s)}$, $Z_{ij}^{(s)}$, $s = 1, 2, 3$, which are the velocity components induced by that element at one particular null point, must be stored along with the twenty-eight defining quantities. For non-symmetric bodies there is one set of $X_{ij}^{(s)}$, $Y_{ij}^{(s)}$, $Z_{ij}^{(s)}$, while there are two sets for bodies with one symmetry plane and three sets for bodies with two or three symmetry planes. In all cases the rows of the induced normal velocity matrices are computed just before storing, so for each element only one $A_{ij}^{(s)}$

109

is stored in the core at any time. Thus, if N is the number of elements formed from the input points (basic elements in cases of symmetry), the total storage required for the elements in the various cases is

Non-Symmetric   : 32 N
One Symmetry Plane   : 35 N
Two or Three Symmetry Planes: 38 N

These requirements are somewhat increased except for the one plane of symmetry case by other considerations. Up until all the elements have been formed storage must be provided for the coordinates of the input points, which then become superfluous once the calculation of induced velocities has begun. Accordingly, this storage is then utilized for the induced velocity components. In all cases of symmetry the induced velocities require at least as much storage as the input points, and there is no trouble. For non-symmetric bodies, however, there is only one set of induced velocities, which thereby require less storage than the coordinates of the input points, since the number of input points exceeds the number of elements. The additional ''wasted'' storage that must be provided for the input points amounts to about 1.7 numbers per element in non-symmetric cases only. (See below for limits on the number of input points.) Also in cases of two or three symmetry planes where (unlike the case of one symmetry plane) the number of intermediate induced velocities due to the individual basic and reflected elements exceeds the final number of combined induced velocities, provision has been made for storing one additional set of induced velocity components — three numbers. This additional storage is not essential, but is required by the particular programming logic employed. With these adjustments the total high speed storage required for the various cases is as follows:

Non-Symmetric   : 33.7 N
One Symmetry Plane   : 35   N
Two or Three Symmetry Planes: 41   N

The IBM 704 and the IBM 7090 for which this method was programmed both have a high speed core of 32,000 storage registers. On the IBM 704 the program of this method requires about 4,000 words, while the supervisory program used requires about 1,000. The compatibility program that allows the

program of the method to be run on the IBM 7090 requires about 4,000 words. Thus on the IBM 704 there are 27,000 storage registers available for the elements, while on the IBM 7090 there are 23,000 available. Thus the core storage limits on the maximum number of elements are as follows;

Core Storage Limits on Element Number

Type of Case	:	IBM 704	IBM 7090
Non-Symmetric	:	800	675
One Symmetry Plane	:	770	650
Two or Three Symmetry Planes:		650	550

The low speed tape storage capacity of the machine is taxed by the induced velocities $X_{ij}^{(s)}$, $Y_{ij}^{(s)}$, $Z_{ij}^{(s)}$, $A_{ij}^{(s)}$, $s = 1, 2, 3$. Since the matrices $A_{ij}^{(s)}$ are used many times during the iterative solution of the linear equations, in the program for the IBM 704 they are stored in duplicate on different tape units, which are then used alternately to eliminate the time required for rewinding a tape. The requirement is imposed that one complete set of $A_{ij}^{(s)}$ be stored on a single tape unit. Thus in the largest cases on the IBM 704 five tape units are completely filled — one for each set of $A_{ij}^{(s)}$ and three for the $X_{ij}^{(s)}$, $Y_{ij}^{(s)}$, $Z_{ij}^{(s)}$. In this scheme, if larger cases were allowed, three additional tape units would be required — one for each set of $A_{ij}^{(s)}$ and one for $X_{ij}^{(s)}$, $Y_{ij}^{(s)}$, $Z_{ij}^{(s)}$. This would mean a total of eight tape units, which is more than was available. Increasing the storage capacity by changing the tape reels is not feasible, since it would have to be done every iteration during the solution of the linear equations. Thus the low speed tape storage limit on the number of elements arises from the fact that a complete set of $A_{ij}^{(s)}$, $s = 1, 2, 3$, must be stored on a single tape-unit. The program for the IBM 7090 does not store $A_{ij}^{(s)}$ in duplicate. Nevertheless, the same tape storage limit was adopted for this program, because of the possibility that this procedure may be adopted in the future. In any case the core storage limits are the critical ones for the IBM 7090 program.

For non-symmetric bodies there is only one matrix $A_{ij}^{(s)}$, while there are two matrices for bodies with one symmetry plane, and three matrices for bodies with two or three symmetry planes. Thus if N is the number of elements

formed from input points, the total number of the $A_{ij}^{(s)}$ for the various cases is:

Non-Symmetric	:	N^2
One Symmetry Plane	:	$2N^2$
Two or Three Symmetry Planes	:	$3N^2$

The tape units used with the IBM 704 and sometimes with the IBM 7090 utilized low density tape. A new 2400 foot reel of this tape provides 900,000 words of storage. Recently the tape units used with the IBM 7090 have utilized high density tape, which increases the storage capacity by a factor of about 2.78. Thus the tape storage limits on the maximum number of elements are as follows:

Tape Storage Limits on Element Number

Type of Case	:	Low Density Tape	High Density Tape
Non-Symmetric	:	945	1580
One Symmetry Plane	:	670	1120
Two or Three Symmetry Planes	:	545	910

In each case the limits for the high density tape are just those for the low density tape multiplied by $\sqrt{2.78} \approx 1.67$.

The actual limit on the number of elements in any case is the smaller of the core limit and the tape limit. From the above it is clear that this limit depends both on the machine and on the type of tape used. By comparing the two tables above it can be seen that, if high density tape is used, the core limits are the critical ones for all types of cases on both machines. If low density tape is used, the core limits are still critical for the IBM 7090 (except that in cases with two or three symmetry planes the core and tape limits are essentially equal) while for the IBM 704 the tape limits are critical except for non-symmetric bodies. Assuming that low density tape is used with the IBM 704 and high density tape with the IBM 7090, the limits on the maximum number of elements are as shown in the table below:

112

Maximum Number of Basic Elements

Type of Case		IBM 704	IBM 7090
Non-Symmetric	:	800	675
One Symmetry Plane	:	670	650
Two or Three Symmetry Planes	:	545	550

If low density tape is used with the IBM 7090, these limits are unchanged except that the limit in cases with two or three symmetry planes is lowered by five elements.

These limits are on the number of elements formed from the input points — basic elements in cases of symmetry. The total effective number of elements that approximate the entire body surface is found by multiplying these numbers by two raised to a power equal to the number of symmetry planes. For convenience the maximum effective number of elements for the various cases in the previous table are listed below:

Maximum Effective Number of Elements

Type of Case		IBM 704	IBM 7090
Non-Symmetric	:	800	675
One Symmetry Plane	:	1340	1300
Two Symmetry Planes	:	2180	2200
Three Symmetry Planes	:	4360	4400

There are also core storage limits on the maximum number of input points. Basically, the input points occupy the same storage as the induced velocity components $X_{ij}^{(s)}$, $Y_{ij}^{(s)}$, $Z_{ij}^{(s)}$. Since each input point has three coordinates, this means that the ratio of maximum number of input points to maximum number of basic elements (core storage limit) equals the number of induced velocity matrices computed. This would fix the maximum number of input points at N, $2N$, and $4N$ in cases of zero, one, and two or three symmetry planes, respectively. (The limit is $4N$ rather than $3N$ in cases of two or three symmetry planes, because storage is provided for a fourth set of induced velocity components, as explained above.) These limits, however, have been adjusted. It is clear from the description of how elements are formed from input points in Section 9.1 that the number of input points must exceed the number of

elements formed. Thus in non-symmetric cases provision must be made for storing more than N input points even though the maximum permissible number of elements is thereby reduced, as mentioned above. It is difficult to imagine a situation for which more than $2N$ input points would be required, so the limits in cases of two or three symmetry planes have been reduced to this value. The maximum numbers of input points permitted by the actual program are as shown below:

Maximum Number of Input Points

Type of Case		IBM 704	IBM 7090
Non-Symmetric	:	1250	1125
One Symmetry Plane	:	1540	1300
Two or Three Symmetry Planes	:	1300	1100

From the manner in which elements are formed from the input points it is clear that the number of input points does not greatly exceed the number of elements. For example, consider a section with 41 n-lines, each of which contains 21 points. Thus this section has a total of $41 \times 21 = 861$ input points, from which $40 \times 20 = 800$ elements are formed. It is felt that the above limits are high enough so that they will never restrict the input.

Due to assumptions made during the programming of this method, the input must satisfy two additional conditions, neither of which is thought to be restrictive. The maximum number of ''columns'' or n-lines of input points cannot exceed 250, while the maximum number of sections into which the body surface is divided cannot exceed 40.

The limits on the number of off-body points are determined in a way similar to that used for the basic elements. It will be recalled that vector ''matrices of influence coefficients'', $X_{vj}^{(s)}$, $Y_{vj}^{(s)}$, $Z_{vj}^{(s)}$, are computed for the off-body points in the same way as they were computed for the null points. This is accomplished by replacing the coordinates of the null points by the coordinates of the off-body points in the portion of the program that computes induced velocities and then repeating the calculations. The core storage limits on the number of off-body points are thus the same as those given

above for the basic elements. Moreover, since storage assignments are permanent, these limits hold regardless of the number of basic elements used to approximate the body surface. The tape storage limits on the number of off-body points are artificial in the sense that they were dictated by programming logic rather than by the tape storage capacity of the machine. It is required that the sets of induced velocity components, $X_{vj}^{(s)}$, $Y_{vj}^{(s)}$, $Z_{vj}^{(s)}$, be stored on three tape units, as the induced velocity components for the null points were. (The tape units on which the $A_{ij}^{(s)}$ were stored are thus not utilized during this portion of the program.) Accordingly, the tape storage limits on the number of off-body points depend on the number of basic elements. The restriction is that the product of the number of off-body points and the number of basic elements be less than the square of the tape storage limit on the number of basic elements for the type of case in question. Thus the tape storage limits on the number of off-body points are at least as large as the corresponding tape storage limits on the number of basic elements. The two limits are equal if the maximum number of basic elements are used to approximate the body surface. In summary, if the core limits are critical for the basic elements (This includes all cases for the IBM 7090.), the limits on the maximum number of off-body points are the same as those for the basic elements, independently of the number of basic elements actually used. If the tape limits are critical for the basic elements, the limits on the number of off-body points may be tape storage limits, which depend on the number of basic elements used, or core storage limits. The limits on the maximum number of off-body points are shown in the table below.

Maximum Number of Off-Body Points

Type of Case		IBM 704	IBM 7090
Non-Symmetric	:	800	675
One Symmetry Plane	:	$(670)^2/N^*$ or 770	650
Two or Three Symmetry Planes	:	$(545)^2/N^*$ or 650	550

*The smaller is the limit

115

9.9 Computation Times

This section presents some analysis that, it is hoped, may prove useful to the user of this method in the estimation of computation times. Basically, experience in the use of this program is necessary before accurate estimates of computation times can be made. It is necessary because the time for a particular case depends not only on the number of elements used to approximate the body surface but also on the geometry of the body in a manner that is sometimes difficult to predict. The following analysis shows the basic dependence of the computation time on the number of elements for various portions of the program and points out where the body geometry is most important. For a known body geometry this analysis defines computation time as a function of element number in terms of certain timing constants. Generally, these timing constants do not represent simple computation times for a basic operation, but are due to several sources. For this reason they have been determined empirically by timing the various cases that have been run on the IBM 704 and the IBM 7090. These constants are thus not known to high accuracy, for the timing of these cases is subject to many sources of error that cannot be taken into account. These errors include clock inaccuracies, machine room procedure, and minor difficulties of machine operation. Ultimately, satisfactory estimates of the timing constants could be obtained from a large number of cases. It is believed that the values given below are accurate enough to be useful, particularly those for the IBM 704 on which considerably more cases have been run than on the IBM 7090 and for which the computation times are several times as large.

For the purpose of estimating computation times it is convenient to divide the total calculation into four parts. These are: (1) the formation of the elements from the input points (Sections 9.2, 9.3, and 9.4); (2) the calculation of the induced velocities (Section 9.5); (3) the solution of the linear equations (Section 9.6); and, (4) the calculation of the total flow velocities (Section 9.7). The computation time of (1) is negligible, while that of (4) is definitely minor. Parts (2) and (3) are the time-consuming ones and either may be the larger. Estimates of these computation times and their dependence on the number of elements, symmetry planes, and onset flows in the case being calculated are discussed below.

116

The time required to form elements from the input points depends only on the number N of elements that are formed. It is independent of the body geometry, the number of symmetry planes, and the number of onset flows. This time is simply proportional to N and is thus negligible compared to the other computation times that vary as N^2. Its only importance is that it is the time that elapses up to the first output, and this portion of the computation is often performed separately. A sufficiently accurate estimate is obtained by simply ignoring the dependence on N and using the time required for the larger cases. On the IBM 704 this portion of the calculation requires 2 to 3 minutes, while on the IBM 7090 it requires half a minute to a minute.

The time required to compute the induced velocities or ''matrices of influence coefficients'' depends on the element number, number of symmetry planes and the body geometry, but it is independent of the number of onset flows. If the induced velocity components were calculated by a single set of formulas, body geometry would not be a factor, and the computation time would simply be proportional to N^2, the square of the number of basic elements, multiplied by two raised to a power equal to the number of symmetry planes. However, the induced velocity components are computed by one of three alternative sets of formulas: source, equation (97); source-quadrupole, equations (57) through (62); or exact, equations (42) through (49). The body geometry is important, because different body shapes use the various sets of formulas for different proportions of the elements. The times required to compute a single set of induced velocity components by each of the three methods are as follows:

Velocity Formula	IBM 704	IBM 7090
Source	$0.17 \cdot 10^{-3}$ min	$0.026 \cdot 10^{-3}$ min
Source-Quadrupole	$0.43 \cdot 10^{-3}$ min	$0.04 \cdot 10^{-3}$ min
Exact	$1.75 \cdot 10^{-3}$ min	$0.31 \cdot 10^{-3}$ min

It can be seen that the ratios of these basic computation times are not the same for the two machines. The difference is due to the fact that these times are not simple instruction times, but include such things as tape reading.

117

From the above table time estimates can be made if the number of induced velocities computed by each type of formulas can be predicted. The last comes rapidly with experience since a few general bodies are typical of all. For example, any simply-connected, convex body is quite similar to an ellipsoid of the same fineness ratio as far as the induced velocity computation is concerned. Also, these timing constants permit a good estimate of the variation of computing time with element number to be made for a given body shape. For many bodies the number of times the velocities induced by each element are computed by the exact or source-quadrupole formulas is approximately independent of element number, and thus the total number of times these formulas are used varies linearly with N, the number of basic elements. The number of applications of the simple source formulas varies accordingly, so that the total number of induced velocities calculated equals N^2 multiplied by two raised to a power equal to the number of symmetry planes. Some examples of the proportion of the induced velocities computed by each of the three sets of formulas in actual cases are given below. To quote the results for a typical case, if a body with three symmetry planes is approximated by 500 basic elements, there are $8 \cdot (500)^2 = 2,000,000$ sets of induced velocity components computed. Of these 50,000 to 100,000 are generally computed by the exact formulas, 100,000 to 200,000 by the source-quadrupole formulas, and the remaining 1,700,000 to 1,850,000 by the simple source formulas. Typical computation times for such a set of induced velocities might be eight hours on the IBM 704 and an hour and a half on the IBM 7090.

The time required for the iterative solution of the sets of linear equations for the values of the surface source density depends on the body geometry, element number, number of onset flows, and number of symmetry planes. The time required for a single iteration is independent of the body geometry. However, the total number of iterations required for convergence for any onset flow is a function only of body geometry and, moreover, a rather strong function. The prediction of the number of iterations required for a given body shape is a skill that comes rapidly with experience. As was the case for the induced velocities, the results for bodies of the same general shape are quite similar. A single iteration consists of two operations. First, the matrices of induced normal velocities are transfered one row at a time from tape storage to core storage. Second, matrix multiplications are performed one row at a time to

118

obtain new sets of values of the surface source densities from the values of the previous iteration. The time required for the first of these operations is simply proportional to the number of elements in the induced velocity matrices, which equals N^2, the square of the number of basic elements, multiplied by the number of matrices. It will be recalled that there is one matrix for non-symmetric cases, two matrices for cases with one symmetry plane, and three matrices for cases with two or three symmetry planes. All matrices for a given case are formed and transfered to core storage during each iteration regardless of which onset flows are actually being computed. The second operation consists of one matrix multiplication for each onset flow that is being computed. The time required is thus proportional to N^2 multiplied by the number of onset flows for which computations are performed during the iteration in question. The two constants of proportionality were determined empirically for the IBM 704 and the IBM 7090. The time required for a single iteration was found to be:

$$\text{IBM 704} \quad : \quad \left[0.07 \text{ (No. of Matrices)} + 0.07 \text{ (No. of Flows)} \right] \left(\frac{N}{100} \right)^2 \text{ min}$$

$$\text{IBM 7090} \quad : \quad \left[0.03 \text{ (No. of Matrices)} + 0.015 \text{(No. of Flows)} \right] \left(\frac{N}{100} \right)^2 \text{ min}$$

Notice that the time for the computations performed in the core is of the same order of magnitude as the tape-reading time. The use of these constants is best illustrated by an example. Consider a body with one plane of symmetry defined by 500 basic elements for which calculations are being performed for onset flows parallel to the x, y, and z coordinate axes. Suppose it is known or estimated that the iterative solutions of the three sets of linear equations will converge in 38, 15, and 47 iterations, respectively. Then there are three onset flows for 15 iterations, two onset flows for 23 iterations, and one onset flow for 9 iterations. There are of course two matrices of induced velocities for all 47 iterations. If the solution is being carried out on the IBM 7090, the above formulas estimate the computation time as

$$\left[0.03(2 \cdot 47) + 0.015(3 \cdot 15 + 2 \cdot 23 + 1 \cdot 9) \right] (5)^2 = 108 \text{ min}$$

The calculation and output of the total flow velocities is a similar operation to a single iteration of the solution of the linear equations, and its

computation time varies in the above-described way with element number, number
of onset flows, and number of matrices. In this case, however, the variation
with number of onset flows is more important than the variation with number of
matrices, because both the flow computation and the amount of output are pro-
portional to the former number. Since the time required for this portion of
the program is a small fraction of the total computation time, it is sufficient-
ly accurate to ignore the dependence on the number of matrices and write the
time as

IBM 704	IBM 7090

$$0.8(\text{No. of Flows}) \left(\frac{N}{100}\right)^2 \text{min} \qquad 0.3(\text{No. of Flows}) \left(\frac{N}{100}\right)^2 \text{min}$$

If velocities are computed at off-body points, a ''row'' of the induced
velocity matrix must be computed for each such point, and similarly a calcu-
lation of total flow velocities is required. Thus the number of sets of in-
duced velocity components calculated at each off-body point is N, the number
of basic elements, multiplied by two raised to a power equal to the number of
symmetry planes. The proportions of these induced velocities calculated by
each of the three sets of formulas must be estimated. Often it turns out
that all the induced velocities at off-body points are calculated by the
simple source formulas. The calculation of total flow velocities at off-body
points simply increases the computation time of that portion of the program by
a percentage equal to the ratio of the number of off-body points to the number
of basic elements.

The basic information, including actual and estimated computation times,
for some typical cases is presented in the tables on the following page. The
accuracy of the time estimates on these tables is about average. No off-body
points are included in any of the cases shown in the table.

Body Shape	Basic Elements	Symmetry Planes Used	Onset Flows	Induced Velocities Computed by each Formula			Iterations For Linear Equations	Computation Times to the Nearest Minute with Estimates in ( )				
				Source	Source-Quadrupole	Exact		Element Formation	Induced Velocities	Solution of Equations	Flow Velocities	Total
Prolate Spheroid Fineness Ratio 10	432	0	1	114,...	..., 2..	..., ...	9	(2)	120 (113)	25 (24)	13 (15)	161 (155)
Oblate Spheroid Fineness Ratio 0.1	432	0	.1	94,...	..., 0..	...,...	14	(2)	104 (105)	44 (39)	13 (15)	163 (162)
Wing-Fuselage Combination	509	2	..	863,...	...,...	...9..	7, 8, 22	(2)	308 (310)	213 (258)	62 (62)	585 (613)
Prolate Spheroid Fineness Ratio 10	527	1	..	52,935	9.,92.	...,...	10, ...	(1)	393 (383)	132 (118)	96 (107)	624 (611)
Contracting Duct Area Ratio 4	525	.	..	...,...	...,...	...,...	24	(2)	477 (512)	193 (185)	22 (22)	690 (722)
Sphere	540	.	.	...,...	...,...	10,700	3, 3, 3	(2)	..09 (..50)	100 (98)	69 (70)	581 (627)

Body Shape	Basic Elements	Symmetry Planes Used	Onset Flows	Induced Velocities Computed by each Formula			Iterations For Linear Equations	Computation Times to the Nearest Minute with Estimates in ( )				
				Source	Source-Quadrupole	Exact		Element Formation	Induced Velocities	Solution of Equations	Flow Velocities	Total
Prolate Spheroid Fineness Ratio 10	432	0	.1	114,...	...,2...	...,...	9	(1)	19 (19)	8 (8)	4 (6)	31 (34)
Oblate Spheroid Fineness Ratio 0.1	432	0	...	94,510	...,2..	37,...	11, 7,..	(1)	19 (18)	32 (17)	17 (17)	68 (51)
Wing-Fuselage Combination	523	2	..	597,...	155,...	68,...	4, 5, 30	(1)	70 (55)	116 (91)	30 (25)	247 (172)
Tri-axial Ellipsoid Axis Ratios:10:10:0.1	540	.	..	2,019,...	131,...	131,...	..., 21	(1)	103 (100)	65 (70)	25 (26)	193 (203)
Contracting Duct Area Ratio 4	525	.	1	2,01.,...	101,...	...,...	24	(1)	78 (76)	69 (69)	7 (8)	154 (156)
Ship Hull	50.	0	.0	2..,000	107,...	...,421	3, 21	(1)	52 (47)	80 (73)	13 (15)	146 (136)

121

10.0 COMPARISON OF THE CALCULATED VELOCITIES WITH ANALYTIC SOLUTIONS

To evaluate the accuracy of this method, the calculated flow velocities were compared with the analytic solutions for the flow on the surface of a sphere, ellipsoids of revolution, and tri-axial ellipsoids. Before the comparisons are discussed, three facts should be mentioned. Since the null points, where the calculated flow velocities are evaluated, are seldom actually on the body surface being approximated, there is some uncertainty as to how the calculated and analytic solutions should be compared. It was decided to relate the two solutions by means of the unit normal vector. For purposes of comparison, a given null point is taken to correspond to the point on the true body surface where the unit normal vector to the surface is identical with the unit normal vector of the element on which the null point in question is located. The accuracy of the calculation obviously increases with the number of elements used to approximate the body surface. In fact, the variation of accuracy with element number is one of the important considerations illustrated by the comparisons. The calculated velocities are always identified by the total effective number of elements used to approximate the body surface regardless of the number of symmetry planes utilized by the computation. This number, which is the number of basic elements multiplied by two raised to a power equal to the number of symmetry planes, is evidently the significant one for accuracy considerations. Finally, for simplicity of presentation the calculated and analytic solutions are generally compared along curves in the body surfaces that lie in the symmetry planes. Many of the calculated cases utilized the symmetry of the bodies, and thus, as explained previously, velocities were not calculated in the symmetry planes. In these cases the velocities in the symmetry planes were obtained by parabolic extrapolation of the velocity components at nearby points ignoring any components known to be zero in the symmetry plane under consideration. The errors resulting from this extrapolation appear to be very small.

The errors discussed in this section are those arising from the approximate mathematical solution of the problem of potential flow about a body . When calculated velocities or pressures are compared to those of a real flow, there is another source of error arising from the fact that a potential flow

is being used to approximate a viscous, compressible, flow. This problem is not discussed here. However, experience with axisymmetric and two-dimensional flows, references 1 and 2, indicates that the calculated results agree with experiment very well in many cases of interest.

10.1 The Sphere

The body shape that received the greatest attention was, naturally enough, the sphere. A considerable number of spheres were calculated using various numbers of elements to approximate the body surface. In all cases the distribution of elements is similar, namely the one shown in figure 27. As can be seen in the figure, the elements are distributed symmetrically about the x-axis in the following manner. Two numbers are selected. The first is the number N_T of elements in the x-direction and the second is the number M_n of elements around the circumference at a given x-location. The semi-circle that is the intersection of the sphere with that portion of the xy-plane for which $y > 0$ is divided in N_T equal arcs each of which subtends an angle of $180°/N_T$ at the center of the semi-circle. The ''latitude'' circles formed by rotating the endpoints of these arcs about the x-axis are taken as the n-lines of the element system. The input points are spaced at equal angles with respect to the x-axis along these ''latitude'' circles, i.e., there is a point every $360°/M_n$ around the circles. Thus the m-lines are ''longitude'' lines. In the example of figure 27 $N_T = 9$ and $M_n = 12$ — a total of 108 elements, spaced every 20° in the x-direction and every 30° around the ''latitude'' circles at constant values of x. This rather crude representation of the sphere is for purposes of illustration only. In the cases actually computed a much larger number of elements were used, but the ratio of the element spacing in the two directions was approximately the same. With this distribution of input points, the two points where the sphere intersects the x-axis (the ''north and south poles'') are each common to M_n elements, and these elements are triangular. It is not a particularly desirable situation, and apparently introduces a certain amount of inaccuracy, particularly when the flow is parallel to the x-axis, i.e., when these concentration points are stagnation points of the flow.

123

Because the element distribution does not have spherical symmetry, the calculated velocity distributions are not exactly the same for various directions of the onset flow. Accordingly, the velocities were calculated for two onset flows, one parallel to the x-axis and one parallel to the y-axis. As can be seen from figure 27, in the case of an onset flow parallel to the x-axis the element distribution has the same symmetry as the true flow (a sort of ''axial'' symmetry), and the computed velocity magnitude is the same on all elements lying between the same two ''latitude'' circles. If the onset flow is parallel to the y-axis, the element distribution does not have the same symmetry as the true flow, and the calculated velocity magnitude will not be exactly the same, for example, at the concentration points on the x-axis as it is at the points on the z-axis.

In the following figures, the calculated velocity at every null point is represented by a symbol. Thus the density of elements may be inferred directly from the figures.

Figure 28 shows the comparison of the analytic solution with two calculated velocity distributions for the case of an onset flow parallel to the x-axis. One calculation was performed with 1334 effective elements ($N_T = 29$, $M_n = 46$), and the other with 4320 ($N_T = 54$, $M_n = 80$). Both calculated cases are quite accurate in the region of maximum velocity. The more accurate case of 4320 elements gives an error of 0.03 percent of free stream velocity in this region, while the other case gives an error of 0.1 percent. The accuracy of both calculations is quite satisfactory except near the stagnation point, which is also the concentration point of the elements. In the 4320 element case, the calculated velocity at the null point nearest the stagnation point (the null point of one of the triangular elements shown in figure 27) is in error by about 1 percent of free stream velocity. The error falls below 0.1 percent at the third null point, $\theta = 8.3°$ in figure 28, and remains below 0.3 percent for all larger values of θ. In the 1334 element case, the error at the null point nearest the stagnation point is about 2 percent of free stream velocity. This error falls below 0.5 percent for $\theta > 10°$.

Figure 29 shows comparisons of the same two calculated velocity distributions with the analytic solution for the case of an onset flow parallel to the y-axis. Comparisons are made along two curves in the body surface. The first, shown in figure 29a, lies in the yz-plane and is thus the ''equator'' of the element distribution of figure 27, while the second, shown in figure 29b, lies in the xy-plane and is thus a ''longitude'' line. It can be seen that the accuracy of the calculated velocities is quite good, particularly that of the 4320 element case. The concentration point of the elements is at $\varphi = 90°$ in figure 29b, and some increase in error can be noticed in this region — up to about 0.6 percent of free stream velocity for the 4320 element case and about twice this for the 1334 element case. It is, however, smaller than the error that occurred near the concentration point in the case of flow parallel to the x-axis.

10.2   Ellipsoids of Revolution

The calculated velocity distributions were compared with analytic solutions for two ellipsoids of revolution, a prolate spheroid of fineness ratio 10 and an oblate spheroid of fineness ratio 1/10. In all cases of ellipsoids of revolution, the input points are distributed on a sphere in the manner described in the previous section, and the y and z coordinates of these points are then divided by the fineness ratio to generate the input points for the ellipsoid. This procedure tends to concentrate points in the regions of high curvature of the body surface. The number of elements used to obtain the calculated velocity distributions are the same as were used for the sphere.

Figure 30 shows the comparison of the analytic solution with two calculated velocity distributions — one obtained using 1334 effective elements and one obtained using 4320 —, for the case of an onset flow parallel to the x-axis. The accuracy is seen to be quite good. The 4320 element case agrees with the analytic solution to plotting accuracy even in the region near the stagnation point where the velocity varies rapidly with position. Figure 31 shows comparisons of these two calculated velocity distributions with the analytic solution for the case of an onset flow parallel to the y-axis. Figure 31a shows the comparison around the circumference of the body in the yz-plane, where the velocity distribution is approximately the same as the

125

solution for an infinite circular cylinder, while figure 31b shows the comparison of the calculated and analytic velocity distributions along the meridian curve in the xy-plane. Again agreement is seen to be good.

Similar comparisons for an oblate spheroid of fineness ratio 0.1 are shown in figures 32 and 33. In the case of an onset flow parallel to the x-axis (figure 32) the maximum velocity ratio on the body surface is 7.18 . The 1334 element case calculates the maximum velocity ratio as 7.09 — an error of 9 percent of free stream velocity in this rather extreme case. In the 4320 element case there is no null point at the location of maximum velocity for the reason explained perviously. The null points closest to the location of maximum velocity have a calculated velocity ratio of 6.90, which agrees with the analytic solution to 0.8 percent of free stream velocity. The use of a parabolic extrapolation gives the calculated maximum velocity for the 4320 element case as 7.16 — an error of 2 percent of free stream velocity. It is felt that these results are quite satisfactory considering the large velocity ratios involved. The comparisons for an onset flow parallel to the y-axis are shown in figure 33. The flow in the yz-plane shown in figure 33a exhibits the only noticeable errors in this case — 0.5 percent of free stream velocity for the 4320 element case and 1 percent for the 1334 element case. Near this plane the curvature of the body surface is quite high and perhaps more elements should be concentrated in this region for better accuracy.

It should be noticed that the concentration point of the elements apparently causes no trouble for either ellipsoid of revolution.

10.3 Tri-Axial Ellipsoids

The one truly three-dimensional family of body shapes for which the analytic solution can be easily obtained consists of ellipsoids all three of whose axes have different lengths. The flows about a considerable number of ellipsoids were calculated and compared with the analytic solutions. The comparisons presented here are typical examples.

The ellipsoid whose axes in the x, y, and z directions have the ratios 1:2:0.5, respectively, is representative of rather thick three-dimensional bodies. The calculated velocities selected for comparison with the analytic solution were obtained from a case utilizing 4320 effective elements to approximate the body surface. The element distribution consisted of 54 in the y-direction and 80 around the elliptical cross-sections at constant values of y. The comparisons for onset flows parallel to the x, y, and z coordinate axes are presented in figure 34. For each onset flow these figures show the velocity distributions along three curves in the body surface — one in each of the symmetry planes. It can be seen that in all cases the velocity in the plane perpendicular to the onset flow vector is a constant independent of position and equal to the maximum velocity of the flow. The analytic and calculated velocity distributions are seen to agree to plotting accuracy, except for the region near the y-axis in the xy-plane for the case of an onset flow parallel to the z-axis (figure 34c). It is believed that this error is due to the relatively high curvature of the body surface in this region and might be removed by concentrating elements there.

11.0 THE CALCULATED FLOW VELOCITIES AND PRESSURES ON
A VARIETY OF BODIES

In this section are presented the calculated flow velocities on some
body shapes that are thought to be of interest. For the most part these
calculated solutions stand alone, although in certain cases comparisons are
made with analytic solutions, with solutions obtained by the method of
reference 1, or with experimental data.

11.1 Wing Fuselage Combinations

This section presents the results of the calculations for two wing-
fuselage combinations, for one of which experimental data were available.
It should be mentioned that the restriction of the method to cases of zero
lift essentially limits the airfoils that may be considered to symmetrical
ones. Also, wing-fuselage combinations have concave corners at the juncture
of the wing and fuselage. Thus, as explained previously, some difficulty might
be expected. However, examination of the results of the calculations has
shown that no significant inaccuracy apparently arises from this source, at
least in the zero-lift, zero-yaw case.

11.11 Warren Wing with Ellipsoidal Fuselage.

The first wing considered is that described in reference 7. The root
and tip airfoil sections of this wing are identical, being a symmetric airfoil
of 6 percent thickness. The leading edge is swept 53.5°, and the taper ratio
is 1/3. The wing is cut off at the tip parallel to the midplane of the wing.
The zero lift, zero yaw pressure distribution on this wing was calculated for
a variety of conditions.

Figure 35 shows the curves of constant pressure coefficient on the
isolated wing in incompressible flow. Two cases were calculated. In the
first the flat tip of the wing was represented by elements in the usual way,
while in the second the tip was not represented by elements, and the end of
the wing was thus left open. This was done to evaluate tip effects. The two
cases have identical pressure distributions except within 5 percent semi-span
of the tip, so only a portion of the pressure distribution for the wing with-
out tip is shown.

Both the left and right halves of the wing were taken into account, and the body therefore has two planes of symmetry. A total of 425 basic elements were employed to approximate the upper surface of the wing on one side of the midplane. The distribution consisted of 17 elements along the semi-span and 25 along the chord of the airfoil section. In addition 50 elements were used to represent the upper half of the wing tip. (1900 total effective elements.)

To a first approximation the flow at non-zero subsonic Mach numbers may be calculated by applying the Goethert transformation to the body. This is accomplished by stretching the body in the direction of the onset flow (x-direction), calculating the incompressible flow about the resulting body, and multiplying the calculated velocity components by suitable factors, (see for example reference 8). This was done for the wing without tip described above, and the resulting curves of constant pressure coefficients are shown in figure 36. A comparison of the last two figures thus shows the effect of Mach number on the pressure distribution.

To exhibit interference effects, the pressure distribution was calculated on the wing-fuselage consisting of the wing with tip described above mounted as a midwing on an ellipsoidal fuselage. The fuselage selected was a prolate spheroid of fineness ratio 8 whose length is 3 times the root chord of the wing. The leading edge of the root airfoil section is located 20 percent of the fuselage length from the front. The calculated curves of constant pressure coefficient are shown in figure 37. The effect of the fuselage on the pressure distribution on the wing can be judged by comparing these isobars with those shown in figure 35. It is also interesting to note the manner in which the isobars on the wing continue over the fuselage. This case is one of two planes of symmetry. The upper surface of the right half of the wing is approximated by 187 elements — 11 along the semi-span and 17 along the chord of the airfoil section. The upper half of the tip is represented by 34 elements. A total of 320 elements define the upper right quarter of the fuselage. The distribution consists of 40 elements along the length of the fuselage and 8 around the quarter circumference. (2164 total effective elements.)

The effect of the wing on the pressure distribution on the fuselage is shown in figure 38. This figure presents the pressure distributions in the midplane of the fuselage both with and without the presence of the wing. The analytic solution for the isolated fuselage is also shown to establish the basic calculation error. It should be noticed that the significant lowering of the pressure on the fuselage caused by the wing is located downstream of the intersection of the wing with the fuselage. This is in accordance with the experimentally observed behavior of swept wings.

11.12   NACA Wing-Fuselage.

To obtain an experimental verification of the accuracy of pressures calculated by this method for the important class of wing-fuselage bodies, calculations were performed for an NACA wing-fuselage combination. The configuration is described in reference 9, which also contains the experimental results. The wing has identical root and tip airfoil sections, both of which consist of an NACA 65A006 airfoil. The 25 percent chord line of the wing is swept 45°, and the taper ratio is 0.6. The fuselage is a pointed body of revolution of basic fineness ratio 12. However, the actual fineness ratio is 10, since one-sixth of the fuselage was cut off to accomodate the sting on which the body was mounted in the wind tunnel. The forward part of the sting was taken into account in the calculations. Tests were conducted at a Mach number of 0.6, and this was accounted for in the calculations in the manner described above. The element distribution used for the calculations differed only slightly from that described in the previous section for the Warren wing with ellipsoidal fuselage.

The calculated curves of constant pressure coefficient for this wing-fuselage are presented in figure 39. The wing tip was left open in the calculation in the manner previously described for the Warren wing, while the wing tested had a rounded tip. Accordingly, the isobars of figure 39 are terminated a short distance from the tip where it is felt they no longer have validity. The experimental curves of constant pressure coefficient are presented in figure 40. By comparing figure 39 and 40 it can be seen that the calculated and experimental isobars have the same general shape over most of the surface of the wing, but that the locations may differ significantly.

130

This difference is due to the fact that the pressure gradient is small over most of the wing surface, and thus small differences in pressure lead to significant differences in the location of the isobars.

To compare the calculated and experimental pressures directly, pressure distributions along the chord of the wing are shown in figure 41 for three locations along the span. It can be seen that the calculated and experimental pressure distributions agree quite well except near the leading edge of the wing where the calculated pressure distribution has a small, sharp, negative peak. To investigate this phenomenon further, the airfoil section was calculated as a two-dimensional body by the method of reference 1. This method has been shown to be highly accurate in a variety of applications. Its calculations agree very closely with those of high order Theodorsen solutions and also with experimental data. The resulting pressure distributions are shown in figure 42 for Mach numbers of zero and 0.6. Also shown is the theoretical incompressible pressure distribution from reference 10. The pressure distributions calculated by the method of reference 1 show a small, sharp, negative pressure peak near the leading edge of the airfoil, and it is accordingly concluded that this peak is real and was correctly predicted by the present method for the three-dimensional case. Why the method of reference 10 fails to predict such a peak is not known. Also unexplained is the failure to obtain such a peak in the wind tunnel test. It is known, however, that the pressure distribution near the leading edge of a thin airfoil is extremely sensitive to the body shape in this region. A very small change in the coordinates of the body could cause the presence or absence of such a peak.

11.2 Ducts

Ducts form an interesting class of body shapes to which the present flow calculation method is applicable, since the restriction to zero lift is not a factor. A duct is actually a case of an interior flow problem and should be calculated as such. That is, the duct should be closed by surfaces at both ends, and the onset flow should be eliminated. The interior flow is then calculated by specifying zero normal velocity on the interior of the duct walls and by specifying non-zero normal velocity distributions on the surfaces across the cross-sections at the ends of the duct. The normal velocities specified

on these surfaces may have any distributions that satisfy continuity, but normally they would be taken to give uniform flow at the ends of the duct. While the method of this report can calculate this type of flow in a perfectly routine manner, the results are subject to inaccuracies related to the inability of this method to handle bodies having concave corners. It is usually necessary to simulate the required interior flow by the flow through the open-ended duct, due to some onset flow. There are several ways that this can be done, and often the particular application will dictate the proper approach. The scheme used for the examples of this section consisted of extending both ends of the duct by means of straight sections of constant cross-sectional shape to a distance relatively large compared to the region of interest, e.g., bend, contraction, etc.. This extended duct with open ends is then taken to be in a uniform onset flow, and the calculations are performed in the same way as for cases of exterior flow. The source density distribution is determined in such a way that the normal velocity now vanishes on the inner surface of the duct. The resulting flow is somewhat irregular near the ''entrance'' of the duct at the end of the extensions, but, if the extensions are long enough, the flow smoothes out and is nearly uniform a considerable distance before the beginning of the region of interest is reached. The magnitude of the velocity in this uniform velocity region is the one of real significance for applications rather than that of the onset flow.

Several ducts of various kinds were calculated. The two main types were: (1) ducts of constant cross-sectional shape with bends and (2) straight ducts with varying cross-sectional area and/or varying cross sectional shape. In most cases the cross-sectional shape of the ducts was either circular or rectangular. The rectangular ducts of course have concave corners, and thus the results for these cases are open to question. An examination of the velocity distributions around the cross-sections of the rectangular ducts showed that the computed velocities were seriously in error near the corners. While the velocities away from the corners are more reasonable, the overall results were not judged accurate enough to be included here. Apparently some rounding of the corners is required. Thus, two circular ducts have been selected for presentation.

11.21 A Straight Circular Contracting Duct having an Area Ratio of Four.

The first duct considered is a straight one of circular cross-section. The flow is thus axisymmetric. The duct consists of a constant diameter section followed by a contraction to a cross-section of half the original diameter. The duct then expands in such a way that it is symmetric about the section of minumum area. The contracting portion of the duct has a profile that is a portion of a sine wave having a zero slope at the location of minimum area and also at the location where the constant diameter section begins. The length of the contracting section is equal to one and a half diameters of the constant diameter region.

For exterior flows about smooth convex bodies like ellipsoids the accuracy of the calculated results is determined largely by the total effective number of elements. The relative number of elements used to approximate the body in the direction of the free stream and in the direction normal to the free stream is not too important as long as the resulting distribution is at all reasonable. The element distribution is somewhat more critical in the case of ducts, and thus certain cases were repeated with the same total number of effective elements but various element distributions.

Figure 43 shows five calculated velocity distributions for the duct in question. Two of these were obtained by means of the axisymmetric method of reference 1, while the other three were obtained by the present method. The cases calculated by the present method are identified by the number of effective elements used axially along the duct and by the number of effective elements used around the circumference. These numbers apply to the entire duct from x = -7 to x = +7 and to the full 360° of circumference even though only part of the duct is shown in the figure. In the smallest case (case 1) the duct is specified by 42 elements longitudinally, 21 on each side of the throat, and by 18 elements circumferentially, one every 20°. Case 2 uses the same number of elements axially as case 1, but has 100 elements around the circumference. In case 3 the number of elements along the length of the duct is doubled relative to case 2, while the number around the circumference is approximately halved. Thus the total number of effective elements is roughly the same for case 2 and case 3. The 42 element axisymmetric solution employed the same axial distribution of elements as cases 1 and 2, and what amounts to

an infinite number of elements around the circumference. The high accuracy axisymmetric solution was obtained by calculating several cases with a very large number of elements and extrapolating the results to the case of infinitely many elements. It may be regarded as the exact solution for the present purpose. The calculated velocity magnitudes V_o in the constant velocity region around $x = 6$ differed slightly in the various cases, and in the figure each velocity distribution has been normalized with respect to its value at $x = 6$ in accordance with the fact that this is the velocity of real significance. Case 2 is seen to be somewhat more accurate than case 3, and the 42 element axisymmetric solution is considerably more accurate than either. From these results it is clear that a very large number of elements is required for good accuracy in cases of ducts having this area ratio, and, moreover, that it is advantageous to employ a relatively large number of elements around the circumference even if it is necessary to reduce the number of elements used longitudinally.

11.22 A Constant Area Circular Duct with a 90° Bend.

The case of a constant area circular duct or pipe that makes a right angle turn was selected as an example of a truly three-dimensional duct. In the curved region, the centerline of the duct is a quarter circle of radius five times the radius of the circular cross-section of the duct. A sketch of half of the duct is shown in figure 44a, which also shows the calculated velocity distributions along the length of the duct at three circumferential locations on the duct wall. The curves A and C, whose velocity distributions are shown in figure 44a, are in the plane of the paper as shown in the sketch — A on the "inside"of the turn and C on the "outside". The curve B is 90° around the circumference from each of these, i.e., at the maximum height above the plane of the paper. The plots were made versus centerline arc length so that all three curves could utilize a common abscissa. The velocities at a given value of centerline arc length are at those points of the curves A, B, and C that lie in the plane normal to the centerline at that location. The straight section of the duct begins at a value of centerline arc length $s = 4.333$ and the end of the duct is at $s = 9.0$. The uniform velocity region around $s = 6$ is the limit of validity of the calculation for applications. The end effects near $s = 9$ can be seen in the figure. The calculated velocity distributions around the circumference of the duct at various locations are

shown in figure 44b. The calculations were performed using 2100 effective
elements — 42 along the length of the duct and 50 around the circumference.

11.3 Interference Problems

11.31 An Ellipsoid at Angle of Attack in a Round Wind Tunnel.

The use of this method of flow calculation makes it possible to predict
the effect of wind tunnel walls on the velocity and pressure distributions on
the surface of a body. The results of one such calculation are presented here.
The body considered is a prolate spheroid of fineness ratio 10 at 10° angle
of attack in a circular wind tunnel whose diameter is equal to the length of
the body. Figure 45 shows the calculated velocity distributions along three
curves on the surface of the body both with and without the presence of the
wind tunnel. Curves A and C are in the midplane of the ellipsoid on the
upper and lower side, respectively. Curve B is 90° around the circumference
from the other two and is thus at the ''side'' of the ellipsoid. It can be
seen that the effect of the tunnel walls is small but definitely noticeable
in some regions. The maximum change in velocity caused by the presence of the
tunnel is 0.4 percent of free stream velocity. The velocity distributions on
the top, bottom, and ''side'' of the tunnel wall are shown in figure 46. The
maximum variation from a uniform flow is 0.7 percent of free stream velocity.
The calculations were performed using 1296 total effective elements. These
were distributed as follows: 720 on the ellipsoid, 20 along its length and
36 around its circumference, and 576 on the wall of the tunnel, 16 axially
and 36 circumferentially.

11.32 An Ellipsoid below a Free Surface. Two Ellipsoids Side by Side.

The method discussed here can also be used to calculate, to a first
approximation, the flow about a body moving beneath a free surface at the
extremes of the speed range. The linearized free surface boundary condition
is such that if the body is moving very slowly (low Froude number) the proper
condition at the surface is satisfied by placing a mirror image of the body
above the surface with a source density distribution identical to that of the
actual body. If the body is moving very rapidly (high Froude number), the
surface condition is satisfied by placing a mirror image of the body above the

surface with a source density distribution equal to the negative of that on the actual body. The first of these situation is such that there is no flow across the free surface and no normal velocity on the image body. This case is thus equivalent to the flow about two identical solid bodies side by side. Both cases can be handled by the symmetry feature of this method, with the second requiring a sign change in the calculation of the effect of certain reflected elements.

The body chosen to illustrate these calculations is a prolate spheroid of fineness ratio 10 whose axis of symmetry is parallel to the free surface and located one diameter below it. Figure 47a shows the calculated velocity distributions along the length of the ellipsoid on the meridian curve nearest the free surface for the case when the ellipsoid is moving parallel to the free surface and along its axis of symmetry. To make the results consistent with the other figures of this report, the velocity distributions are shown for the case of a stationary ellipsoid in the presence of a uniform onset flow. In addition to the low and high Froude number flows, the analytic solution for the ellipsoid alone in an unbounded fluid is also shown. Figure 47b shows the calculated velocity distributions around the circumference at the location of maximum diameter for the case of an onset flow (or movement of the body) parallel to the free surface and perpendicular to the axis of symmetry of the body. The same three cases are shown as in figure 47a. The calculated cases utilized 4320 effective elements − 2160 for the ellipsoid and the same number for its image. The distribution consisted of 54 elements along the length of the ellipsoid and 40 around its circumference.

11.4 Ship Hulls

11.41 General Remarks.

The flow about a ship hull is another example of flow in the presence of a free surface that can be calculated to a first approximation by the present method. The speeds of ships are such that this is a case of flow at low Froude number, and thus, as was mentioned earlier, the linearized free surface condition is approximately satisfied by placing a mirror image of the hull above the surface with the same source density distribution as the actual

hull . Since the ship hull pierces the surface, the true situation is thus approximated by the flow of an unbounded fluid about a single, closed, ''double hull'' body, which consists of the portion of the ship hull below the free surface plus the mirror image of this portion in the free surface. Thus in using the present method it is necessary to approximate by quadrilateral elements, not only the ship hull itself, but also its image in the free surface, and accordingly in a given case only half of the total effective elements are on the actual hull. From the point of view of the method, ships then will always have two symmetry planes — the midplane or ''keel plane'', which is a real symmetry plane, and an artificial symmetry plane coincident with the free surface. Ships with ''fore and aft'' symmetry have a third symmetry plane. In some applications it is advantageous to assume this last symmetry even if it is only approximately true, since it doubles the number of effective elements. To make the results for ships consistent with the other calculated results, the flows in the examples below have been computed assuming the body to be stationary in the presence of a uniform onset flow.

In normal practice hull shapes are specified by polynomials. The coordinates used to describe a ship are as given in reference 11. The coordinate x denotes distance along the length of the ship, and the shape is normalized so that the bow is at $x = +1$ and the stern at $x = -1$. The coordinate z denotes depth below the free surface. The keel or the location of maximum depth of the hull is at $z = z_M$, i.e., z_M is the draft of the ship. Distances perpendicular to the midplane of the ship are represented by the coordinate y. The maximum distance of points on the hull from the midplane is y_M, and thus the beam of the ship is $2y_M$. The polynomial representation of the ship hull expresses y/y_M as a function of x and z/z_M. The region of definition of the polynomials is the rectangle $-1 \leq x \leq +1$, $0 \leq z/z_M \leq 1$. If the side view of the hull is not rectangular, e.g., if the bow curves to meet the keel smoothly, the hull will not completely fill this rectangle of definition, except in the sense that $y = 0$ over part of the region. A polynomial cannot of course be zero over a region, and where the actual ship is absent, the polynomial representation gives small, variable, possibly even negative, values of the thickness y. While this may be acceptable for some purposes, it is not permissible in the present application.

Usually, the inclusion of this region will prevent the convergence of the iterative solution of the linear equations for the values of the source density. It is possible, however, that absurd results could be calculated. The body shape used with this method should terminate where the actual shape terminates. If the input points are generated from the polynomial representation, the curve on which $y = 0$ must be calculated.

In many cases the cross-sections of the hull in a plane normal to the x-axis intersect the plane $y = 0$ normally or nearly so, i.e., with slopes nearly parallel to the free surface. To approximate this condition, the polynomials defining hull shapes must have terms of very high order in z/z_M.

All the results presented below were calculated for the case of an onset flow parallel to the x-axis, i.e., along the length of the ship. Normally, the case of an onset flow parallel to the y-axis, i.e., the flow about a ship in yaw, was also calculated, but these results were felt to be of less interest.

11.42 Velocity Distributions on Two Ship Hulls.

Calculations were performed for two hull shapes. The polynomial representations of these shapes were furnished by personnel of the David Taylor Model Basin.

The first ship hull is a relatively simple, idealized shape, which is designated the simple ship hull. Its polynomial representation is as follows:

$$(y/y_M) = \left[1 - x^2 - (x^2 - x^4)(z/z_M)^{10} \right] \left[1 - 0.3(z/z_M)^8 - 0.7(z/z_M)^{150} \right] \qquad (141)$$

Since only even powers of x appear in equation (141), the hull has a ''fore and aft'' symmetry about the plane $x = 0$. The thickness y is zero only on the boundary of the rectangle of definition of the polynomial. Accordingly, the keel is the line $y = 0$, $z/z_M = 1$, $-1 \leq x \leq +1$ and the bow is the line $x = +1$, $y = 0$, $0 \leq z/z_M \leq 1$. The shape is well suited to approximation by quadrilateral elements in the manner employed by this method. In particular, there is no concentration point of the elements as there is for smooth bodies like spheres. The limits of the surface, bow, stern, keel, and waterline,

are simply taken as ''n-lines'' and ''m-lines'' of the elements distribution.
In fact the selection of input points was quite routine, except for one diffi-
cult region, which seems to occur in many ships. The slope of the surface at
the keel varies rapidly with distance along the hull near the bow. In this
case, for example, at the bow the unit normal vector to the surface at the
keel has a zero z-component and a y-component of almost unity, while at 5
percent of the length of the ship the unit normal vector at the keel has a
z-component of almost unity and a y-component equal to about 0.01. (The unit
normal has a small x-component at both locations.) Thus the unit normal
vector at the keel rotates almost 90° in 5 percent of the length of the ship.
This fact necessitated a concentration of elements near the keel in the
vicinity of the bow (and, by symmetry, a similar concentration at the stern).
The total number of effective elements used in the calculations was 3816 —
1908 on the actual hull and an equal number on its reflection in the free
surface. The basic element distribution consisted of 42 along the length of
the ship in the x-direction and 30 around the hull at a constant value of x
from waterline to waterline. An additional 156 elements were concentrated
near the keel at the bow and a like number at the stern.

The simple ship hull on which the flow was calculated had a beam-length
ratio of 0.118 and a draft-length ratio of 0.047, i.e., $y_M = 0.118$ and
$z_M = 0.094$. Plan and side views of the hull are shown in figure 48a, which
also shows the calculated velocity distributions along the waterline and the
keel. Figure 48b shows the calculated velocity distributions around cross-
sections of the hull at several values of x together with the cross-sec-
tional shapes at those locations. From the latter curves it can be seen that
the maximum velocity on a cross section is attained at the waterline if the
cross-section is near the middle of the ship, but at the keel if the cross-
section is near the bow. The maximum velocity on a cross-section about mid-
way between the bow and the middle of the ship occurs neither at the keel
nor the waterline but somewhere in between. All velocity curves in figure 48
are terminated at the last null points appropriate to the particular velocity
distributions. This accounts for the fact that the curves end at different
values of the abscissae.

The second ship hull is a realistic approximation to a ''Series 60''
merchant ship having a beam-length ratio of 0.1333 and a draft-length ratio
of 0.5333. This ship and its polynomial representation are described in re-
ference 11. The polynomial contains 140 terms, consisting of powers of x
from 0 through 13 and powers of (z/z_M) from 0 through 6 and also the powers
20, 40, and 200. The side view of the ship is not rectangular, but the bow
is curved, beginning at about 80 percent of the draft, and smoothly joins the
keel at about 5 percent of the length of the ship. At the stern of the ship,
$x = -1$, the thickness y is not quite zero but has a small positive value.
In the calculations, elements were distributed only on the surface defined by
the polynomial, and the stern of the ship was thus left open in a manner
similar to the wing tips described in Section 11.1. This leads to an error
in the calculated velocities over the last three or four percent of the length
of the ship. The slope of the keel changes rapidly near the bow, and elements
were concentrated in this region as was done for the simple ship hull. Such
a concentration was unnecessary at the stern. A total of 2024 effective
elements were used in the calculations, -- 1012 on the actual hull and the
same number on its image in the free surface. The basic element distribution
consisted of 34 along the length of the ship and 28 around the cross sections
of the hull from waterline to waterline. An additional 60 elements were con-
centrated near the bow in the vicinity of the keel. For illustrative purposes,
a half model of the series 60 merchant ship hull was constructed showing the
distribution of elements. A photograph of this model is shown in the frontis-
piece. The bow is on the upper left in the photograph, and the concentration
of elements near the keel can be seen. The dots on the elements show the
locations of the null points.

The calculated velocity distributions along the keel and the waterline
are shown in figure 49a, while the velocity distributions around cross-sections
of the hull at several values of x are shown in figure 49b, together with the
cross-sectional shapes for those locations. All curves are terminated at the
last null points appropriate to the particular velocity distributions.

11.43 The Effects of Variation of Ship Thickness. Evaluation of the Validity of Thin Ship Theory.

The velocity distributions on ship hulls may also be calculated by an approximate method known as thin ship theory. According to this theory, for the case of an onset flow parallel to the x-axis, the disturbance velocity components, $V_x - 1$, V_y, and V_z, at all points of the hull vary linearly with the thickness of the ship, i.e., with beam-length ratio y_M, for a given normalized ship geometry. Thus the present method of flow calculation may be used to evaluate the validity of thin ship theory by calculating the flow about a particular hull shape for several beam-length ratios and determining whether or not the variations of the disturbance velocity components with thickness are linear. If the variations are linear, it still must be verified whether or not the slopes are those predicted by thin ship theory.

The investigation was conducted using the simple ship hull of Section 11.42. In addition to the case of a beam-length ratio of 0.118 described in that section, calculations were performed for this hull with beam-length ratios of half and twice this value leaving the draft unchanged. Each of the three cases can be obtained from any other by multiplying the y-coordinates of the input points by the proper factor. Thus corresponding input points in the three cases have the same x and z coordinates, and this is approximately true of corresponding null points, so that the variation with ship thickness of the disturbance velocity components at a given xz location may be determined by examining the velocities at corresponding null points in the three cases. Three locations along the ship were selected for examination — one near the bow (x = 0.985), one near the middle of the ship (x = 0.025), and one approximately midway between (x = 0.925). At each location three null points were selected — the one nearest the keel $(z/z_M \approx 1)$, the one nearest the waterline $(z/z_M \approx 0+)$, and one at a depth equal to about half the draft $(z/z_M \approx 0.5)$. The calculated disturbance velocity components for these nine locations are shown as functions of beam-length ratio in figure 50. Also shown are the straight lines having the same slope as these curves at zero beam-length ratio. It can be seen that some components at some locations are almost linear with beam-length ratio, while others are not. The greatest deviations from linear behavior occur at the location near both the keel and the bow, figure 50i.

141

The behavior of the x disturbance component at the intermediate x-location (x = 0.525) is quite interesting. In figures 50d and 50e it is seen that this component at first increases with beam-length ratio, but reaches a maximum and thereafter decreases and eventually changes sign. The magnitude of this component is not large in these cases, but the behavior is evidently of a sort that could not be predicted by a linearized theory.

12.0 ACKNOWLEDGEMENTS

An extraordinarily large debt of gratitude is owed by the authors to Miss Sue Faulkner. Her highly significant contributions to the construction of this method and the preparation of this report included: checking all mathematical derivations; inputting and monitoring the progress of all cases run on the computing machine; designing, drawing, and supervising the inking of all the figures in this report; and, calculating all the required analytic solutions. The importance of her efforts cannot be overestimated.

The formidable job of programming this method for the IBM 704 and 7090 computing machines was performed by two computing analysts. The majority of the work was done by Mr. Ron Dunbar, while the initial programming was done by Mr. Ken Alexander.

13.0 REFERENCES

1. Smith, A. M. O., and Pierce, Jesse:-Exact Solution of the Neumann Problem. Calculation of non-Circulatory Plane and Axially Symmetric Flows About or Within Arbitrary Boundaries. Douglas Aircraft Company Report No. ES 26988, April, 1958.

2. Hess, J. L.:-Calculation of Potential Flow About Bodies of Revolution Having Axes Perpendicular to the Free Stream Direction. Douglas Aircraft Company Report No. ES 29812, May, 1960.

3. Kellogg, O. D.:-Foundations of Potential Theory. Frederick Ungar Publishing Company, 1929, also available through Dover Publications, Inc.

4. Levy, R. H.:-Preliminary Report on a Proposed Method of Calculating Pressure Distributions Over Arbitrary Bodies. Canadair Limited Report No. RAA-00-113, October, 1959.

5. Hardy, G. H.:-A Course of Pure Mathematics, The MacMillan Company, New York, 1945, p.262.

6. Stratton, J. A.:-Electromagnetic Theory. McGraw-Hill Book Company, Inc., New York, 1941.

7. Hall, I. M., and Rogers, E. W. E.:-The Flow Pattern on a Tapered Swept-Back Wing at Mach Numbers between 0.6 and 1.6. British FM 2617, November 1957.

8. Sears, W. R., editor:-High Speed Aerodynamics and Jet Propulsion, Vol. VI, General Theory of High Speed Aerodynamics. Princeton University Press, Princeton, New Jersey, 1954.

9. Loving, D. L., and Estabrooks, B. B.:-Transonic-Wing Investigation in the Langley 8-Foot High-Speed Tunnel at High Subsonic Mach Numbers and at a Mach Number of 1.2. Analysis of Pressure Distribution of Wing-Fuselage Configuration Having a Wing of $45°$ Sweepback, Aspect Ratio 4, Taper Ratio 0.6, and NACA 65A006 Airfoil Section. NACA RM L51F07, September, 1951.

10. Abbott, I. H., and Von Doenhoff, A. E.:-Theory of Wing Sections. Dover Publications, Inc., New York, 1959.

11. Kerwin, J. E.:-Polynomial Surface Representation of Arbitrary Ship Forms. Journal of Ship Research, Vol. 4, No. 1, June, 1960.
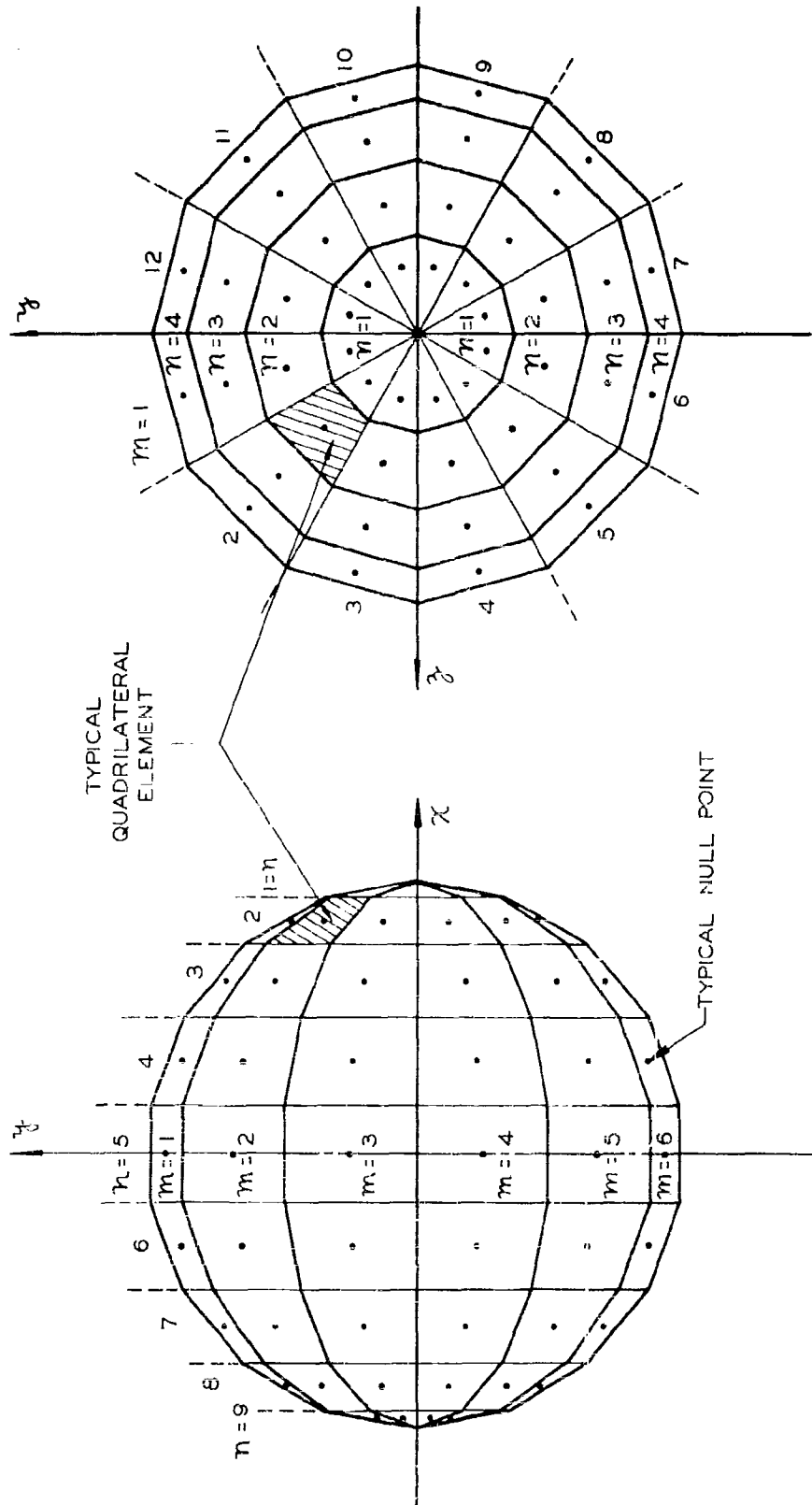
Figure 27. - Distribution of elements on a sphere.

TYPICAL
QUADRILATERAL
ELEMENT

TYPICAL NULL POINT
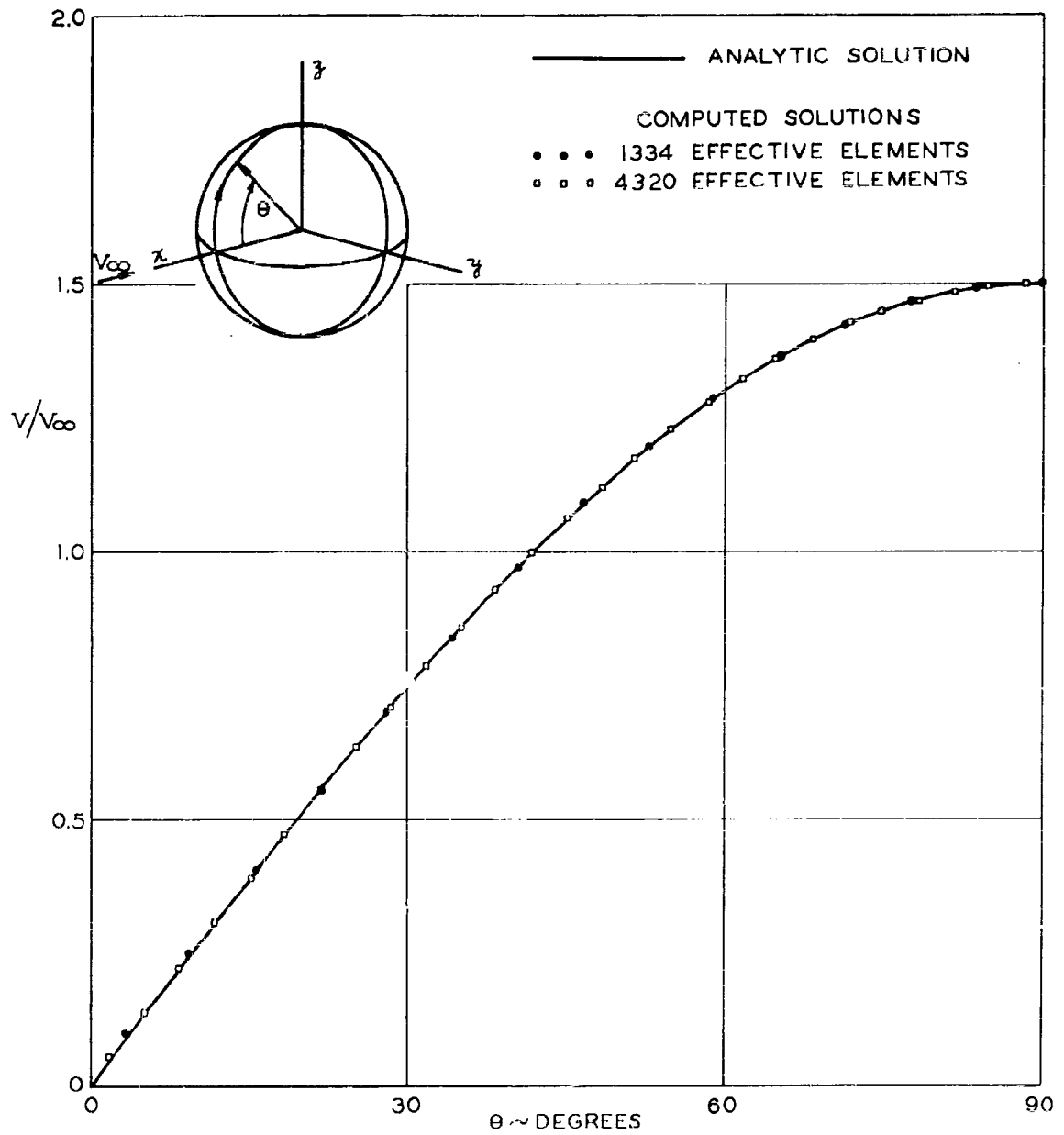
Figure 28. - Comparison of analytic and calculated velocity distributions on a sphere for an onset flow parallel to the x-axis.

146
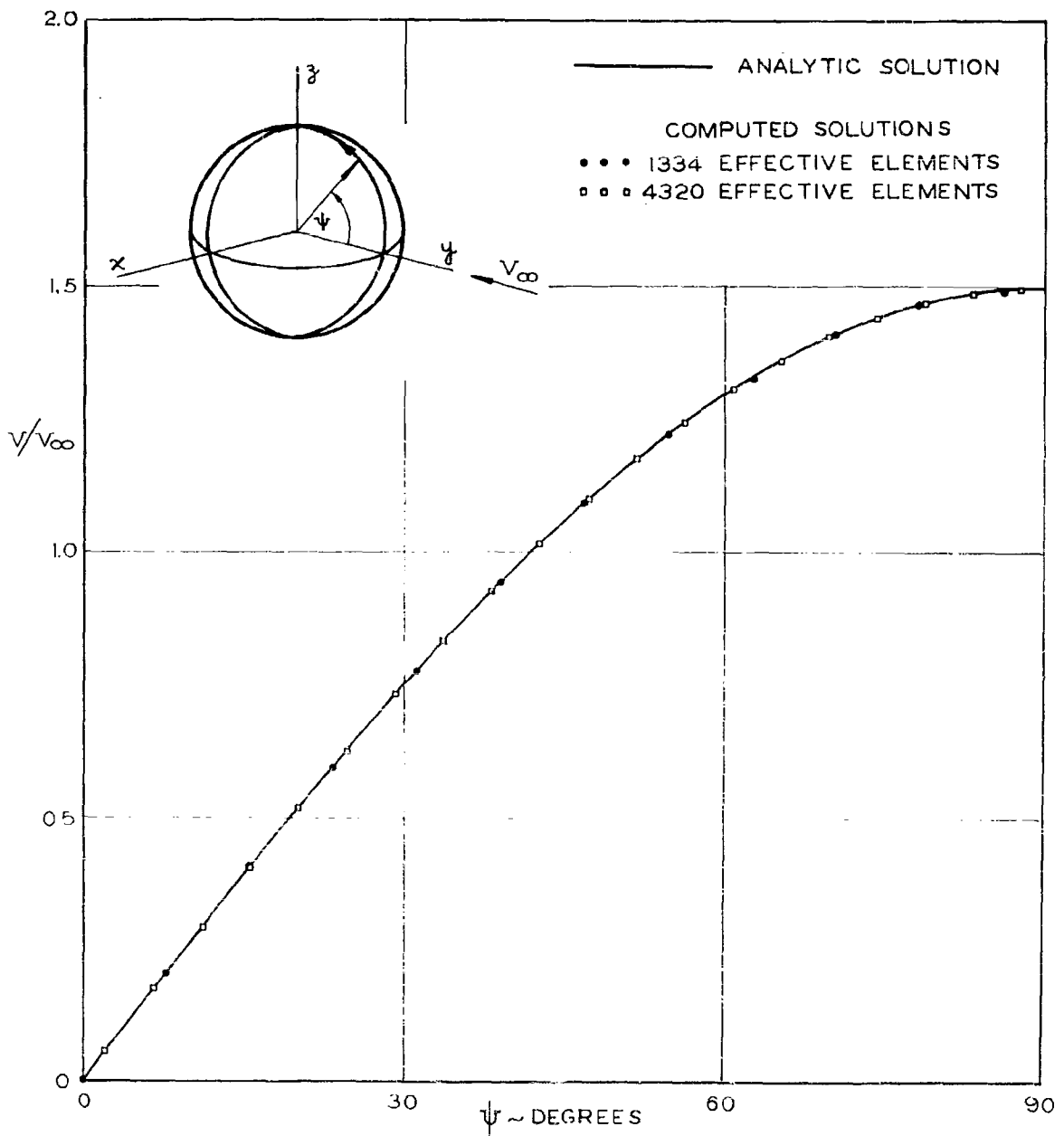
Figure 29. - Comparison of analytic and calculated velocity distributions on a sphere for an onset flow parallel to the y-axis. (a) Velocities in the yz-plane
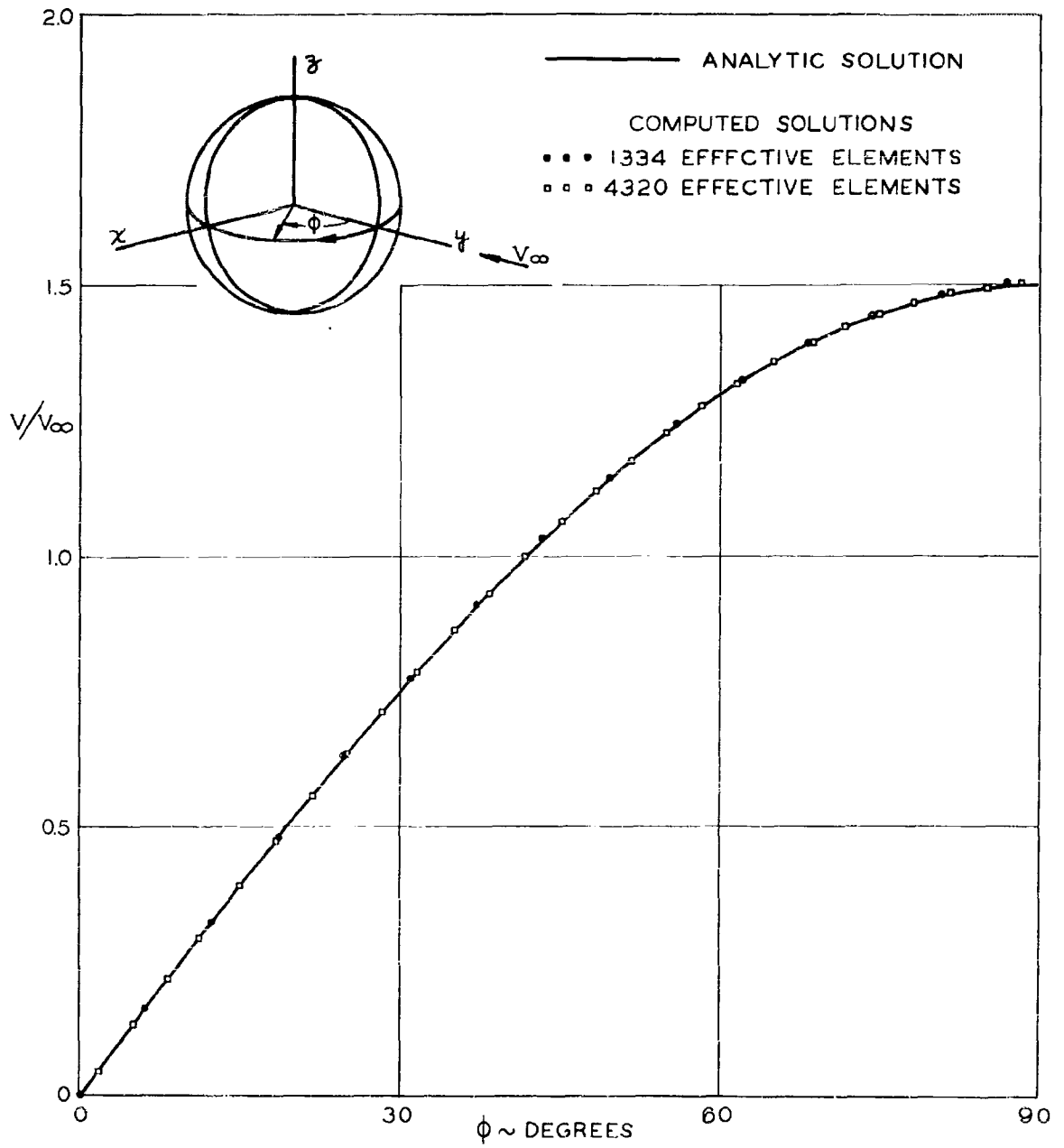
Figure 29. - Continued   (b) Velocities in the xy-plane.
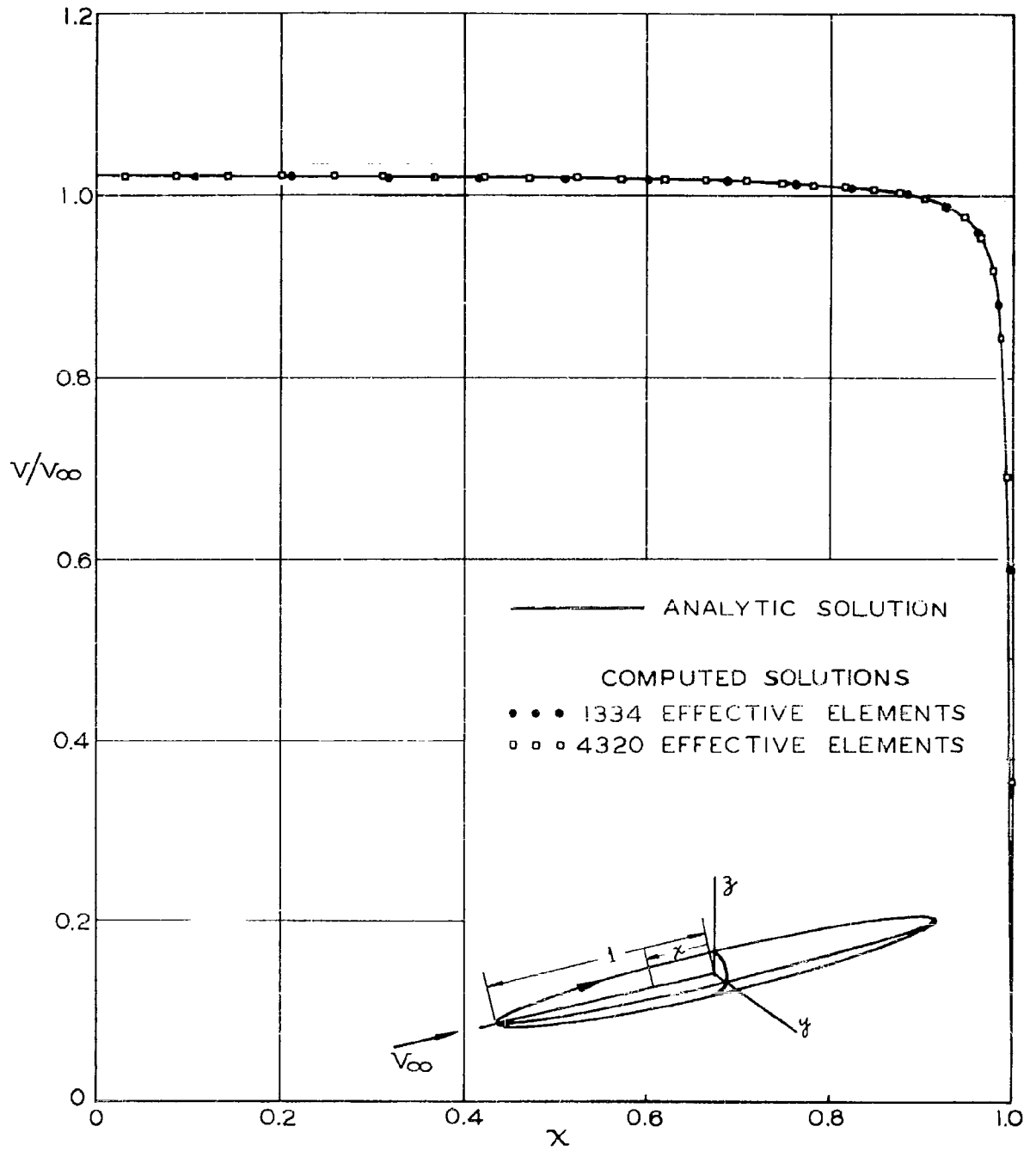
Figure 30. - Comparison of analytic and calculated velocity distributions on a prolate spheroid of fineness ratio 10 for an onset flow parallel to the x-axis.
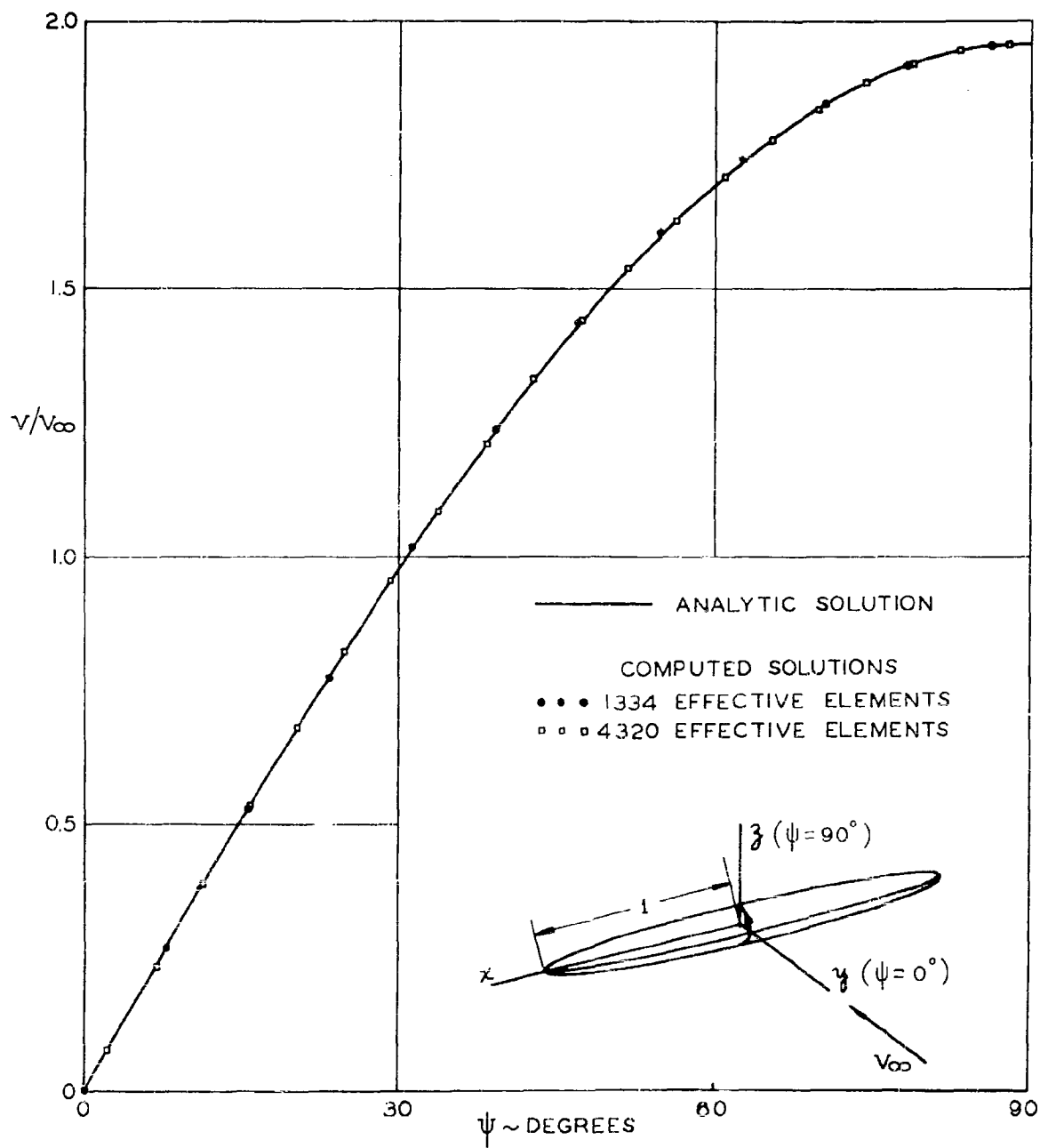
Figure 31. - Comparison of analytic and calculated velocity distributions on a prolate spheroid of
fineness ratio 10 for an onset flow parallel to the y-axis. (a) Velocities in the yz-plane.

150
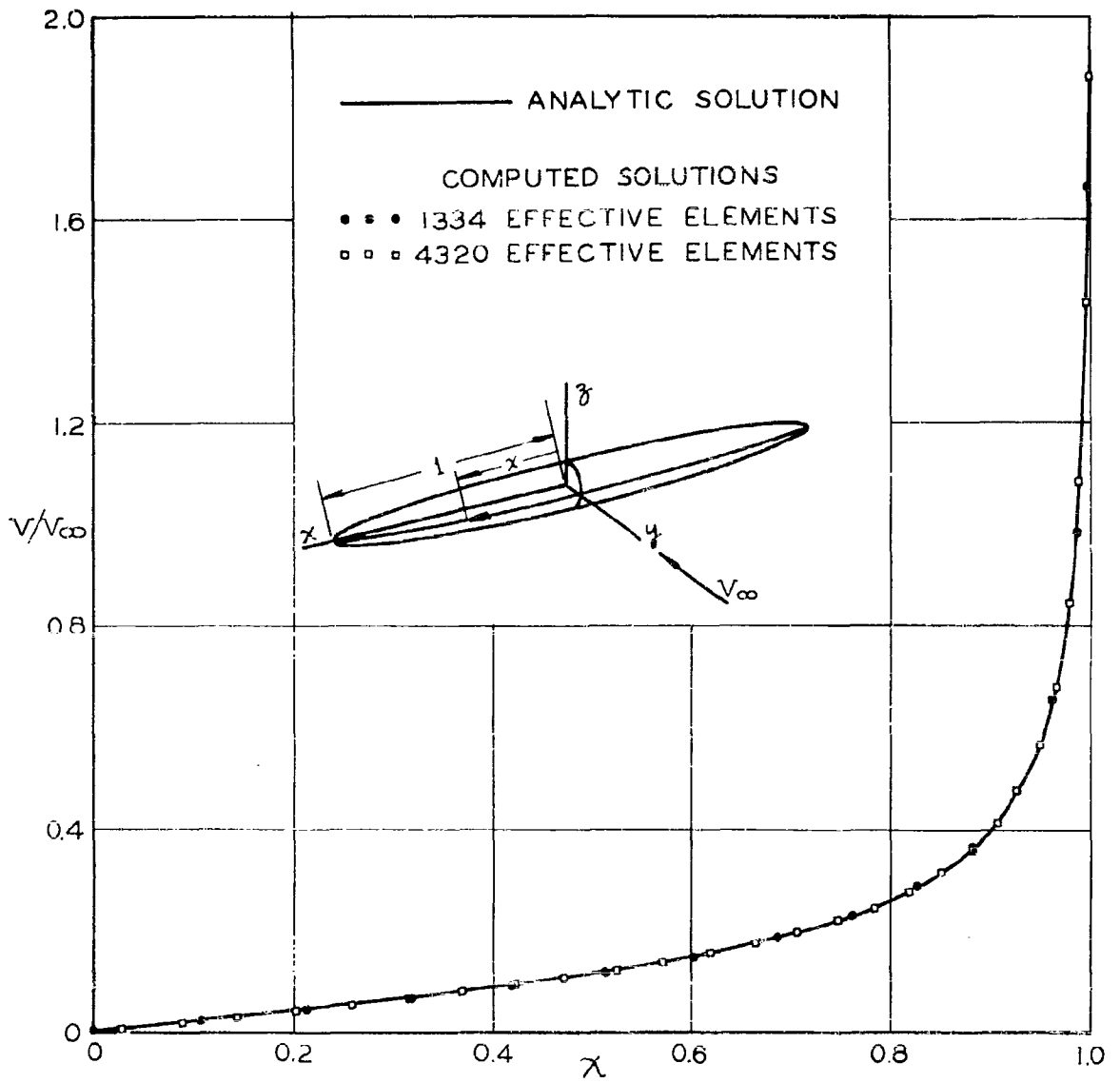
Figure 31. - Continued   (b) Velocities in the xy-plane.

151
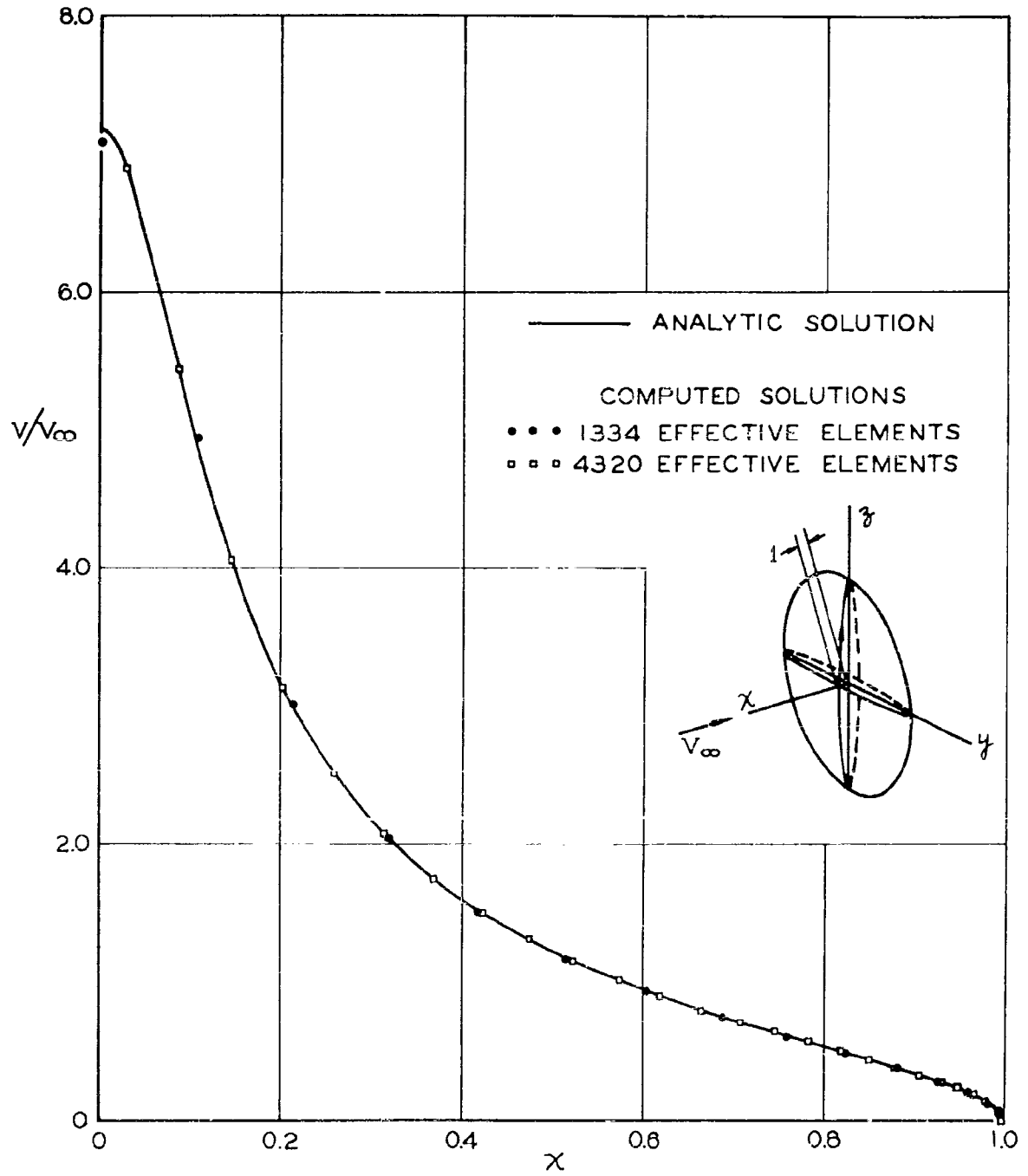
Figure 32. - Comparison of analytic and calculated velocity distributions on an oblate spheroid of fineness ratio 0.1 for an onset flow parallel to the x-axis.

152
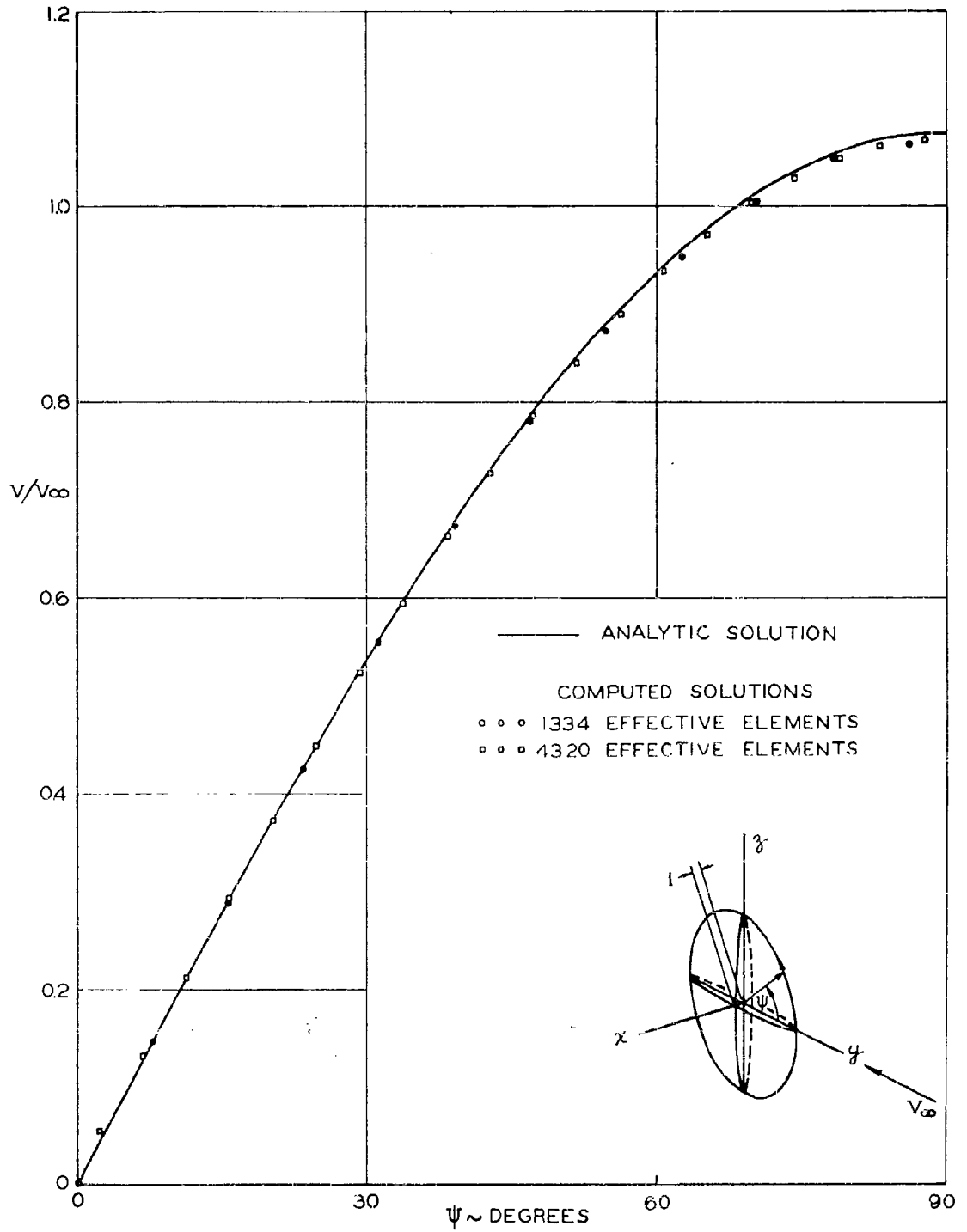
Figure 33. - Comparison of analytic and calculated velocity distributions on an oblate spheroid of fineness ratio 0.1 for an onset flow parallel to the y-axis. (a) Velocities in the yz-plane.
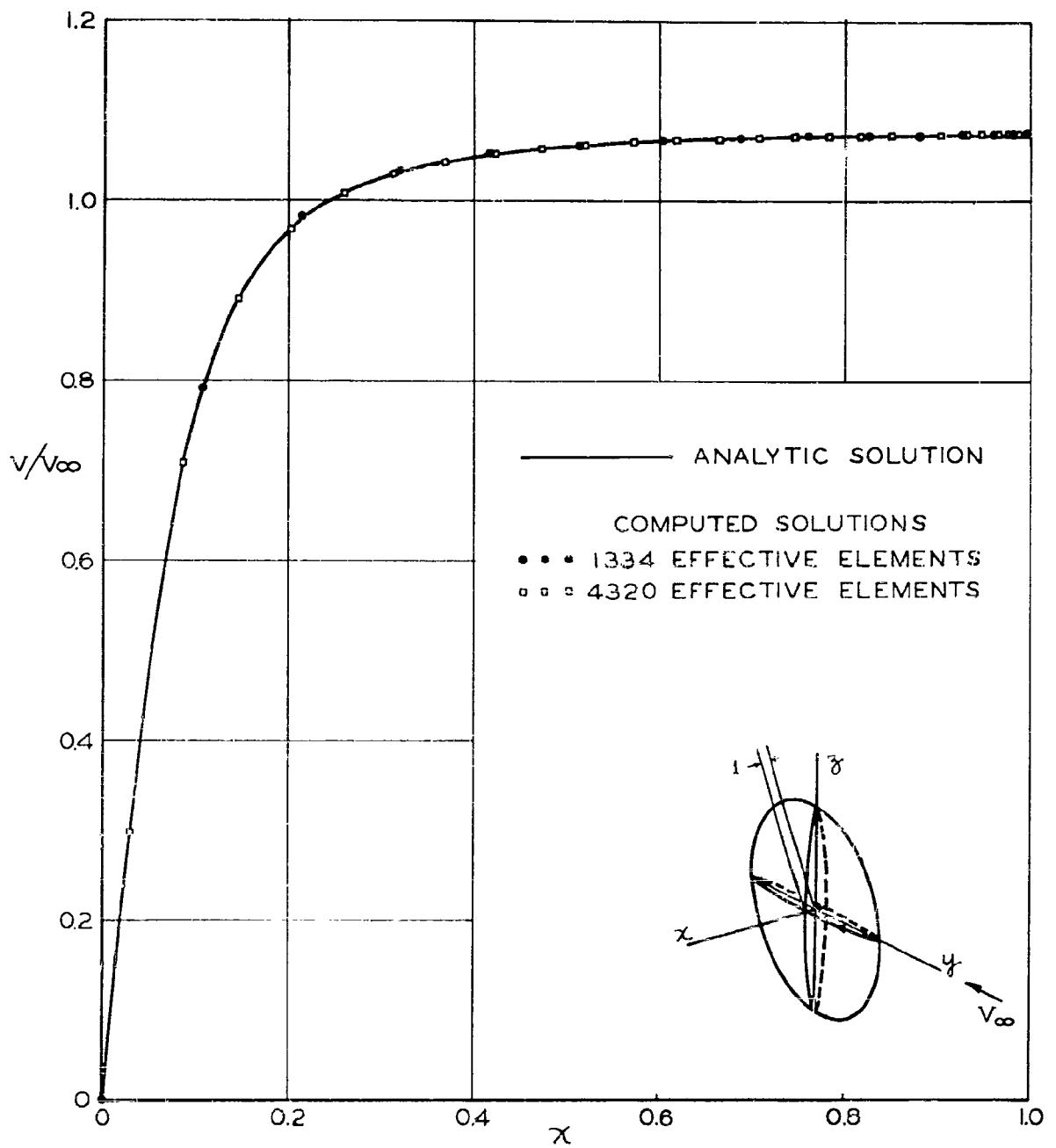
Figure 33. - Continued   (b) Velocities in the xy-plane.
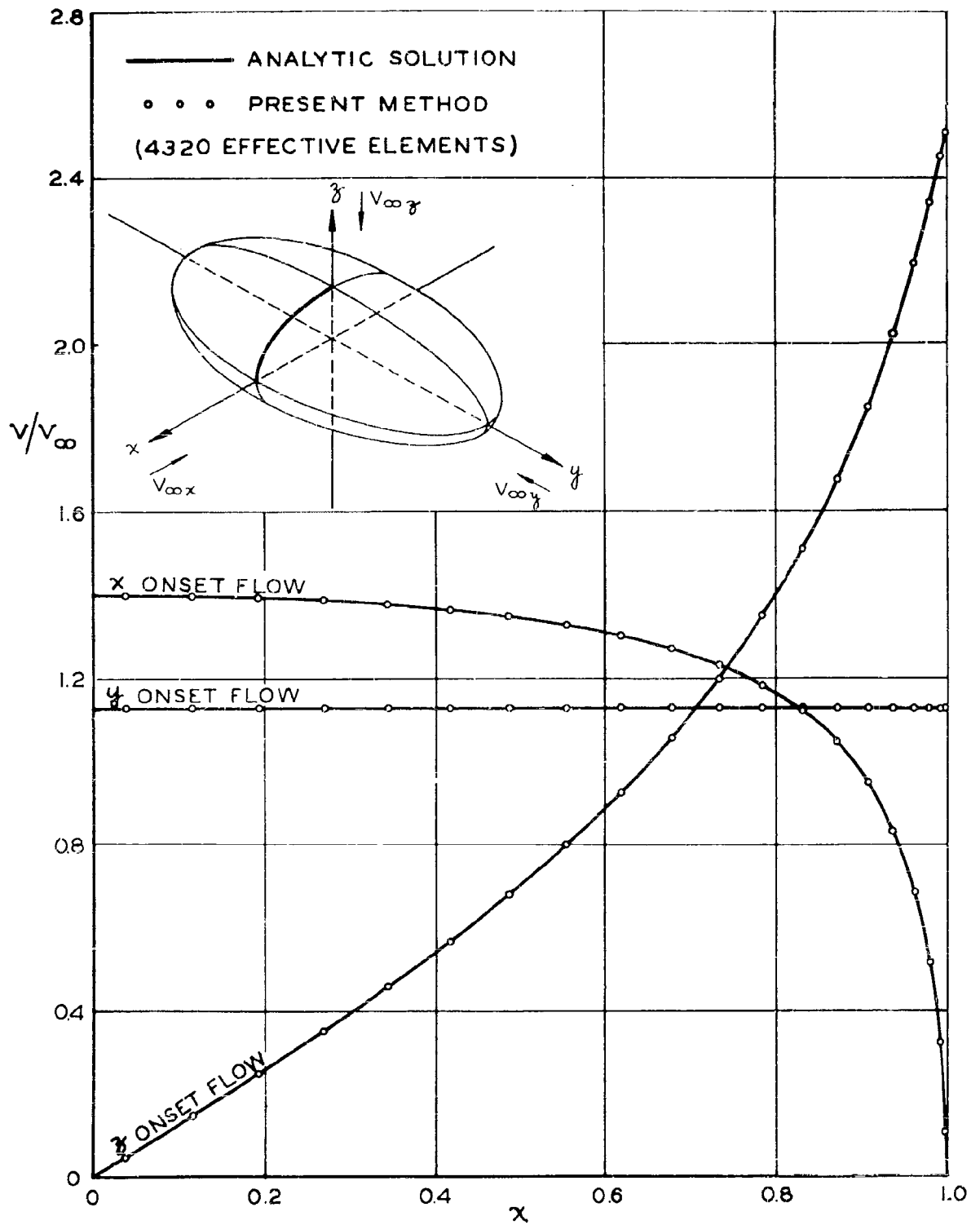
Figure 34. - Comparison of analytic and calculated velocity distributions on an ellipsoid with axes ratios 1:2:0.5. (a) Velocities in the xz-plane.
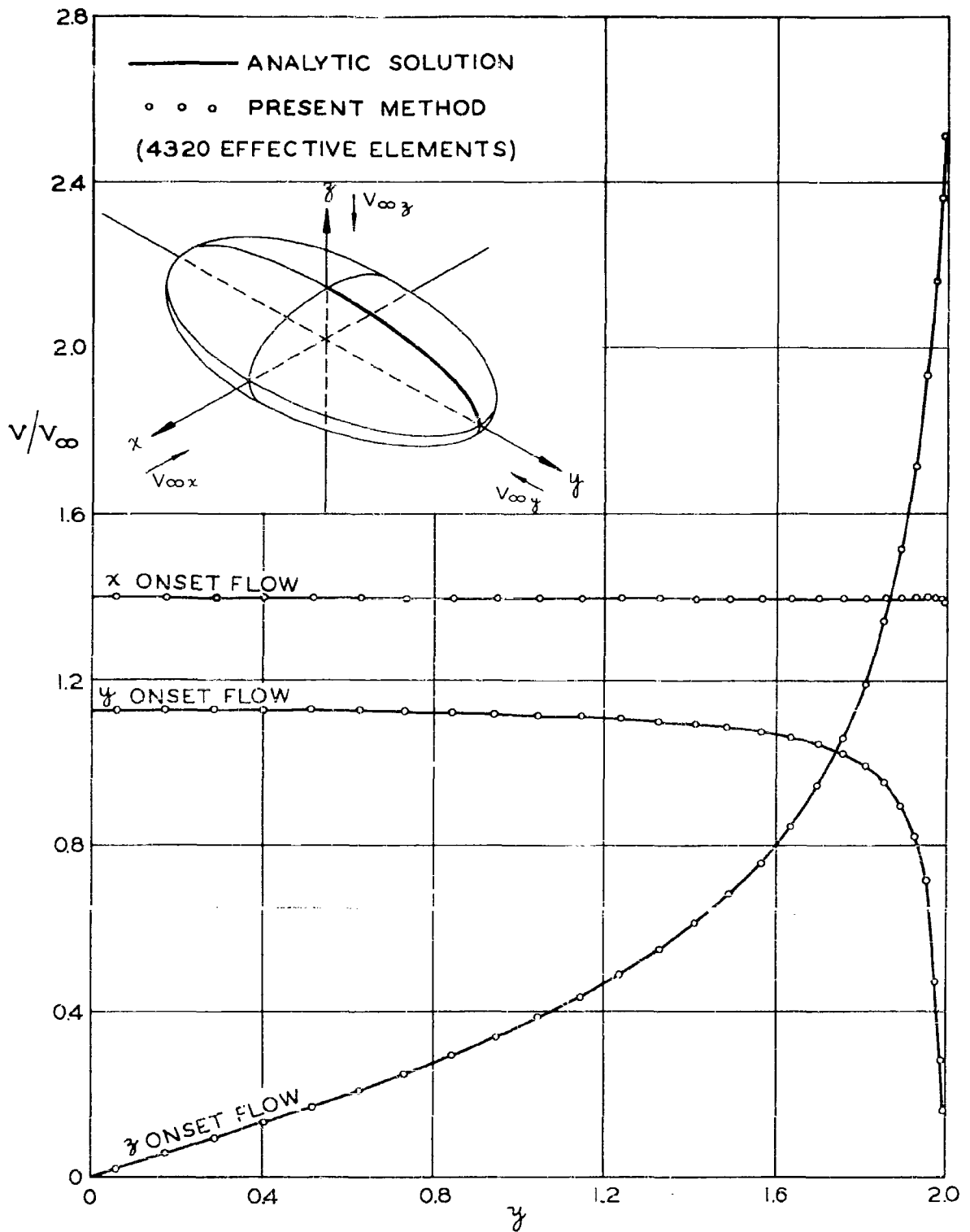
Figure 34. - Continued   (b) Velocities in the yz-plane.
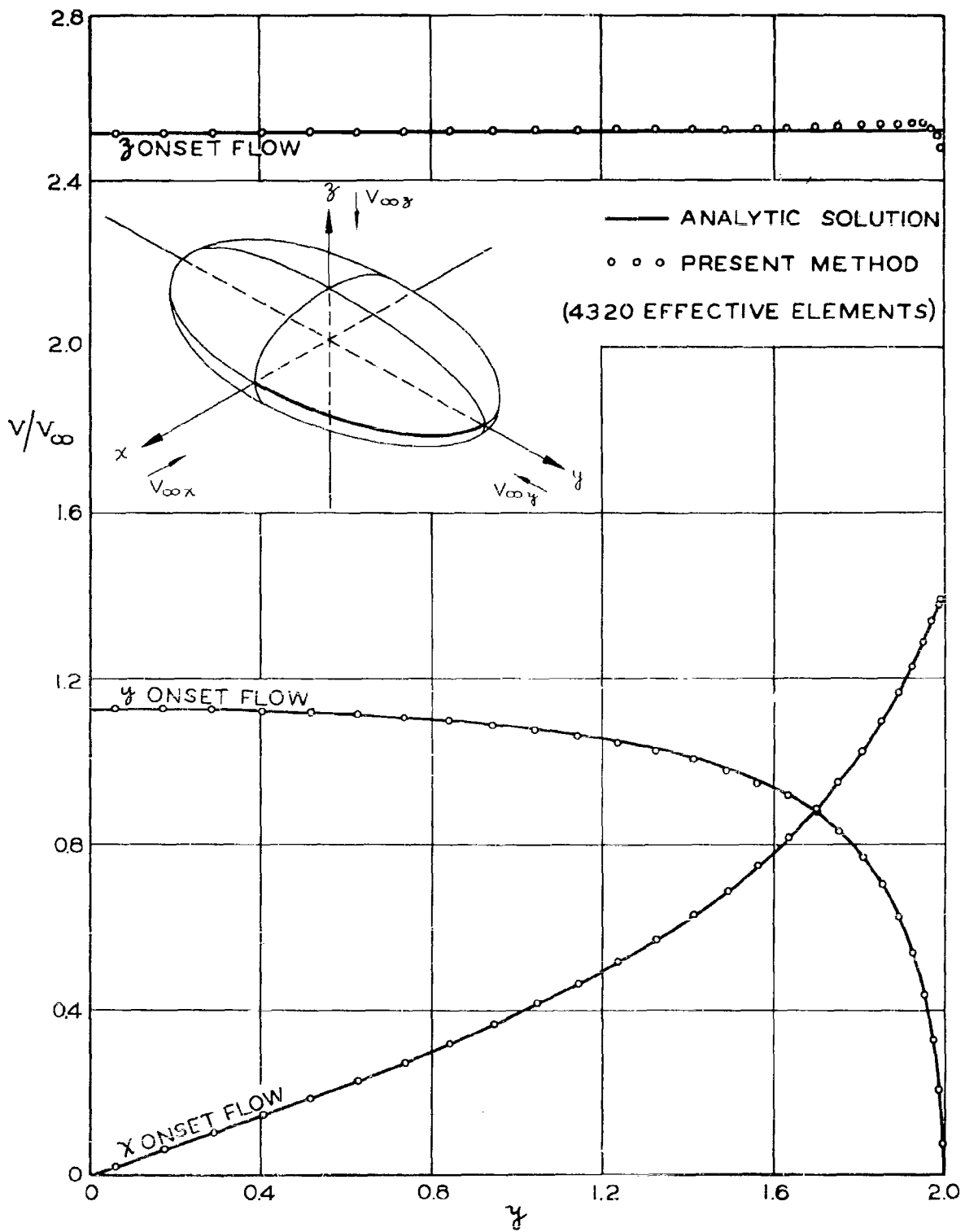
Figure 34. - Continued   (c) Velocities in the xy-plane.
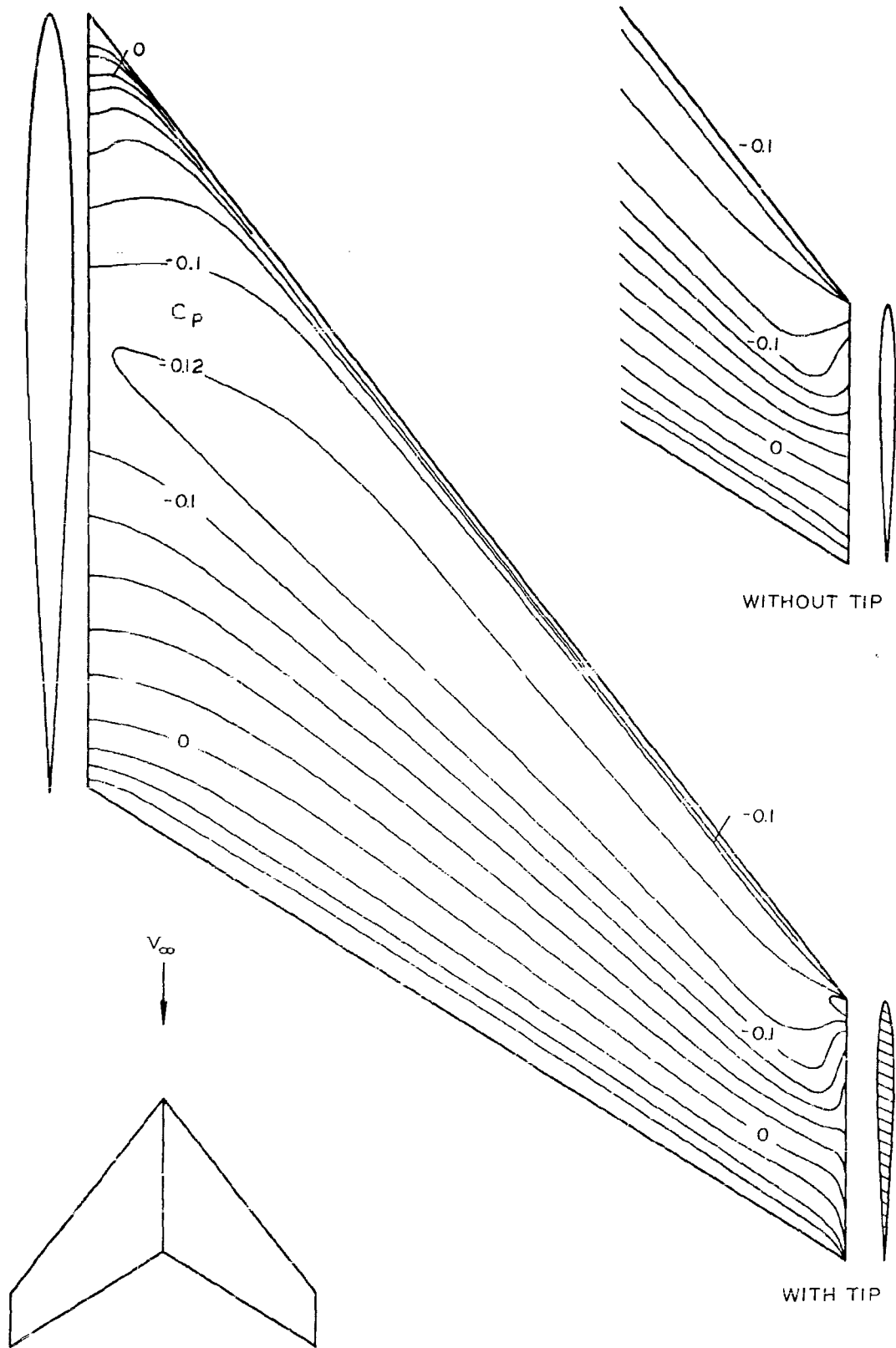
Figure 35. - Calculated isobars on the Warren wing with and without tip in incompressible flow.
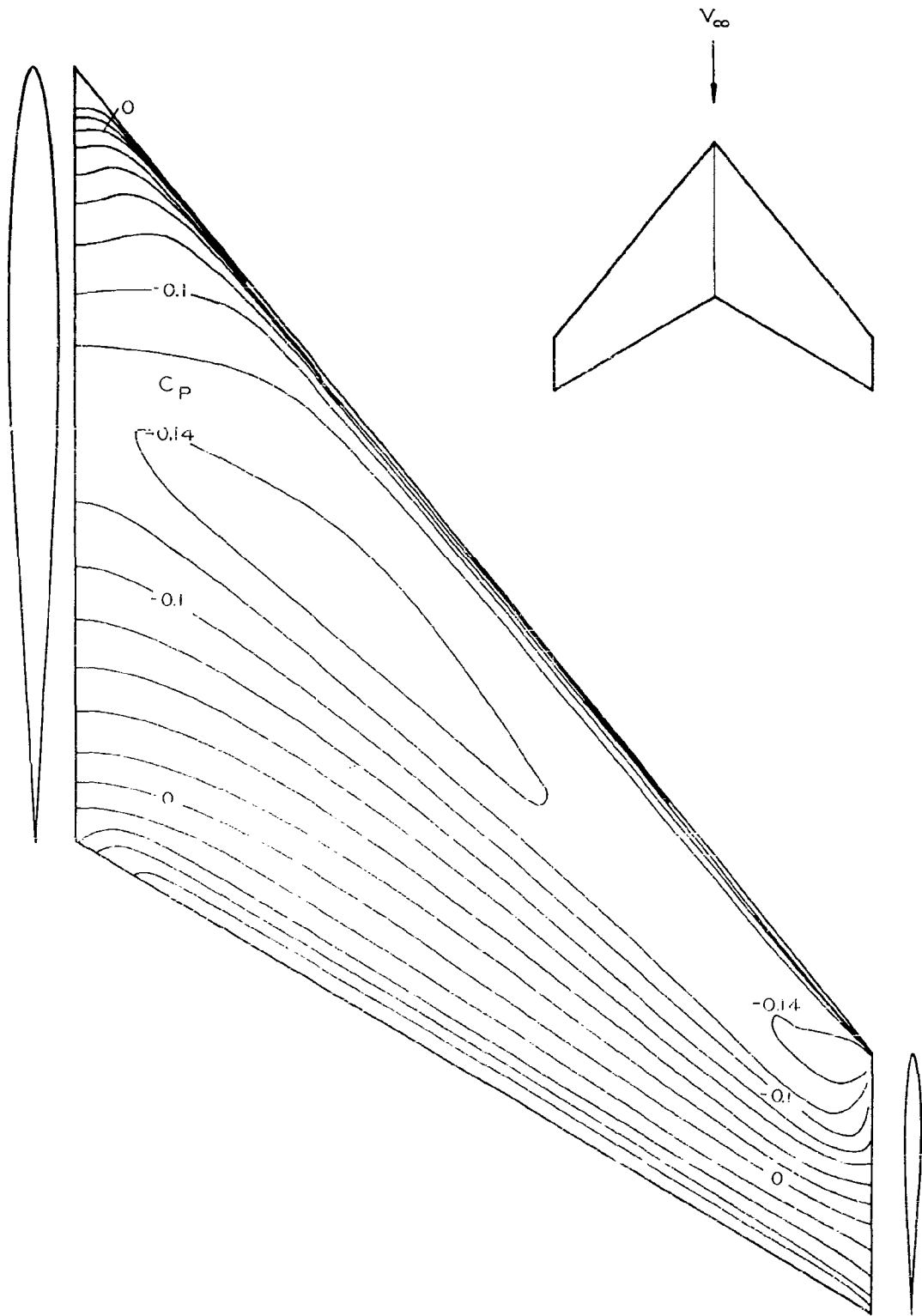
Figure 36. - Calculated isobars on the Warren wing without tip for a Mach number of 0.6.
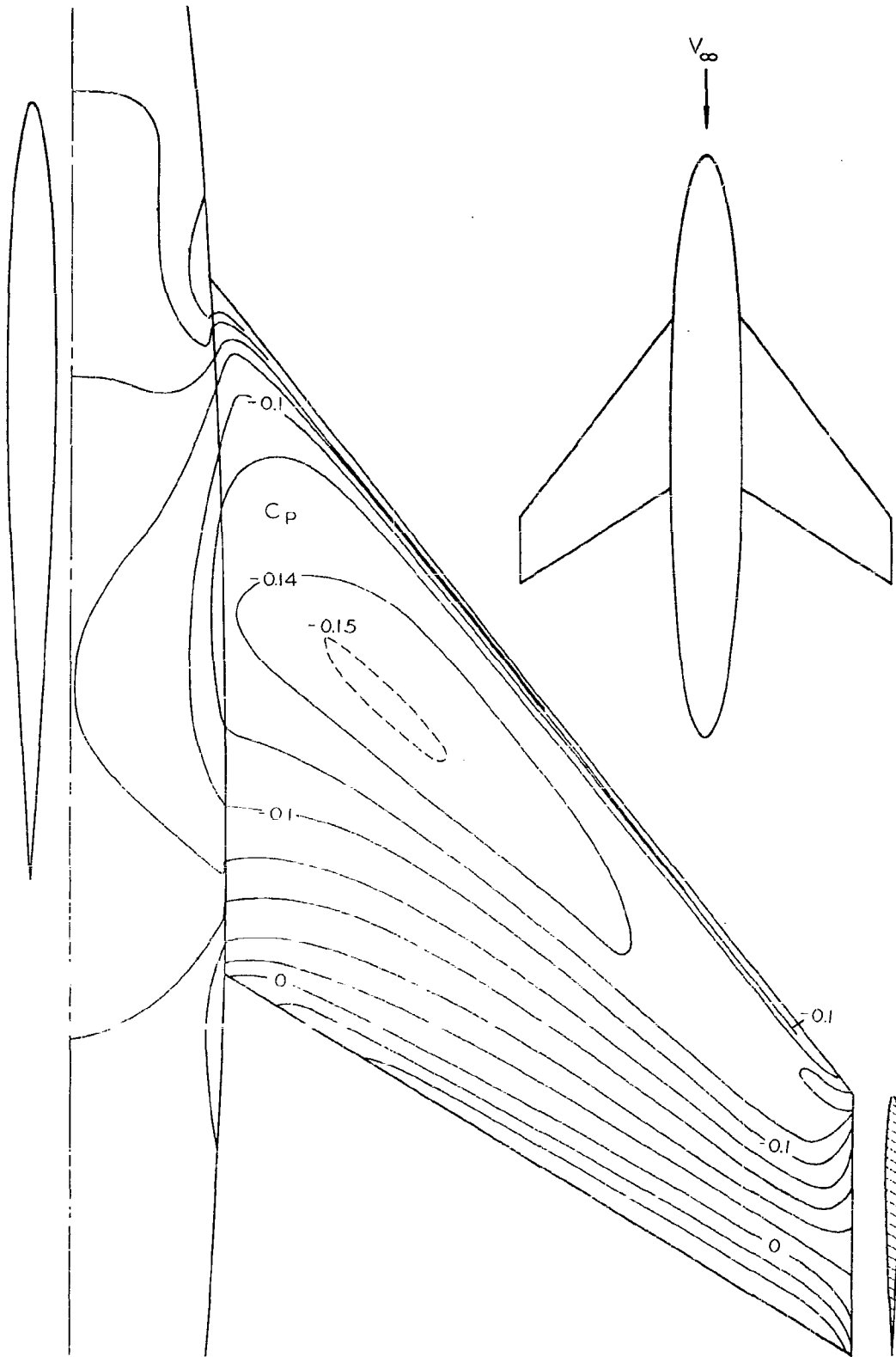
Figure 37. - Calculated isobars in incompressible flow on a wing-fuselage consisting of the Warren wing on an ellipsoidal fuselage.
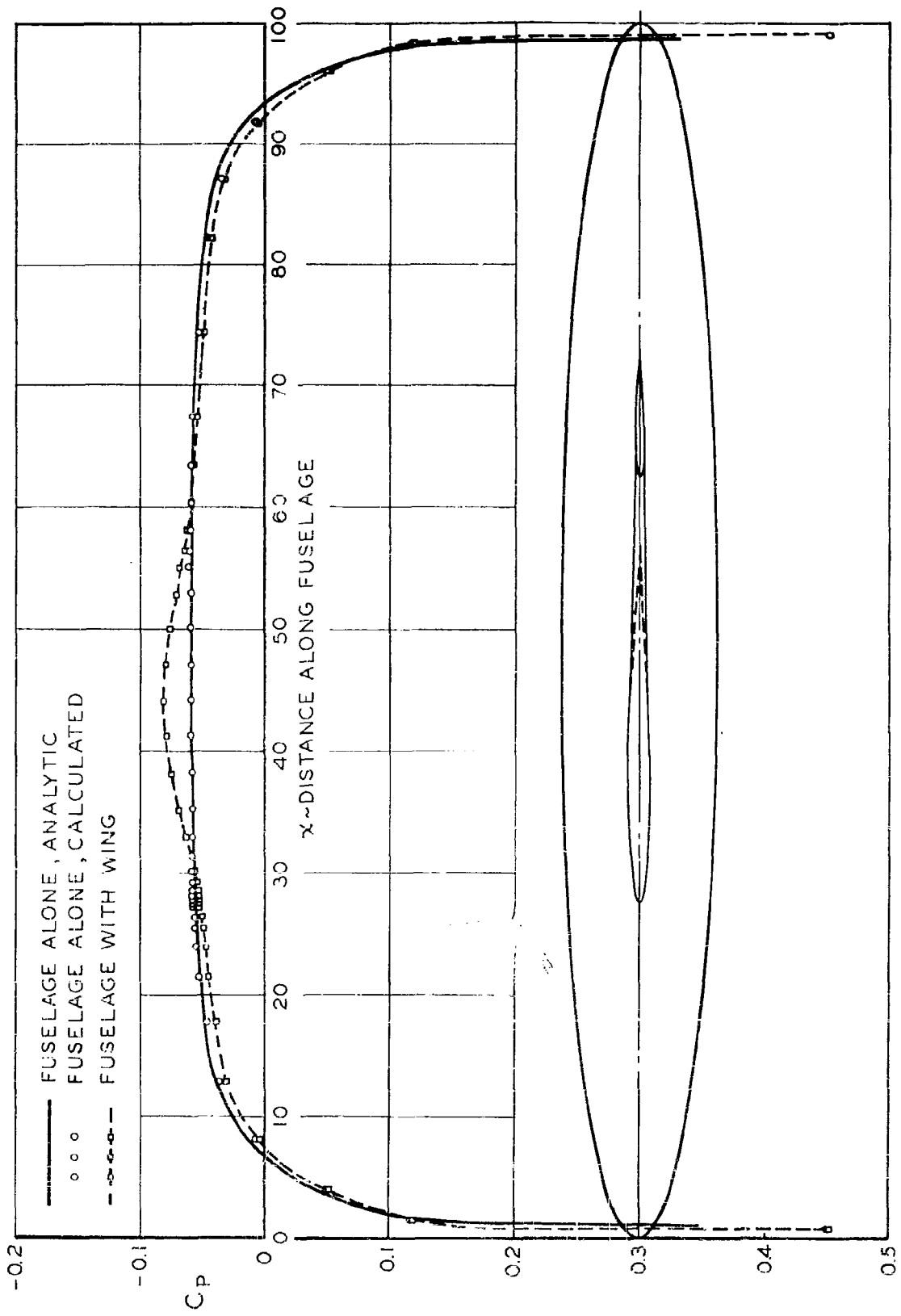
Figure 38. - Pressure distributions in the midplane of an ellipsoidal fuselage with and without the presence of the Warren wing.

161
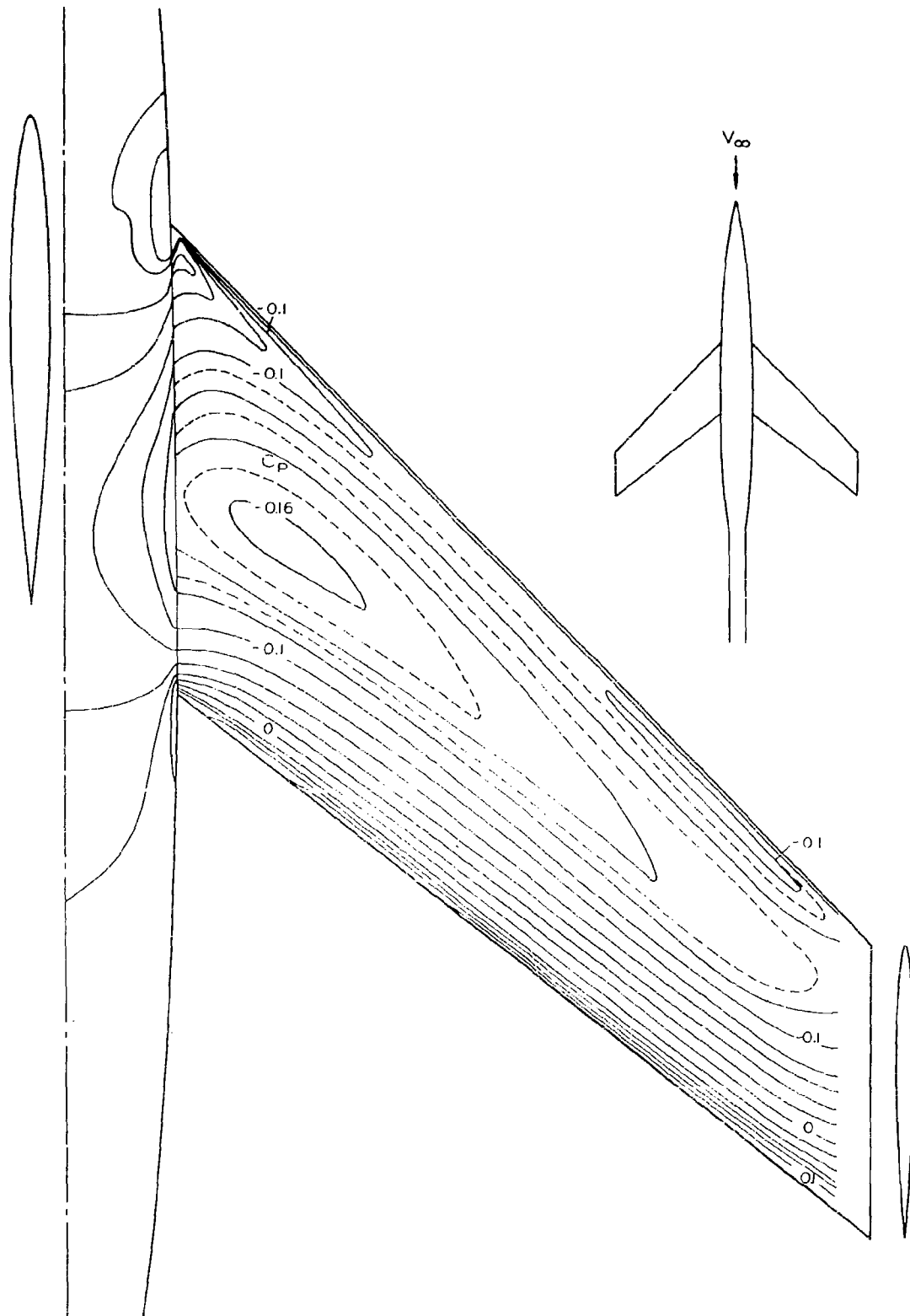
Figure 39. - Calculated isobars on an NACA wing-fuselage for a Mach number of 0.6.
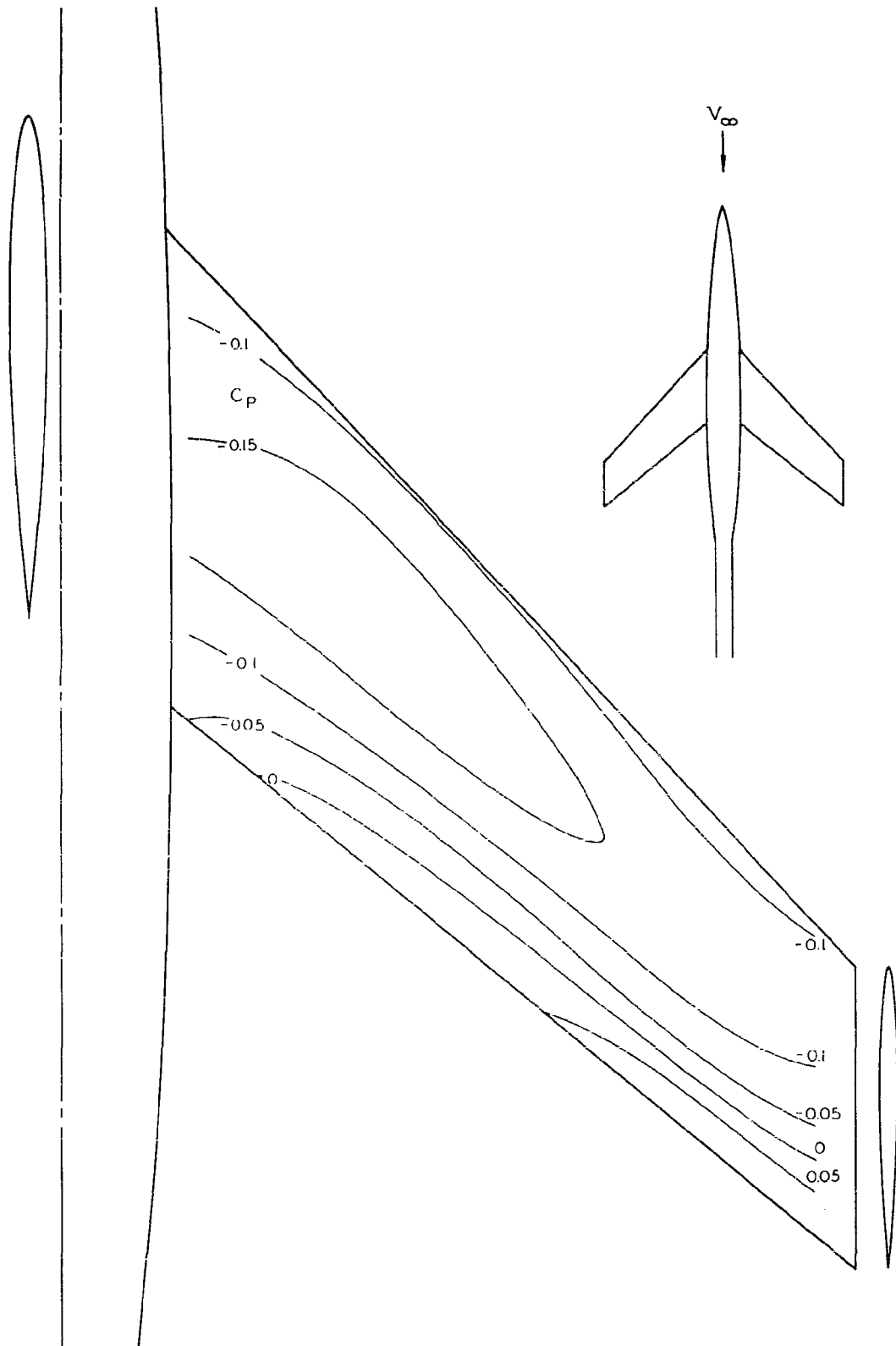
Figure 40. - Experimental isobars on an NACA wing fuselage for a Mach number of 0.6.
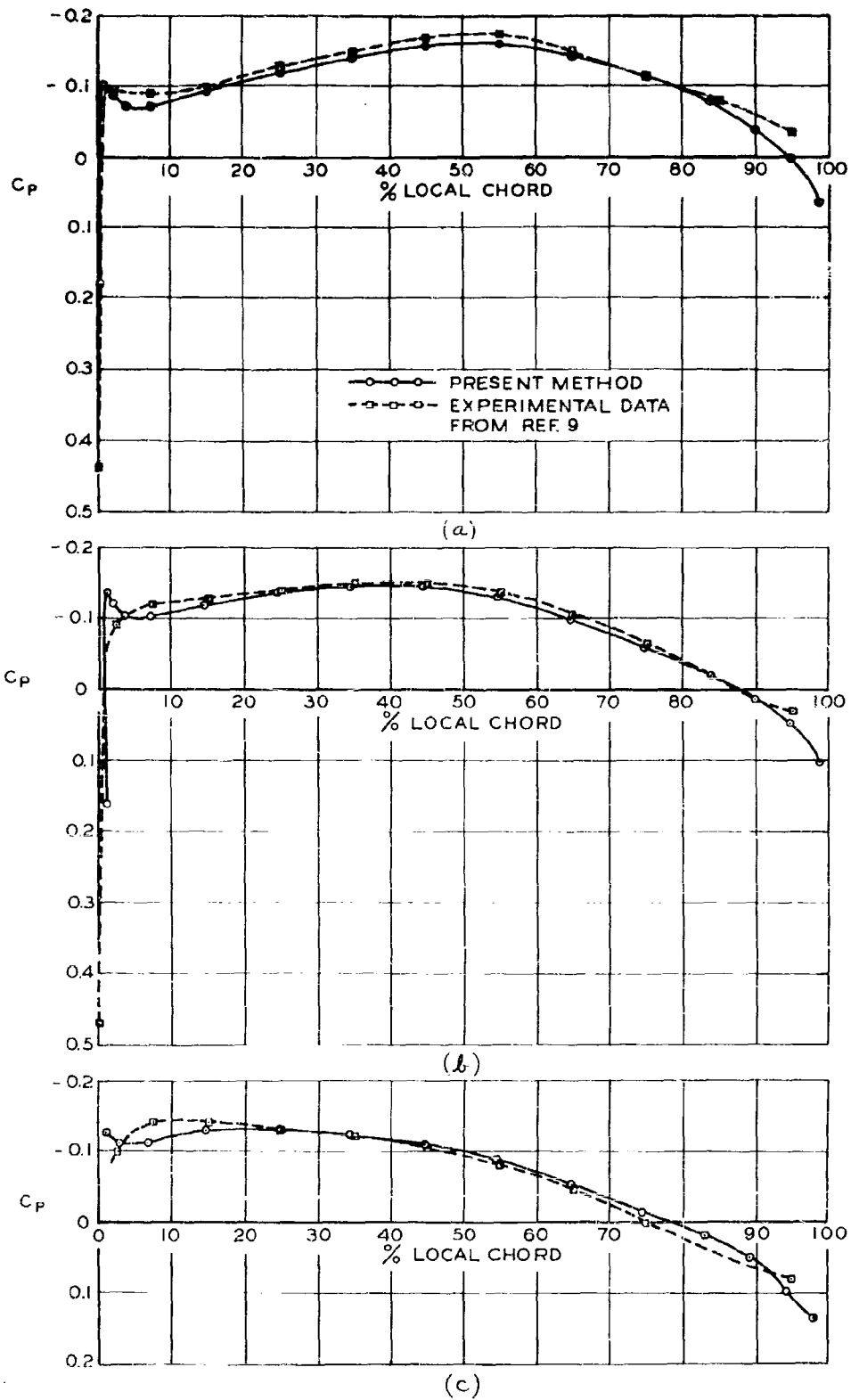
Figure 41. - Comparison of calculated and experimental pressure distributions on the NACA wing
in the presence of the fuselage for a Mach number of 0.6. (a) 20 percent semi-span.
(b) 60 percent semi-span. (c) 95 percent semi-span.

164
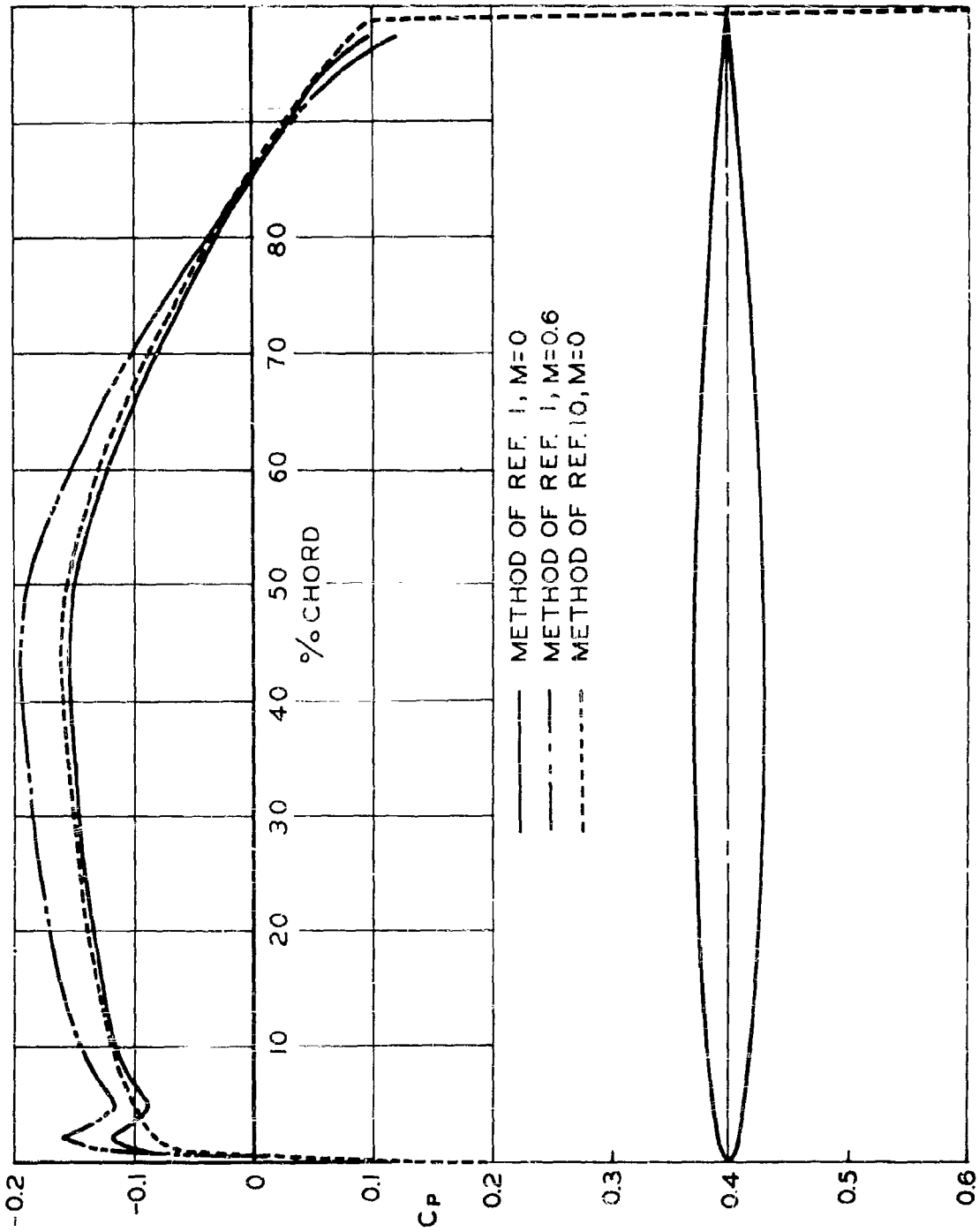
Figure 42. - Calculated two-dimensional pressure distributions on an NACA 65A006 airfoil.

165
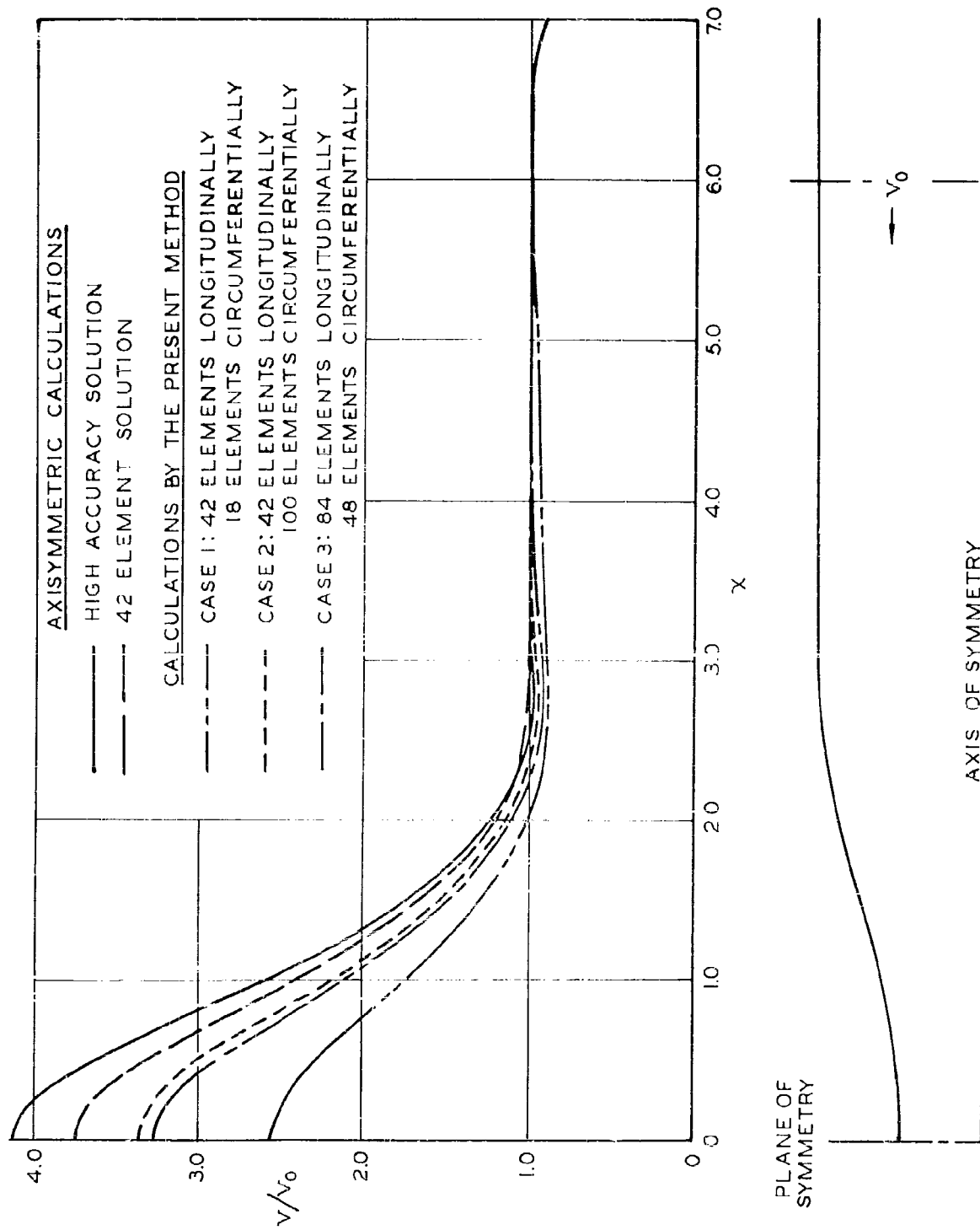
Figure 43. - Calculated velocity distributions on the wall of a straight circular contracting duct having an area ratio of four.
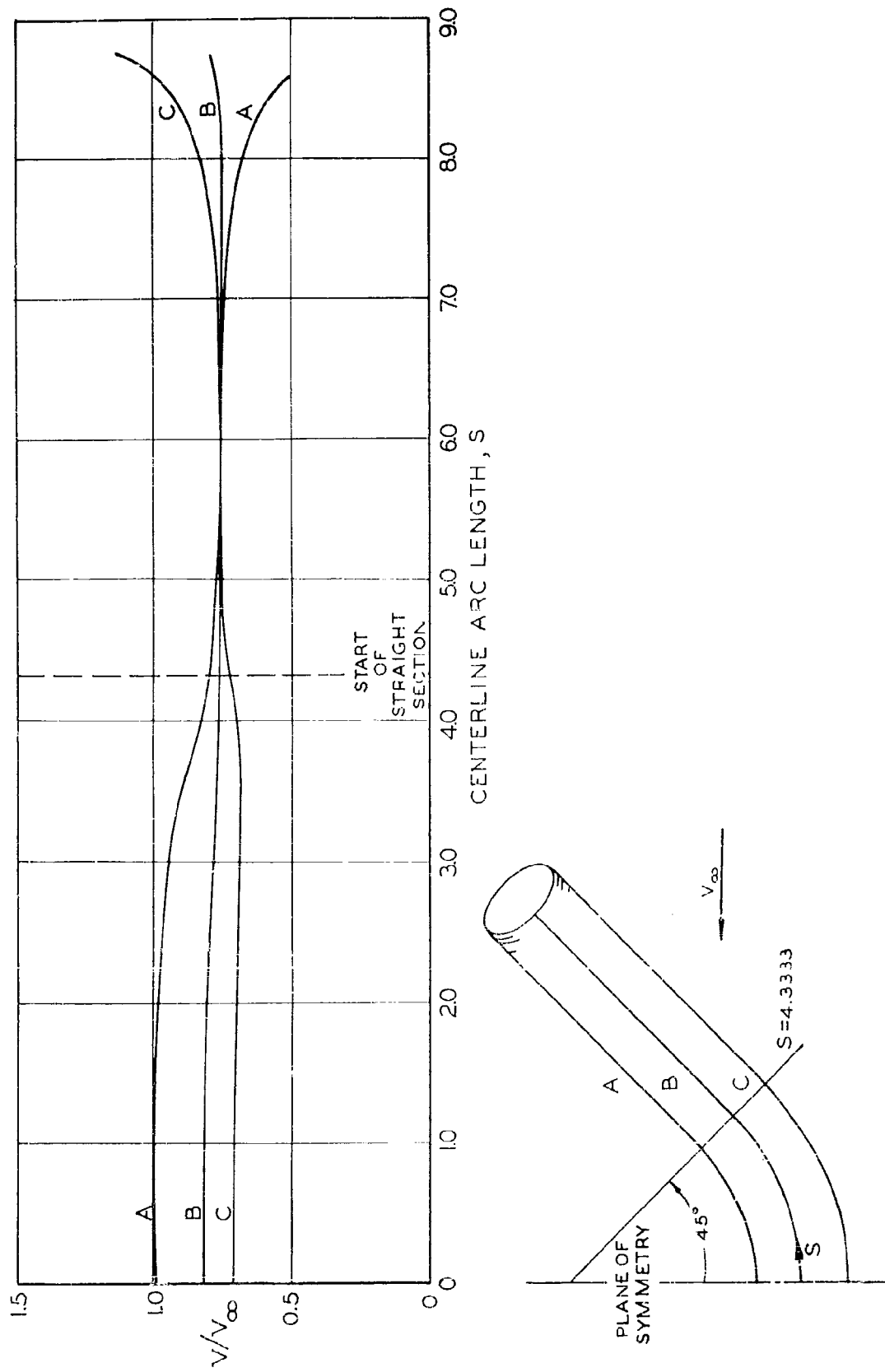
Figure 44. - Calculated velocity distributions on the wall of a constant area circular duct with a 90° bend.
(a) Velocity distributions along the length of the duct.

167
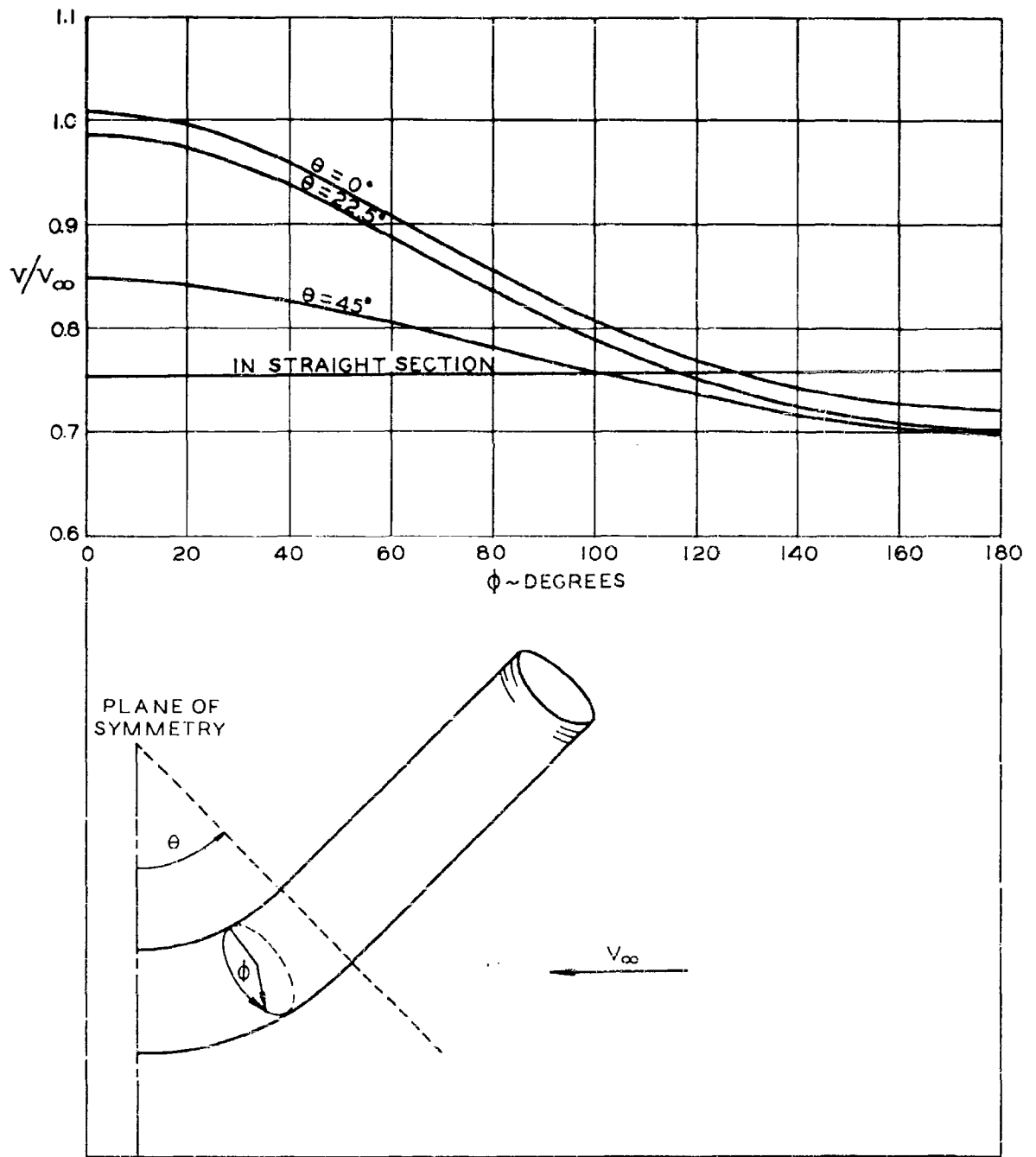
Figure 44. - Continued   (b) Velocity distributions around the circumference of the duct.
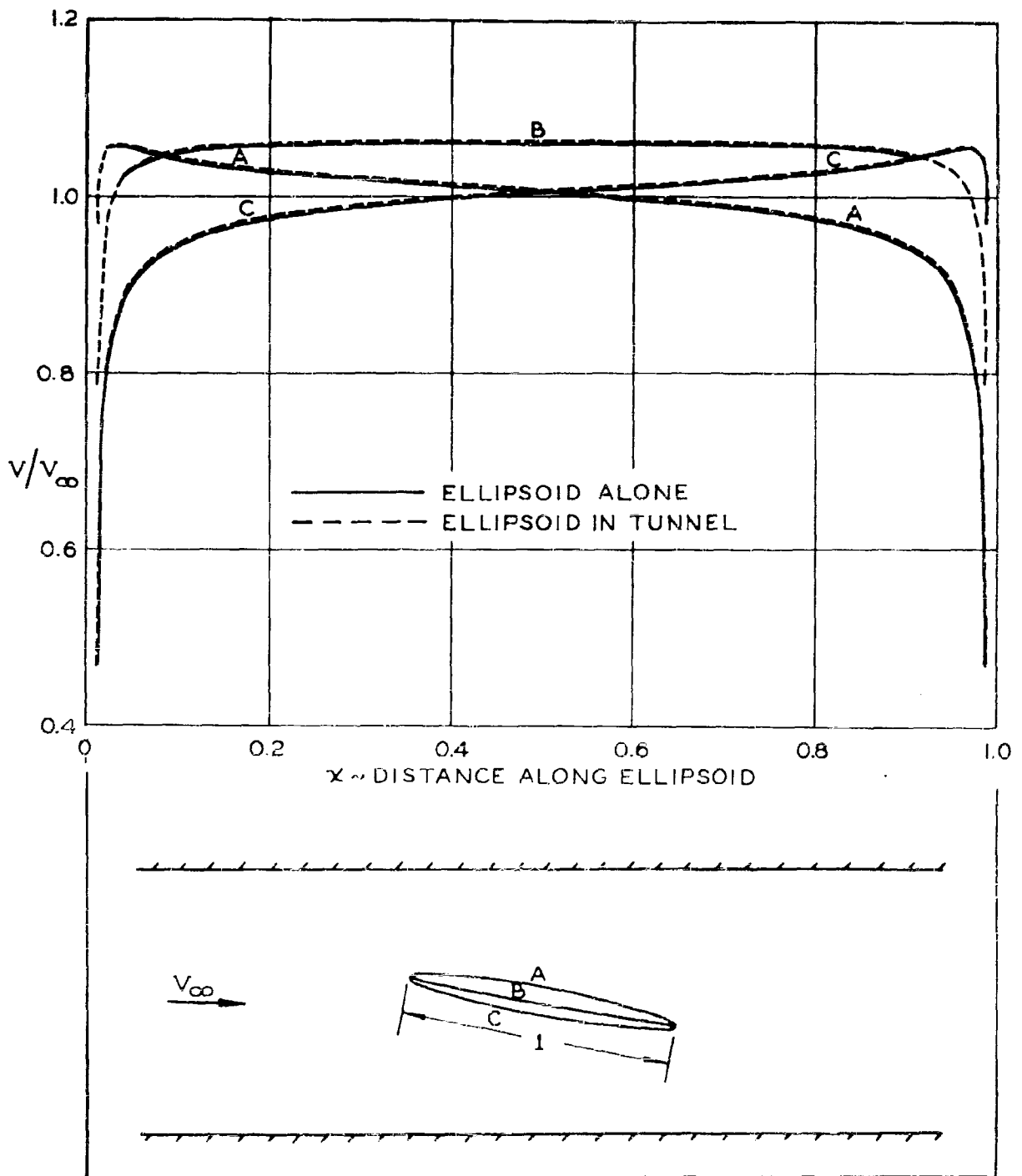
Figure 45. - Calculated velocity distributions on an ellipsoid at 10° angle of attack with and without the presence of a round wind tunnel.
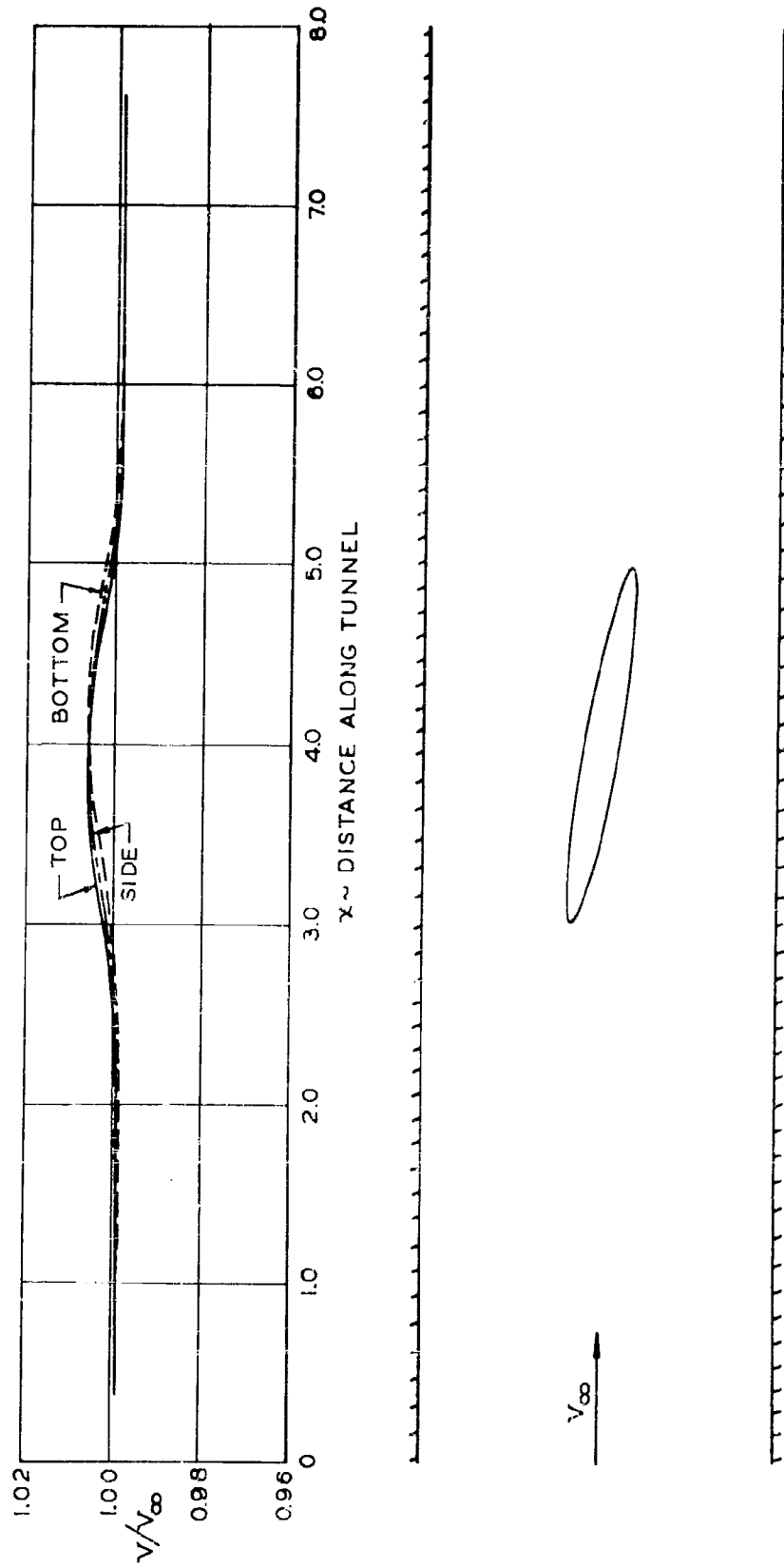
Figure 46. - Calculated velocity distributions along the walls of a round wind tunnel containing an ellipsoid at 10° angle of attack.
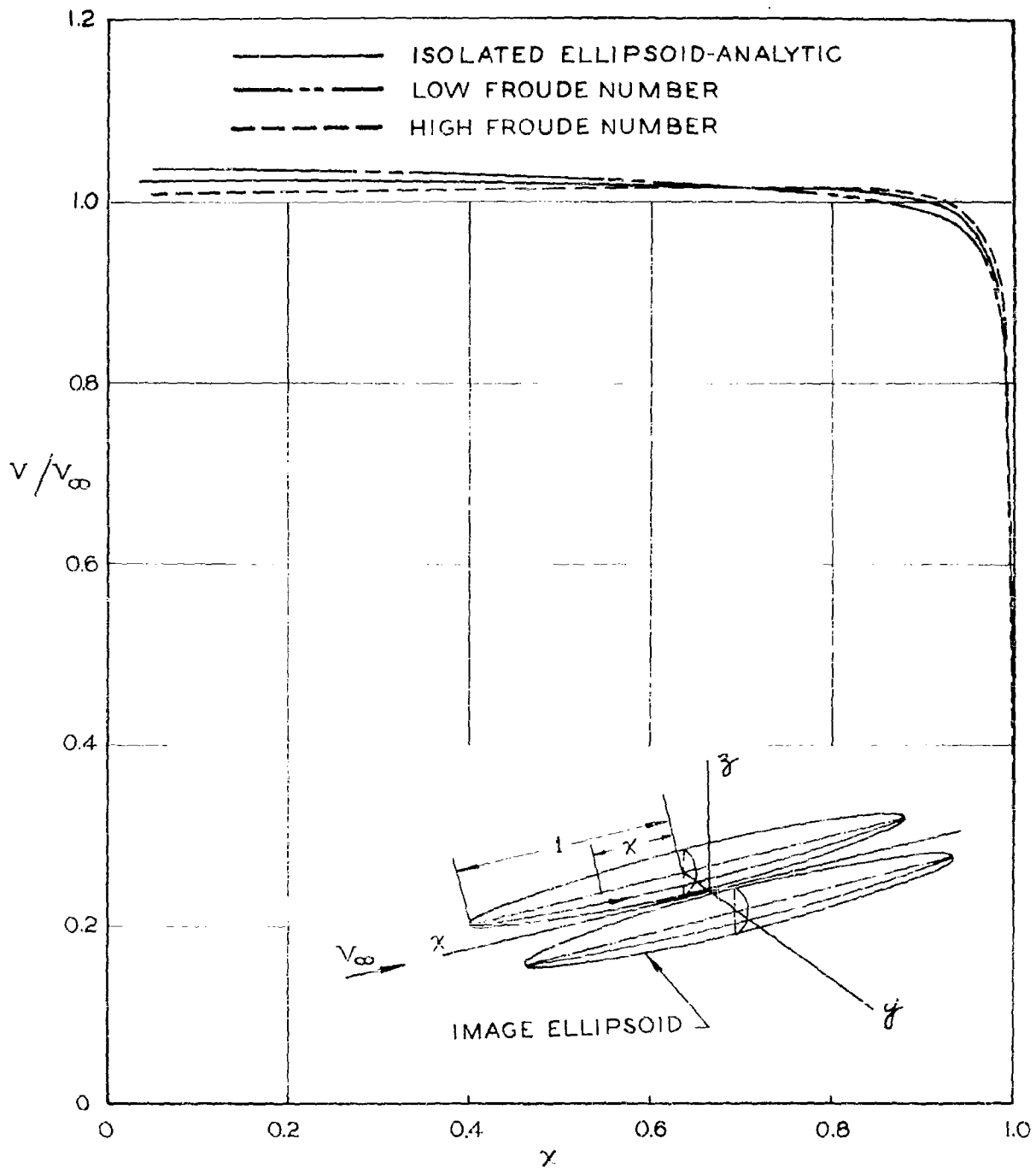
Figure 47. - Calculated velocity distributions on an ellipsoid with and without the presence of a free surface in the xz-plane. (a) Onset flow parallel to the x-axis.
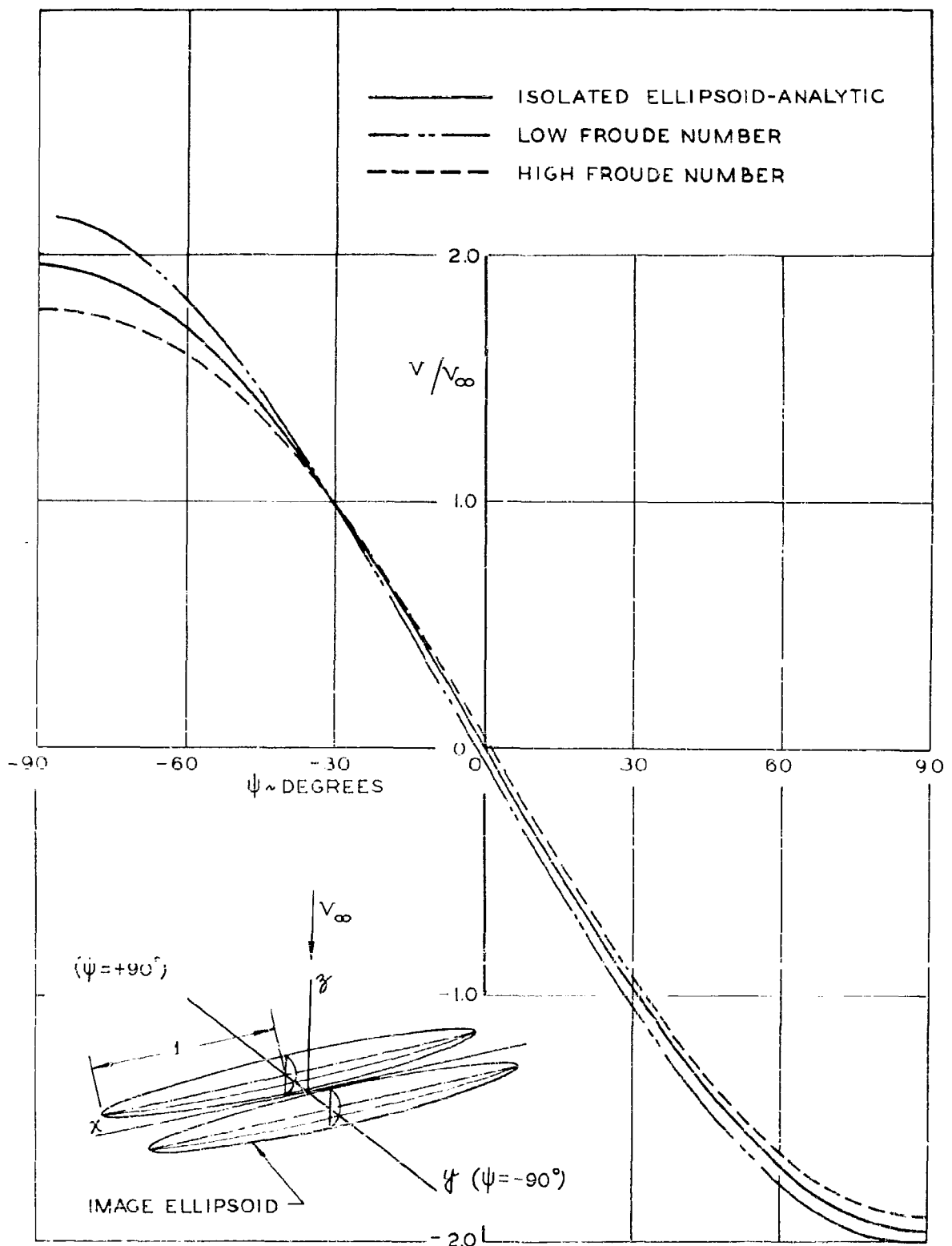
Figure 47. - Continued   (b) Onset flow parallel to the z-axis.
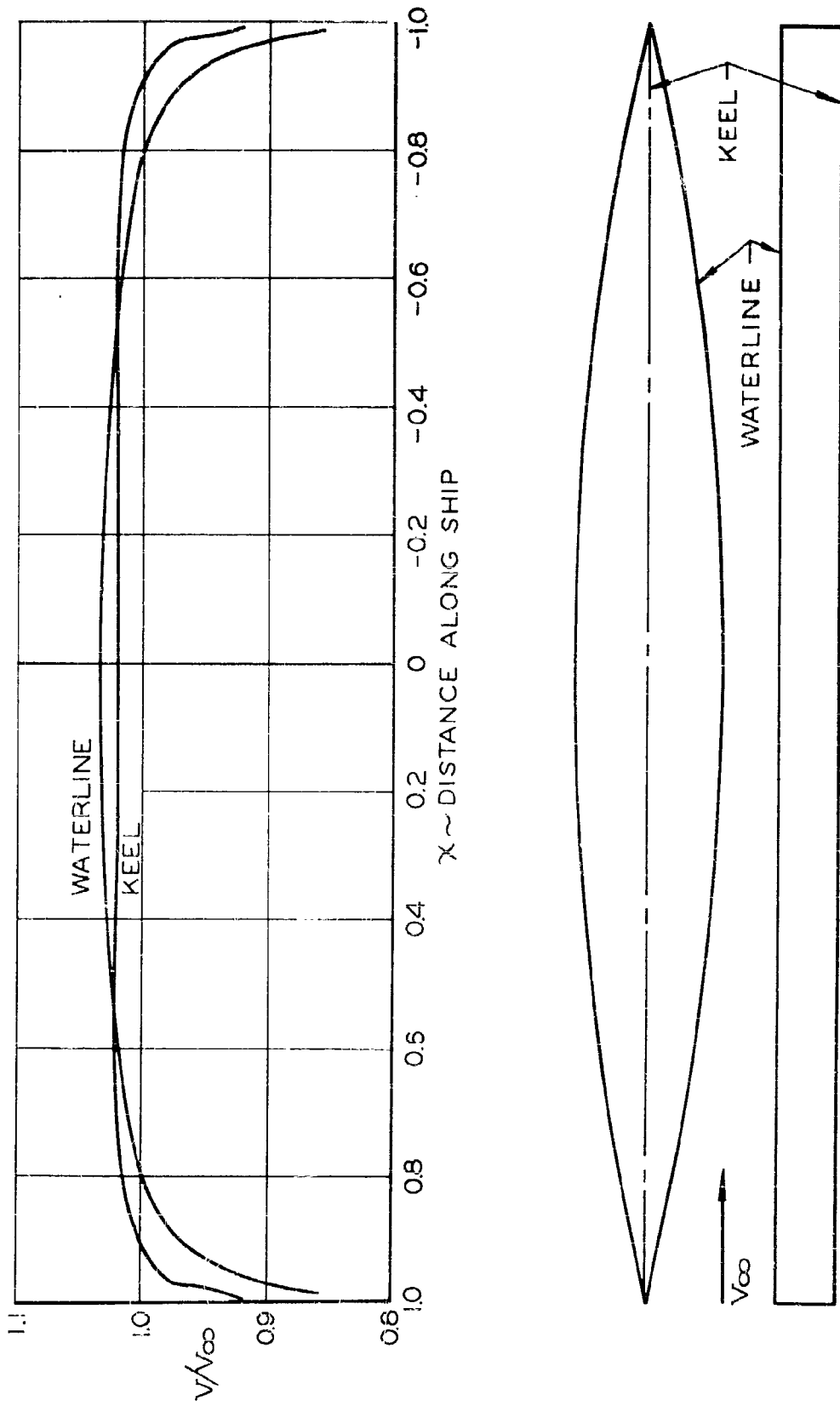
Figure 48. - Calculated velocity distributions on a simple ship hull. (a) Velocity distributions along the waterline and the keel.
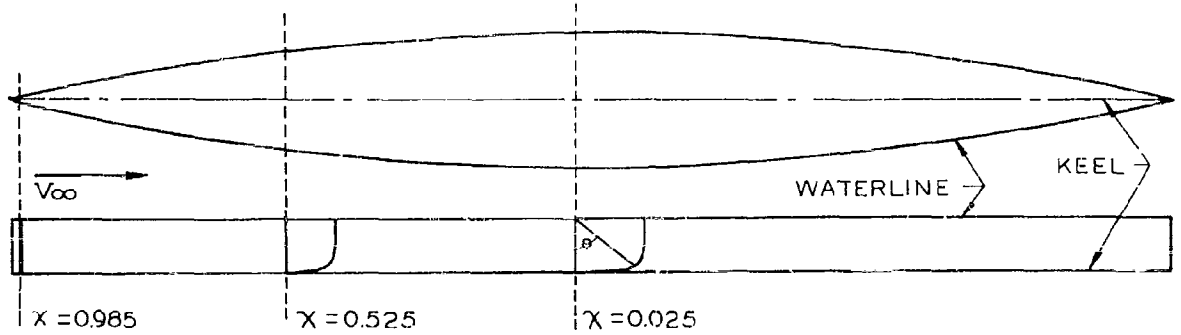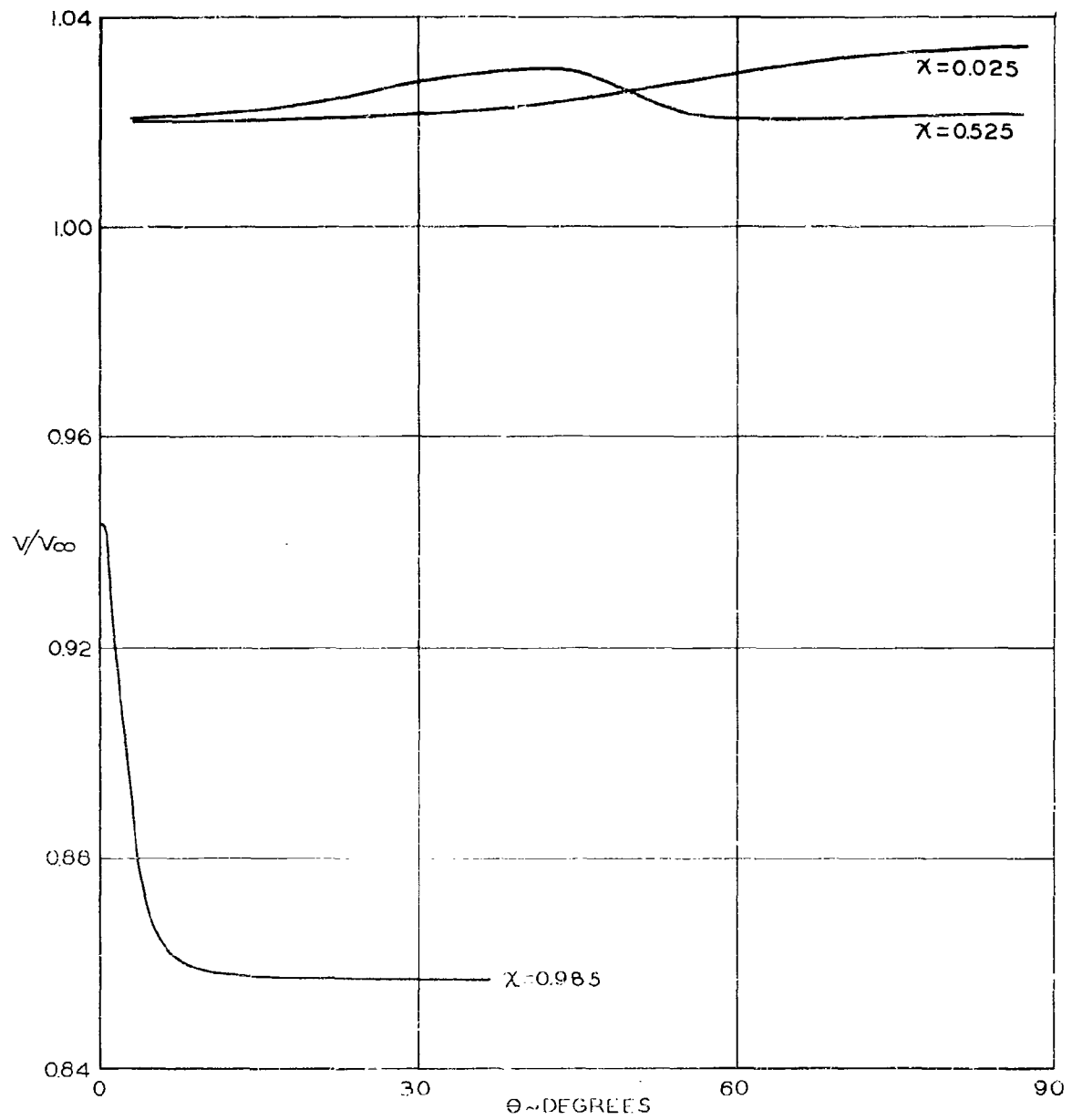
Figure 48. - Continued   (b) Velocity distributions around cross-sections of the hull.

174
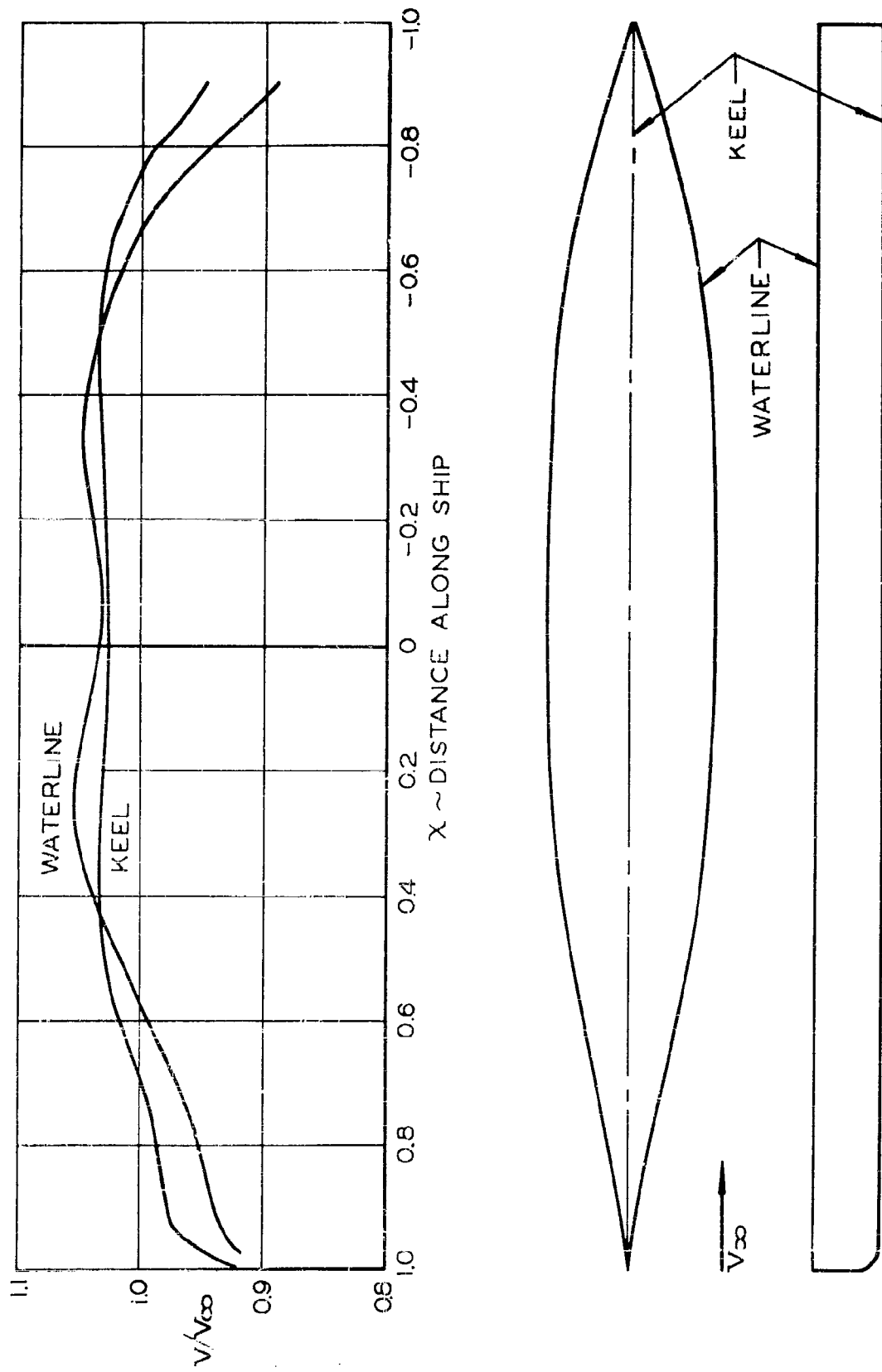
Figure 49. - Calculated velocity distributions on a series 60 merchant ship hull. (a) Velocity distributions along the waterline and the keel.

175
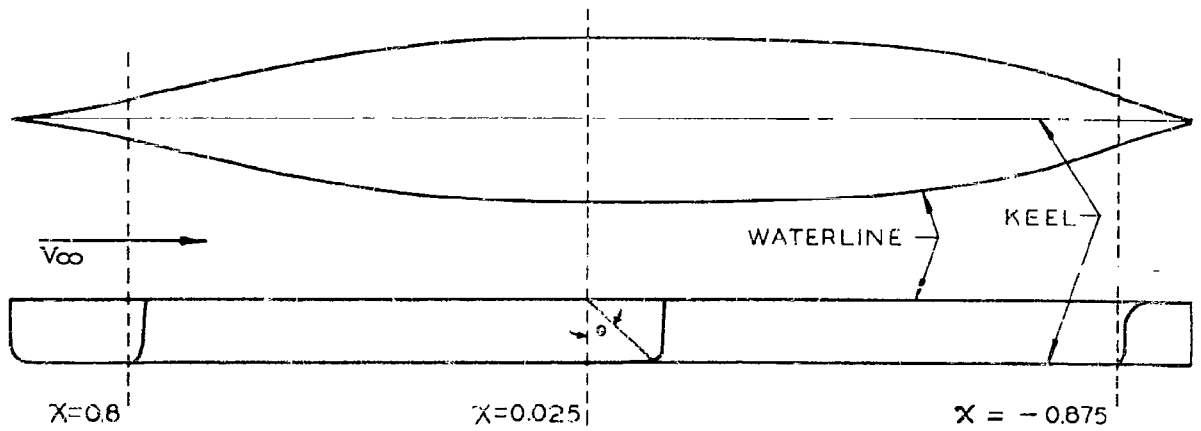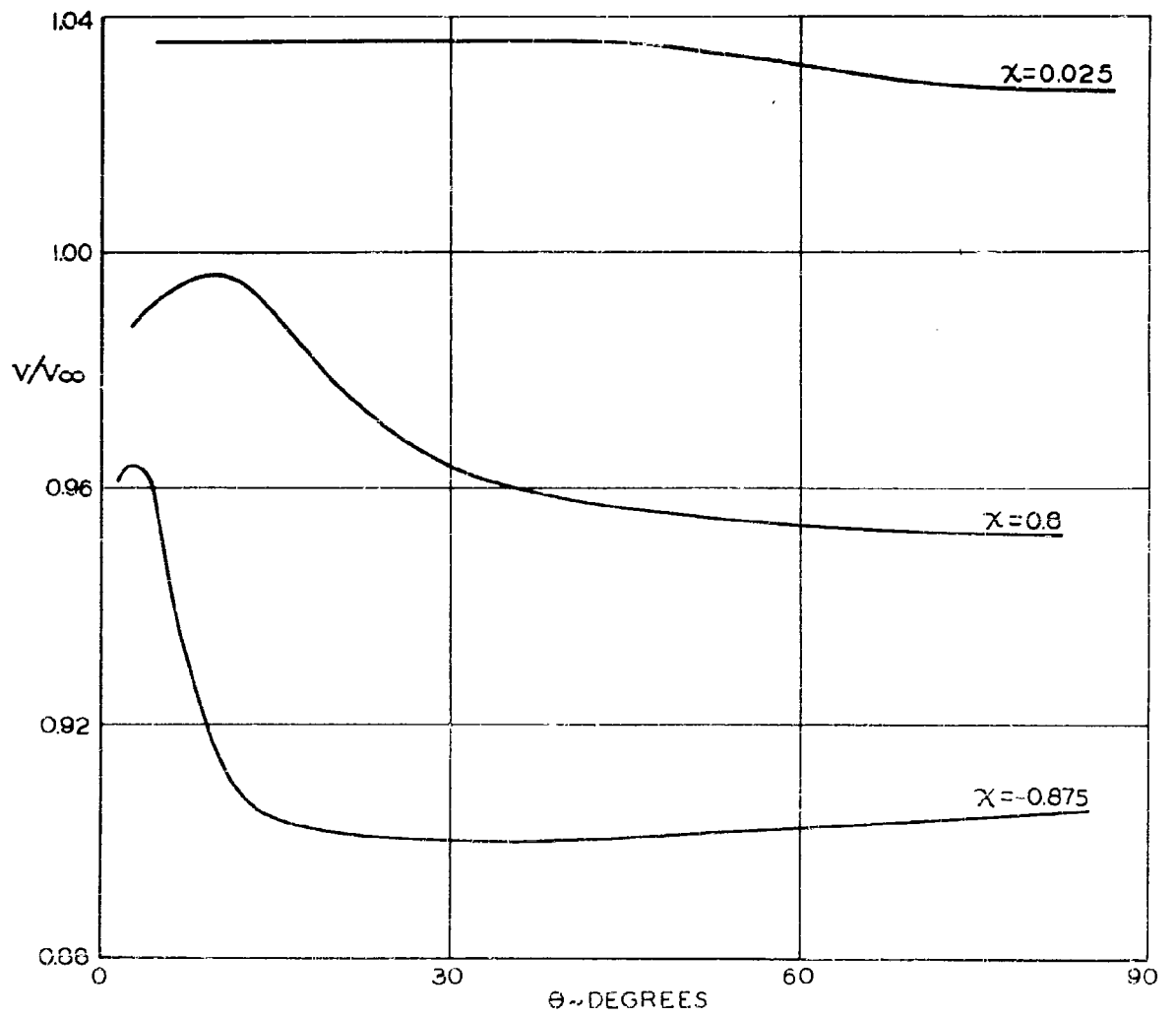
Figure 49. - Continued   (b) Velocity distributions around cross-sections of the hull.

176
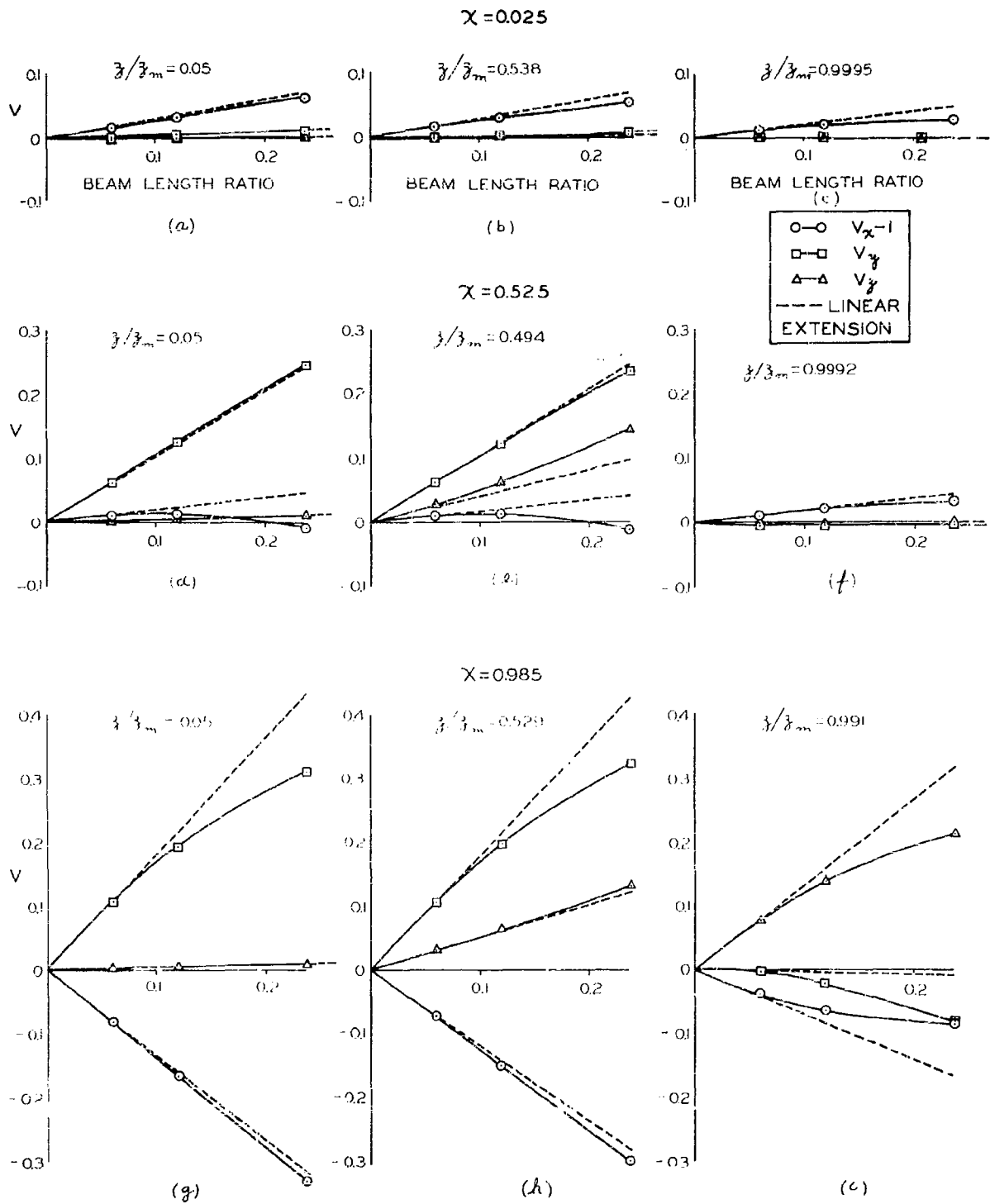
Figure 50. - Disturbance velocity components as functions of beam-length ratio for various locations on the simple ship hull.

177

U. S. Government Agencies

Chief, Bureau of Naval Weapons
Department of the Navy
Washington 25, D. C.
Code RRRE

Chief, Bureau of Naval Weapons
Department of the Navy
Washington 25, D. C.
Code RAAD-3

Chief, Bureau of Naval Weapons
Department of the Navy
Washington 25, D. C.
Att: Code DLI-31

Office of Naval Research
Department of the Navy
Washington 25, D. C.
Att: Code 438

Office of Naval Research
Department of the Navy
Washington 25, D.C.
Code 461

Commanding Officer and Director
Davia Taylor Model Basin
Carderock, Maryland
Att: Code 513 (200 Copies)

Commander
U. S. Naval Weapons Laboratory
Dahlgren, Virginia
Att: Technical Library

Commander
U.S. Naval Ordnance Test Station
Inyokern, China Lake, California
Att: Technical Library

Commander
U.S. Naval Ordnance Laboratory
White Oak, Silver Spring, Maryland

Commander
U.S. Naval Air Missile Test Center
Point Mugu, California

United States Naval Academy
Annapolis, Maryland
Att: Librarian

U.S. Naval Postgraduate School
Aeronautics Department
Monterey, California
Att: Dr. R. M. Head

U.S. Naval Postgraduate School
Monterey, California
Att: Librarian

Chief, Bureau of Ships
Department of the Navy
Washington 25, D.C.
Att: Code 320 (Lab N.G.T.)

Chief, Bureau of Ships
Department of the Navy
Washington 25, D.C.
Att: Code 335 (Technical
Information Branch)(3 Copies)

Chief, Bureau of Ships
Department of the Navy
Washington 25, D.C.
Att: Code 345 (Ship Silencing
Branch)

Chief, Bureau of Ships
Department of the Navy
Washington 25, D.C.
Att: Code 420 (Preliminary
Design Branch)

Chief Bureau of Ships
Department of the Navy
Washington 25, D.C.
Att: Code 421 (Preliminary
Design Branch)

Chief Bureau of Ships
Department of the Navy
Washington 25, D. C.
Att: Code 440 (Hull Design Branch)

Chief Bureau of Ships
Department of the Navy
Washington 25, D.C.
Att: Code 442 (Scientific and Research)

Special Projects Office
Department of the Navy
Washington 25, D.C.
Att: Chief Scientist

Director
U.S.Naval Research Laboratory
Code 2020
Washington 25, D.C.(6 Copies)

Commander
New York Naval Shipyard
Brooklyn, New York

Commander
Norfolk Naval Shipyard
Portsmouth, Virginia

Commanding Officer
Office of Naval Research
Navy 100, Fleet Post Office
New York, New York
(15 Copies)

Commanding Officer
Office of Naval Research
Branch Office
1000 Geary Street
San Francisco 9, California

Commanding Officer
Office of Naval Research Branch Office
346 Broadway
New York 13, New York

Commanding Officer
Office of Naval Research Branch Office
The John Crerar Labrary Building
85 East Randolph Street
Chicago 1, Illinois

Commanding Officer
Office of Naval Research Branch Office
495 Summer Street
Boston 10, Massachusetts

Commanding Officer
Office of Naval Research Branch
Office
1030 East Green Street
Pasadena 1, California

Commander
Long Beach Naval Shipyard
Long Beach, California

Commander
Mare Island Naval Shipyard
Vallejo, California

Commander
Pearl Harbor Naval Shipyard
Navy 120, Fleet Post Office
San Francisco, California

Commander
Philadelphia Naval Shipyard
Philadelphia, Pennsylvania

Commander
Portsmouth Naval Shipyard
Portsmouth, New Hampshire

Commander
Puget Sound Naval Shipyard
Bremerton, Washington

Commander
Office of Aerospace Research
Washington 25, D.C.

Air Force
Office of Scientific Research
SRR
Washington 25, D.C.
Att: Dr. Carl Kaplan

Air Force
Office of Scientific Research
Mechanics Division
Washington 25, D.C.

Commander
Aeronautical Systems Division
Wright-Patterson Air Force Base
Dayton, Ohio
Att: Aeronautical Research Laboratory

Commander
Wright Air Development Division
Att: WCRRD
Wright-Patterson Air Force Base,
Dayton, Ohio

Commander
Wright Air Development Center
Wright-Patterson Air Force Base
Dayton, Ohio
Att: WCLSW, Mr. P. Antonatos

Commander
Aeronautical Systems Division
Wright-Patterson Air Force Base
Dayton, Ohio
Att: Flight Dynamics Laboratory(ASRMD)

Commander
Wright Air Development Center
Wright-Patterson Air Force Base
Dayton, Ohio
Att: Dr. G. Guderley

Arnold Engineering Development
Center Library
P.O.Box 162
Tullahoma, Tennessee

Ballistics Research Laboratory
Aberdeen Proving Ground
Aberdeen, Maryland

Air University
Maxwell Air Force Base
Alabama

United States Air Force Academy
Lowry Air Force Base
Denver, Colorado

Director
National Aeronautics and Space
Administration
1512 H Street, Northwest
Washington 25, D.C.

National Aeronautics and Space
Administration
Langley Aeronautical Laboratory
Langley Field, Virginia
Att: Librarian

Director
National Aeronautics and Space
Administration
Ames Aeronautical Laboratory
Moffett Field, California

Library
Lewis Flight Propulsion Laboratory
21000 Brookpark Road
Cleveland 11, Ohio

NASA High Speed Flight Test Station
Edwards Air Force Base, California

National Bureau of Standards
Department of Commerce
Washington 25, D.C.
Att: Dr. G. B. Schubauer

National Science Foundation
Division of Mathematical, Physical
and Engineering Sciences
Washington 25, D.C.

Documents Service Center
Armed Services Technical
Information Agency
Arlington Hall Station
Arlington 12, Virginia (10 Copies)

UNIVERSITIES

Brown University
Graduate Division of Applied
Mathematics
Providence 12, Rhode Island
Att: Dr. R. Probstein

Guggenheim Aeronautical Laboratory
California Institute of Technology
Pasadena 4, California
Att: Dr. Clark B. Millikan

California Institute of Technology
Pasadena 4, California
Att: Professor Paco Lagerstrom

California Institute of Technology
Pasadena 4, California
Att: Professor H. W. Liepmann

California Institute of Technology
Pasadena 4, California
Att: Professor H. J. Stewart

California Institute of Technology
Pasadena 4, California
Att: Professor T. Y. Wu

Jet Propulsion Laboratory
California Institute of Technology
4800 Oak Grove Drive
Pasadena 3, California

California State Polytechnic College
Aeronautical Engineering
San Luis Obispo, California
Att: Professor Lester W. Gustafson

University of California
209 Mechanical Engineering Building
Berkeley 4, California
Att: Professor Edmund V. Laitone

University of California
209 Mechanical Engineering Building
Berkely 4, California
Att: Professor J.V. Wehausen

University of California
at Los Angeles
College of Engineering
Los Angeles 24, California
Att: Dr. John Miles

Case Institute of Technology
Cleveland, Ohio
Att: Dr. G. Kuerti

Cornell University
Graduate School of Aeronautical
Engineering
Ithaca, New York
Att: Dr. W. R. Sears

University of Florida
Department of Aeronautical Engineering
Gainesville, Florida
Att. Professor William H. Miller

University of Florida
Dept. of Aeronautical Engineering
Gainesville, Florida
Att: Professor D.T. Williams

Harvard University
Div. of Engineering and Applied
Physics
Pierce Hall
Cambridge 38, Massachusetts
Att: Gordon McKay Library

Harvard University
Mathematics Department
Cambridge 38, Massachusetts
Att: Professor Birkhoff

Harvard University
Dept. of Applied Physics and
Engineering Science
Cambridge 38, Massachusetts
Att: Dr. H. W. Emmons

Harvard University
Dept. of Applied Physics and
Engineering Science
Cambridge 38, Massachusetts
Att: Professor Carrier

Harvard University
Dept. of Applied Physics and
Engineering Science
Cambridge 38, Massachusetts
Att: Prof. Goldstein

University of Illinois
Dept. of Aeronautical Engineering
Urbana, Illinois
Att: Dr. Allen I. Ormsbee

University of Illinois Library
Serials Department
Urbana, Illinois

Iowa State University
Iowa City, Iowa
Att: Professor Hunter Rouse

Johns Hopkins University
Department of Aeronautics
Baltimore 18, Maryland
Att: Dr. F.H.Clauser

Johns Hopkins University
Applied Physics Laboratory
P.O.Box 244-Rt. 1
Laurel, Maryland
Att: Technical Reports Office

Johns Hopkins University
Applied Physics Laboratory
8621 Georgia Avenue
Silver Springs, Maryland
Att: Dr. F. N. Frenkiel

University of Maryland
Institute for Fluid Mechanics
and Applied Mathematics
College Park, Maryland
Att: Professor J. M. Burgers

Massachusetts Institute of Technology
Aeronautical Engineering Library
Building 33
Cambridge 39, Massachusetts

Massachusetts Institute of Technology
Cambridge 39, Massachusetts
Att: Dr. Leon Trilling

Massachusetts Institute of Technology
Cambridge 39, Massachusetts
Att: Professor Holt Ashley

Massachusetts Institute of Technology
Cambridge 39, Massachusetts
Att: Professor J. E. Kerwin

Massachusetts Institute of Technology
Cambridge 39, Massacgusetts
Att: Professor Marten Landahl

University of Michigan
Dept. of Aeronautical Engineering
Ann Arbor, Michigan
Att: Professor Arnold Kuethe

University of Michigan
College of Engineering
Dept. of Engineering Mechanics
Ann Arbor, Michigan
Att: Professor C. S. Yih

University of Minnesota
Dept. of Aeronautical Engineering
Rosemount Aeronautical Laboratories
Rosemount, Minnesota

Guggenheim School of Aeronautics
New York University
University Heights
New York 53, New York
Att: Librarian

North Carolina State College
Head of Mechanical Engineering Dept.
Raleigh, North Carolina
Att: Dr. R. W. Truitt

Ohio State University
Research Foundation
Columbus 10, Ohio
Att: Library

The Pennsylvania State University
Engineering Library
University Park, Pennsylvania

Pennsylvania State University
University Park, Pennsylvania
Att: Professor George F. Wislicenus

Polytechnic Institute of Brooklyn
Aerodynamics Laboratory
527 Atlantic Avenue
Freeport, New York
Att: Dr. Antonio Ferri

Brooklyn Polytechnical Institute
Brooklyn, New York
Att: Dr. Martin Bloom

James Forrestal Research Center
Dept. of Aeronautical Engineering
Princeton, New Jersey
Att: Professor C.D.Perkins, Chairman

Purdue University
School of Aeronautical Engineering
Lafayette, Indiana
Att: Library

University of Southern California
Engineering Center
935 West 37th Street
Los Angeles 7, California
Att: Dr. Raymond Chuan

Stanford University
Palo Alto, California
Att: Professor I. Flugge-Lotz

Stanford University
Palo Alto, California
Att: Professor Nicholas G. Hoff

Stevens Institute of Technology
5th and Hudson Street
Hoboken, New Jersey
Att: Dr. John P. Breslin

University of Texas
Defense Research Laboratory
P.O.Box 8029
Austin, Texas
Att: Professor M.J. Thompson

Virginia Polytechnic Institute
Aerospace Engineering Dept.
Blacksburg, Virginia
Att: Dr. H. A. Hassan

University of Washington
Dept. of Aeronautical Engineering
Seattle 5, Washington
Att: Professor R. E. Street

West Virginia University
Aeronautical Engineering Department
Morgantown, West Virginia
Att: Professor L. Z. Seltzer

INDUSTRIAL AND RESEARCH COMPANIES

Armour Research Foundation
10 West 35th Street
Chicago 16, Illinois
Att: Document Librarian

Avco-Everett Research Laboratory
2385 Revere Beach Parkway
Everett 49, Massachusetts
Att: Dr. Richard H. Levy

AVCO Manufacturing Corp.
2385 Revere Beach Parkway
Everett 49, Massachusetts
Att: Dr. A. Kantrowitz

AVCO Research Library
2385 Revere Beach Parkway
Everett 49, Massachusetts

Aeronutronics Systems, Inc.
1234 Air Way
Glendale, California
Att: Dr. L. Kavanau

The Boeing Company
P.O.Box 3107
Seattle 14, Washington
Att: Mr. G. Schairer

Bowles Engineering Corporation
9347 Fraser Street
Silver Spring, Maryland
Att: R. E. Bowles, President

Chance-Vought Corporation
Dallas, Texas
Att: W. C. Schoolfield

Convair
San Diego Division
San Diego 12, California
Att: Mr. C. W. Frick

Cornell Aeronautical Laboratory, Inc.
4455 Genesee Street
Buffalo 21, New York
Att: Librarian

General Dynamics Corporation
Electric Boat Division
Groton, Conn
Att: Frank Walker Caldwell

General Electric Company
2900 Campbell Avenue
Schenectady 6, New York
Att: Library

General Electric Company
Research Laboratory
Schenectady, New York
Att: Dr. H. T. Nagamatsu

Grumman Aircraft Engineering Corp.
Bethpage, New York
Att: Mr. C. Tilgner, Jr.

Grumman Aircraft Engineering Corp.
Bethpage, Long Island, New York
Att: Fluid Mechanics Section

Hughes Aircraft Company
Florence Ave. at Teal Street
Culver City, California
Att: Dr. A. E. Puckett

United Aircraft Corporation
East Hartdford, Connecticut
Att: Mr. J. G. Lee

Hydronautics Inc.
200 Monroe Street
Rockville, Maryland
Att: Phillip Eisenberg, President

Lockheed Missile Systems Division
Research and Development Laboratory
Sunnyvale, California
Att: Dr. W. Griffith

Lockheed Aircraft Corporation
Burbank, California
Att: Mr. L. A. Rodert

The Glenn L. Martin Company
Aerophysics Research Staff
Flight Vehicle Division
Baltimore 3, Maryland

McDonnell Aircraft Corporation
St. Louis, Missouri
Att: Mr. G. S. Graff

Norair
Division of Northrop Aircraft, Inc.
Hawthorne, California
Att: Dr. W. Pfenninger

North American Aviation, Inc.
4300 East 5th Avenue
Columbus, Ohio
Att: Mr. R. M. Crone

North American Aviation, Inc.
Aerophysics Department
12214 Lakewood Boulevard
Downey, California
Att. Dr. E. R. van Driest

The Rand Corporation
1700 Main Street
Santa Monica, California
Att: Library

Republic Aviation Corporation
Conklin Street
Farmingdale, Long Island, New York
Att: Dr. W. J. O'Donnell

Therm Incorporated
Aerophysics Section
Ithaca, New York
Att: D. E. Ordway, Head

MISCELLANEOUS

Institute of the Aeronautical
Sciences
2 East 64th Street
New York 2k, New York

Pacific Aeronautical Library
Institute of the Aeronautical
Sciences
7660 Beverly Boulevard
Los Angeles 36, California

Applied Mechanics Review
Southwest Research Institute
8500 Culebra Road
San Antonio, Texas

Dr. Theodore von Karman
1501 East Marengo Avenue
Pasadena, California (Zone 5)

Society of Naval Architects and
Marine Engineers
74 Trinity Place
New York, New York

Douglas Aircraft Company. Report No. ES 40522

CALCULATION OF NON-LIFTING POTENTIAL FLOW ABOUT ARBITRARY THREE-DIMENSIONAL BODIES, by John L. Hess and A.M.O. Smith. 15 March 1962. 177p. incl. Figs.

UNCLASSIFIED

This report describes a general method of solving the title problem with the aid of an electronic computer. The required formulas are derived and the computational procedure explained in detail. The accuracy of the method is exhibited by comparing the calculated velocities with the analytic solutions for various ellipsoids. The results of the calculations for a variety of bodies are presented, including wing-fuselages, ducts, a body in a wind tunnel, two bodies side by side and ship hulls.

Douglas Aircraft Company. Report No. ES 40622

CALCULATION OF NON-LIFTING POTENTIAL FLOW ABOUT ARBITRARY THREE-DIMENSIONAL BODIES, by John L. Hess and A.M.O. Smith. 15 March 1962. 177p. incl. Figs.

UNCLASSIFIED

This report describes a general method of solving the title problem with the aid of an electronic computer. The required formulas are derived and the computational procedure explained in detail. The accuracy of the method is exhibited by comparing the calculated velocities with the analytic solutions for various ellipsoids. The results of the calculations for a variety of bodies are presented, including wing-fuselages, ducts, a body in a wind tunnel, two

---

Douglas Aircraft Company. Report No. ES 40622

CALCULATION OF NON-LIFTING POTENTIAL FLOW ABOUT ARBITRARY THREE-DIMENSIONAL BODIES, by John L. Hess and A.M.O. Smith. 15 March 1962. 177p. incl. Figs.

UNCLASSIFIED

This report describes a general method of solving the title problem with the aid of an electronic computer. The required formulas are derived and the computational procedure explained in detail. The accuracy of the method is exhibited by comparing the calculated velocities with the analytic solutions for various ellipsoids. The results of the calculations for a variety of bodies are presented, including wing-fuselages, ducts, a body in a wind tunnel, two bodies side by side and ship hulls.

Douglas Aircraft Company. Report No. ES 40622

CALCULATION OF NON-LIFTING POTENTIAL FLOW ABOUT ARBITRARY THREE-DIMENSIONAL BODIES, by John L. Hess and A.M.O. Smith. 15 March 1962. 177p. incl. Figs.

UNCLASSIFIED

This report describes a general method of solving the title problem with the aid of an electronic computer. The required formulas are derived and the computation.l proce. accuracy of the me... ...th the ana... results of the calculati...